Review

Progress on Germanium-Tin Nanoscale Alloys

Jessica Doherty, Subhajit Biswas, Emmanuele Galluccio, Christopher A. Broderick, Adria Garcia-Gil, Ray Duffy, Eoin O'Reilly, and Justin D. Holmes

Chem. Mater., **Just Accepted Manuscript** • DOI: 10.1021/acs.chemmater.9b04136 • Publication Date (Web): 24 Apr 2020

Just Accepted

is published by the American Chemical Society. 1155 Sixteenth Street N.W., Washington, DC 20036

Progress on Germanium-Tin Nanoscale Alloys

Jessica Doherty[1], Subhajit Biswas[1*], Emmanuele Galluccio[2], Christopher A. Broderick[2], Adria Garcia-Gil[1], Ray Duffy[2], Eoin O'Reilly[2] and Justin D. Holmes[1]

[1]School of Chemistry & Advanced Materials and Bioengineering Research (AMBER) Centre, University College Cork, Cork, T12 YN60, Ireland, [2]Tyndall National Institute, University College Cork, Cork, Ireland.

*To whom correspondence should be addressed: Tel: +353 (0)21 4905143; E-mail: s.biswas@ucc.ie (SB)

Abstract

Group IV alloys have attracted interest in the drive to create Si compatible, direct bandgap materials for implementation in complementary metal oxide semiconductor (CMOS) and beyond CMOS devices. The lack of a direct bandgap in Si and Ge hinders their incorporation into optoelectronic and photonic devices, without the induction of undesirable strain. Alloying of Ge with Sn represents a novel solution to the lack of light emission in group IV compounds, with an indirect-to-direct bandgap transition predicted for Ge at a Sn incorporation greater than 6.5 at. %. Recently, the initiatives on GeSn alloy research has turned its focus on nanoforms to keep track with the miniaturization of Si-related platforms for application in nano/optoelectronics, photonics and energy devices. Here, we review recent advances in the growth and application of $Ge_{1-x}Sn_x$ nanomaterials. An overview of theoretical band structure calculations for $Ge_{1-x}Sn_x$ and the effect of band-mixing is briefly explored to highlight the significance of Sn inclusion in Ge for band gap engineering. Different fabrication methods for growing $Ge_{1-x}Sn_x$ alloy nanostructures are delineated and corelated with thin films growth. This highlight the requirement of low-temperature and kinetically-driven non-equilibrium processes for growing these metastable nanoscale alloys. The optical and electrical properties for both $Ge_{1-x}Sn_x$ strain-relaxed one-dimensional (1D) nanostructures and nanoparticles are reported as well as recent key research findings on $Ge_{1-x}Sn_x$ thin films, highlighting the potential application of these materials in photonic, nanoelectronic and optotelectronic devices.

1. INTRODUCTION to $Ge_{1-x}Sn_x$ ALLOY

The race to create alternative, Si compatible, scalable, tuneable device materials over the past number of years has led to a focus on group IV elements. Alloying group IV semiconductors, such as Ge or Si with group IV metals such as Sn and Pb, can lead to a direct bandgap semiconductor, as in III-V materials, but with the distinct advantage over III-Vs of being Si compatible. A number of researchers have reported both theoretically and experimentally that a direct bandgap can be achieved in Ge by alloying the semiconductor with Sn,[1,2] lowering the separation between the indirect (L) and direct (Γ) valleys (140 meV in bulk Ge) in the conduction band.[3] A direct bandgap group IV semiconductor would be beneficial for efficient band-to-band tunnelling devices, such as a tunnelling field effect transistor (TFET),[4,5] for lasing platforms[6,7] and for the development of mid-IR photonic devices, such as waveguide amplifiers and multi-wavelength light sources.[8] Figure 1(a) denotes the historical germanium-tin ($Ge_{1-x}Sn_x$) alloy benchmarks; as reported by Wirths *et al* [9]; including the development in $Ge_{1-x}Sn_x$ nanostructures,

There have been many reports in the literature on $Ge_{1-x}Sn_x$ thin films and their applications in electronics[10], optoelectronics[11,12] and photonics.[7] However, due to the lattice mismatch between Ge and Sn, thin films often experience large amounts of strain. Compressive strain shifts the energy gap to lower wavelengths, therefore, in order to achieve a direct bandgap, more Sn incorporation is necessary.[13,14] This higher incorporation of Sn then becomes increasing difficult to achieve due to the low equilibrium solubility of Sn in Ge (< 1 at. %) and the tendency for Sn to segregate at high growth temperatures.[15–17] Some solutions have been proposed to reduce strain incorporation in $Ge_{1-x}Sn_x$ films, such as introducing a Ge buffer layer[6], or increasing the thickness of the $Ge_{1-x}Sn_x$ layer[18,19]. A promising solution to overcome strain induced in $Ge_{1-x}Sn_x$ thin films is to move towards one dimensional (1D) $Ge_{1-x}Sn_x$

nanostructures; a nanowire morphology allows for increased strain relaxation compared to thin films due to free sidewall facets.[20] The move from $Ge_{1-x}Sn_x$ thin films to nanowires also reduces the Sn required to achieve a direct bandgap as the compressive strain is effectively relaxed. Introduction of Sn into the Ge crystal to form $Ge_{1-x}Sn_x$ alloy nanoparticles also enables tunable bandgap in the near-infrared region through regulating their composition and size due to the quantum confinement effect. A further decrease in nanostructure size can also result in increased quantum effects, resulting in a blue shift of bandgap energies to visible region.

This review summarizes recent developments in the growth and characterization of $Ge_{1-x}Sn_x$ nanostructures, and their application in electronic, optoelectronic and other devices, due to a surge in number of research reports on the $Ge_{1-x}Sn_x$ alloy nanomaterials in the last five years (Figure 1(b)). A comprehensive review of $Ge_{1-x}Sn_x$ materials and their applications up to 2015 has been reported by Zaima *et al.*[17] There were very few reports on $Ge_{1-x}Sn_x$ nanostructures; specially on 1D nanowires; until 2003,[21] with only a few reports following up to 2015.[22] This review will primarily focus on the growth and application of recent $Ge_{1-x}Sn_x$ nanostructures, highlighting their optical and electronic properties and recent developments in $Ge_{1-x}Sn_x$ device fabrication. The most promising $Ge_{1-x}Sn_x$ nanostructures, such as nanowires and nanoparticles, will be discussed in terms of their growth and characterisation in comparison to the $Ge_{1-x}Sn_x$ thin films. Firstly, however, a brief overview of the theoretical insights into $Ge_{1-x}Sn_x$ materials is outlined to provide an essential historical starting point for what has become an increasingly popular alloy.

2. THEORETICAL PERSPECTIVE ON $Ge_{1-x}Sn_x$

The realization that $Ge_{1-x}Sn_x$ alloys could exhibit a direct bandgap was first predicted theoretically in 1982,[23] based on qualitative analysis of trends revealed by simple linear interpolation between the band structures of Ge and α-Sn. This prediction, which was supported by more rigorous density functional theory (DFT) calculations in 1989,[24] predates the growth of crystalline $Ge_{1-x}Sn_x$, and indeed served as a key motivation for early attempts to establish fabrication of $Ge_{1-x}Sn_x$ alloys.[25,26] These early theoretical reports laid the foundation for the strong interest in $Ge_{1-x}Sn_x$ alloys – both from theoretical and experimental perspectives – that has developed over the last three decades. As further theoretical and experimental data emerged it was realized that relatively modest Sn compositions were sufficient to bring about a direct bandgap, stimulating further activity related to theorizing potential growth methods, as well as to initial analysis of the optical and electrical properties, and the overall potential for band structure engineering in $Ge_{1-x}Sn_x$ for device applications.[27, 28]

In this section we provide a brief overview of theoretical investigations of $Ge_{1-x}Sn_x$ alloys, focusing respectively in Sections 2.1 and 2.2 on the evolution of the alloy band structure and on key physical properties relevant to proposed device applications.

2.1. Band structure of $Ge_{1-x}Sn_x$

Beginning with Ge, the lowest energy conduction band (CB) state at the Γ point lies only approximately 140 meV higher in energy than the L-point conduction band minimum. The aim of realizing direct bandgap group IV materials has for this reason centered primarily on engineering the band structure of Ge, since in principle one need only shift the Γ-point CB edge states downwards by 140 meV relative to the L-point states in order to achieve a direct bandgap. This could be achieved via application of tensile strain in pure Ge, to take advantage of the

significantly higher pressure coefficient associated with the direct Γ-Γ bandgap (12.9 meV/kbar) compared to that associated with the fundamental Γ-L bandgap (4.3 meV/kbar).[29,30] However, high levels of tensile strain (> 2%) are required to achieve this Γ-L crossover, testing critical thickness limits and complicating fabrication. Although tensile strained Ge has been successfully demonstrated in photodetector applications,[29] the aforementioned growth challenges limit its potential as a gain medium since even higher tensile strains are required to push the L valleys sufficiently far above the Γ-point CB minimum in energy to allow for efficient laser action under electrical injection. These issues, combined with the predicted rapid reduction in energy of the Γ-point CB edge states relative to those at L with increasing Sn composition, have therefore led to $Ge_{1-x}Sn_x$ alloys being favored in recent years as the leading contender to obtain a direct bandgap Ge-based gain medium to facilitate the development of all-group IV semiconductor lasers for Si photonics applications.

Since the initial qualitative analysis of the $Ge_{1-x}Sn_x$ band structure[23], the evolution of the band structure of $Ge_{1-x}Sn_x$ alloys has attracted significant attention from a theoretical perspective. Theoretical analysis of the $Ge_{1-x}Sn_x$ band structure has for the most part centered on applications of the empirical pseudopotential method (EPM) or tight-binding method (TBM) in the virtual crystal approximation (VCA). In the VCA each atom in the alloy assigned the (identical) properties of an average "$Ge_{1-x}Sn_x$" atom. This has the advantage that it allows calculations to be performed for a primitive unit cell, removing complications associated with zone folding in atomistic supercell calculations. However, this comes at the cost of neglecting effects related to the differences in size and chemical properties between the constituent elements of the alloy, so that effects such as alloy band mixing (hybridisation) and carrier localization do not manifest as in real alloys.

VCA-based calculations have successfully demonstrated the emergence of a direct bandgap due to a more rapid decrease in energy of the lowest CB at Γ than at L in response to Sn incorporation and have predicted bandgap values which are in good overall agreement with experimental measurements. However, predictions of the Sn composition at which $Ge_{1-x}Sn_x$ becomes a direct bandgap semiconductor have varied over a broad range. Since the initial prediction that approximately 26 at.% Sn would be required to bring about a direct bandgap,[24] theoretical analysis has continuously revised this composition downwards in response to emerging experimental data. Simple linear interpolation between the high-symmetry point energies in Ge and α-Sn suggests the emergence for a direct band gap for ~20 at.% Sn. This is, for example, close to the value of 17 at.% calculated by Moontragoon *et al*. using the EPM in the VCA.[31] Subsequent VCA-based analysis using the EPM and TBM has largely relied on reparameterization which drives the emergence of a direct bandgap to lower Sn compositions, with more recent calculations reducing the crossover composition to 11[32,33] and subsequently to 6.5 at.%,[34] bringing theoretical calculations more into line with experimental measurements.[35,36]

This trend has suggested an inability on the part of theory to produce quantitative predictions for $Ge_{1-x}Sn_x$ without reference to existing experimental data. That this should turn out to be the case for calculations employing the VCA was identified at an early stage. Early analysis by He and Atwater[37] noted the inability of calculations based on the VCA to accurately predict the magnitude of the Sn-induced band gap reduction. Later, comparisons by Moontragoon *et al*.[31] between EPM calculations carried out in the VCA and direct atomistic alloy supercell calculations demonstrated significant deviations in results. These results suggest that atomic-

scale alloying effects neglected in the VCA – e.g. band mixing (hybridization) and carrier localization, associated with the differences in size and chemical properties between Ge and Sn – likely play important roles in determining the evolution of the band structure and emergence of a direct bandgap in $Ge_{1-x}Sn_x$ alloys. Nonetheless, there has been a proliferation of VCA-based approaches to model the $Ge_{1-x}Sn_x$ band structure in the literature, due to both to interpretational simplicity and low computational demand.

This situation has begun to change over the past 5 years, with the emergence of a number of studies employing more accurate (non-VCA) atomistic supercell calculations in conjunction with sophisticated electronic structure methods based on DFT.[38–40] However, while first principles calculations are in general more reliable due to their limited number of free parameters, they have not produced a clear consensus regarding the nature of the indirect to direct bandgap transition. Indeed, despite DFT-based analyses agreeing on the qualitative properties of the alloy band structure, they retain significant quantitative differences; between 4.5 to 11 at.%; in the predicted Sn composition at which a direct bandgap emerges.[38–41]

Despite three decades of attention, it therefore appears that current theoretical calculations have failed to produce an unambiguous predictive description of the $Ge_{1-x}Sn_x$ band structure which can be used, e.g., to underpin further theoretical analysis of material properties relevant to device applications. Motivated by this problem, as well as by new experimental data, our group has recently undertaken detailed theoretical analysis of the indirect to direct bandgap transition in $Ge_{1-x}Sn_x$. Pressure-dependent measurements by Eales et al.[42] have provided initial evidence suggesting that the the pressure coefficient associated with the fundamental bandgap in $Ge_{1-x}Sn_x$ is intermediate between that of the indirect (fundamental) Γ-L and direct Γ-Γ bandgaps of

Ge for samples with x ~ 6-7%. This suggests that the alloy direct band gap is hybridised in nature in this composition range, consisting of an admixture of Ge Γ- and L-point CB edge character; measurements on a further sample with x ~10% showed conventional direct-gap character for 10% Sn. This data suggests the continuous evolution of a direct bandgap in $Ge_{1-x}Sn_x$ with increasing Sn composition x, via transfer of Ge Γ-point CB edge character to the alloy conduction band edge, driven by Sn-induced hybridisation. These conclusions have been supported by alloy supercell calculations carried out using both DFT and TBM approaches[43], in which the hybridized nature of the alloy CB edge is directly verified via the calculated bandgap pressure coefficient. Initial analysis has demonstrated that this Sn-induced hybridization is strongly sensitive to short-range alloy disorder (Sn clustering)[42,43], suggesting that systematic analysis of realistic, disordered $Ge_{1-x}Sn_x$ alloy supercells is required to quantitatively understand the nature of the indirect to direct bandgap transition. Further experimental investigations are in addition required to determine the extent to which band mixing effects are present and important in $Ge_{1-x}Sn_x$ alloys.

Nonetheless, emerging experimental evidence of the importance of alloy band mixing effects in $Ge_{1-x}Sn_x$ has the potential to provide critical insight into the failure of previous analysis to quantitatively describe the indirect to direct bandgap transition. The continuous evolution of the character of the CB edge with increasing Sn composition is in stark contrast to the widespread assumption of an indirect to direct bandgap crossover occurring at a single, critical Sn composition. In VCA-based calculations this alloy band mixing is not present due to the limitations of the underlying assumptions, and calculations contain clearly distinguishable Γ- and L-point CB states which pass through one another at a clearly defined composition. In DFT-based alloy supercell calculations the presence of a hybridized CB alloy edge has been directly noted,[38] or evidenced in unfolded supercell band structures,[41] and is to be expected

given the small separation in energy between the Γ- and L-point CB edge states in Ge. However, the assumptions employed in qualitative analysis of DFT band structure calculations has remained the same as that employed in VCA-based approaches: band mixing effects are neglected and individual supercell states are identified as being purely "Γ-like" or "L-like" and the composition at which the former passes through the latter in energy is reported.

The potential consequences of band mixing effects for alloy material properties are not solely of importance for determining the Sn composition range in which the alloy attains a direct bandgap. The presence of hybridized CB states can further be expected to impact key material properties relevant to device applications, including optical transition strengths, electron mobility, etc. Previous theoretical work on alloy band mixing in III-V $Ga_{1-x}In_xP$ alloys has demonstrated that quantitative understanding of hybridization between extended (Bloch) states in disordered semiconductor alloys requires direct electronic structure calculations for ultra-large supercells to overcome the limitations associated with periodicity and zone folding in the smaller supercells to which first principles calculations are limited (by computational expense). Such analysis is therefore required for $Ge_{1-x}Sn_x$ alloys soon, to support experimental efforts to realize $Ge_{1-x}Sn_x$-based semiconductor devices.

2.2. Theoretical insight into the physical properties of $Ge_{1-x}Sn_x$

The optical, thermal, and electrical properties of $Ge_{1-x}Sn_x$ have been investigated and reported throughout the last 30 years; in many instances predating experimental verification. Due to the progression towards a direct bandgap with increasing Sn content in $Ge_{1-x}Sn_x$ materials, the optical properties of $Ge_{1-x}Sn_x$ have been widely considered and investigated. A detailed

theoretical analysis of the optical properties, bandgap, band width *etc*. of $Ge_{1-x}Sn_x$ was reported before experimental data was produced,[44] potentially fueling the desire to produce a single crystalline, direct bandgap $Ge_{1-x}Sn_x$ material. The optical properties, such as bandgap, bowing parameter, optical gain *etc*. of $Ge_{1-x}Sn_x$ are of importance due to the indirect to direct transition undergone by Ge upon sufficient incorporation of Sn (> 6.5 at. % Sn).[34,45,46] Theoretically, the bandgap in $Ge_{1-x}Sn_x$ can be tuned between 0.6 eV and 0.0 eV by altering the Sn inclusion.[45] The tunability of this bandgap is a valuable commodity in both optoelectronics and photonics, making $Ge_{1-x}Sn_x$ materials particularly suitable for incorporation in photodiodes covering the broad mid-IR range. Regarding the theoretical insight into the optical properties of GeSn nanoscale materials, most of the initiatives were focused on calculating the electronic band structure and optical gain in quantum well structure such as GeSn/SiGeSn and Ge/SiGeSn quantum wells.[47,48] Meanwhile, the theoretical studies about Ge/GeSn and GeSn/SiGeSn quantum dots have also been performed to some extent.[49] However, very little work has been done to systematically investigate the optical properties of $Ge_{1-x}Sn_x$ nanowires in theory. Very recently, using effective mass theory, is has been shown that the direct-band gap semiconductor is more difficult to be realized in low-dimensional $Ge_{1-x}Sn_x$ nanowires compared to bulk $Ge_{1-x}Sn_x$.[50] One of the main reasons is that the electron effective-mass of $Ge_{1-x}Sn_x$ alloy at the Γ-valley is less than that at the *L*-valley, which will lead to the quantum confinement induced energy of the electron at the Γ-valley larger than that at the *L*-valley. Thus, $Ge_{1-x}Sn_x$ nanowires with large diameter and Sn content have higher chance to become the direct-band-gap semiconductor. With increasing Sn content, the proportion of the occupied electron concentration at the Γ-valley will increase substantially, which can enhance the light-emitting efficiency in $Ge_{1-x}Sn_x$ nanowire lasers. A remarkable gain peak value can also be obtained with the increase in Sn content to achieve a positive net peak gain in $Ge_{1-x}Sn_x$ nanowire lasers even at a very low diameter of 24 nm, which is not the case for pure Ge nanowires.

In terms of electrical properties, theoretical studies of $Ge_{1-x}Sn_x$ show similar or enhanced values of hole mobility and concentrations compared with doped Ge counterparts.[51] A biaxial compressive strain, which forms due to lattice mismatch between Ge and Sn, lifts the light-hole band in the upward direction thus enhancing hole mobility. High hole mobility is very useful for high-performance p-channel MOSFETs. A 2D analytical model including quantum effects revealed that GeSnOI MOSFETs with a channel thickness of 5 nm yields the lowest threshold voltage (Vth) and subthreshold slope (SS); where the SS increase marginally with increasing Sn concentration ranging 0 – 6 at.%.[52] Due to its direct bandgap and silicon compatibility, $Ge_{1-x}Sn_x$ has been billed as an ideal material for the fabrication of post-CMOS band-to-band tunnelling field effect transistors (TFETs). Wang *et al.*[53] modelled $Ge_{1-x}Sn_x/Si_yGe_{1-x-y}Sn_x$ staggered heterojunction n-channel tunnelling field effect transistors (hetero-NTFETs) using a non-local empirical pseudopotential method. Hetero-NTFETs theoretically exhibited a steeper subthreshold swing, a higher ON-state current and a larger ON-OFF current ratio compared with $Ge_{1-x}Sn_x$ homojunction n-channel tunnelling FET devices. Sant and Schenk[54] also performed modelling analysis of $Ge_{1-x}Sn_x/Si_yGe_{1-x-y}Sn_x$ hetero tunnel FETs, but also explored the role of strain. Their simulations of $Ge_{1-x}Sn_x/Si_yGe_{1-x-y}Sn_x$ hetero-TFETs determined that compressive strain in $Ge_{1-x}Sn_x$ widens the design space for TFET applications while tensile strain reduces it. Haehnel *et al.*[55] explored the influence of drain doping, short channel and Sn content in p-channel Ge(Sn) heterojunction band-to-band tunnelling FETs. In their work they investigated the influence of a reduction of the channel length down to 15 nm on transistor performance.

3. FABRICATION OF $Ge_{1-x}Sn_x$ MATERIALS

From the first reported growth of microcrystalline $Ge_{1-x}Sn_x$ by Oguz *et al.*[25] to the present day, the fabrication of $Ge_{1-x}Sn_x$ materials has predominantly been as thin films. The recent

development and success on the growth of $Ge_{1-x}Sn_x$ nanomaterials, such as nanowires and nanoparticles, owes significantly to the studies on the growth of GeSn thin films. The understanding of the growth techniques used in the fabrication of $Ge_{1-x}Sn_x$ thin films provides essential knowledge, *e.g.* growth temperature, precursors, epitaxy, strain *etc*., and a strong platform for the fabrication of $Ge_{1-x}Sn_x$ nanostructures. Thus, it would be remiss not to detail some of the historical development and recent research on the growth and fabrication of $Ge_{1-x}Sn_x$ thin films.

The growth of $Ge_{1-x}Sn_x$ thin films has been reported using many fabrication techniques, including chemical vapour deposition (CVD), molecular beam epitaxy (MBE), sputtering, solid phase epitaxy and co-evaporation of Ge and Sn via physical vapor deposition (PVD).[56–61] The use of MBE dominated early $Ge_{1-x}Sn_x$ thin film growth,[21,25,26,62] with a shift to CVD growth occurring in the early 2000's.[27,63–67] The shift towards the CVD growth was instigated by the fact that MBE grown $Ge_{1-x}Sn_x$ films were not offering device quality (e.g. low crystallinity, formation of crystal defects etc.) films due to the very low growth temperature window (100 - 200 °C). High Sn content $Ge_{1-x}Sn_x$ with decent crystal quality to show clear photoluminescence (PL) signal was challenging via MBE growth. This shift in film growth towards CVD method was initiated by the development of different suitable CVD precursors, primarily $PhSnD_3$ and deuterated Stannane (SnD_4) as Sn precursor and Ge_2H_6 as Ge source, which allow the CVD growth of GeSn films at a temperature range between 250-350 °C.[68] The use of $SnCl_4$ as a Sn precursor further ease the CVD growth of $Ge_{1-x}Sn_x$ alloy films due to the accessibility and stability of the $SnCl_4$ compared to SnD_4. $SnCl_4$ precursor allowed the $Ge_{1-x}Sn_x$ growth via both atmospheric pressure and low pressure CVD methods.[56] GeH_4 has attracted lot of recent attention as a Ge precursor due to its low cost and thermal stability[69,70], although high order Ge hydrides (e.g. Ge_3H_8, Ge_4H_{10} etc.) are also attractive precursors due to

their weak Ge-Ge molecular bond, promoting high growth rates and large Sn incorporation.[71] Having a suitable growth temperature range (250-450 °C), as higher and lower temperature can result in Sn segregation and films with low crystal quality and Sn incorporation respectively, in combination with strain relaxation; such as the use of virtual substrate; is key in achieving high-quality, Sn-rich $Ge_{1-x}Sn_x$ semiconductor thin films.

Low-temperature CVD efforts have led to the growth of $Ge_{1-x}Sn_x$ thin films with Sn incorporation far in excess of the equilibrium concentration ($x \geq 0.10$).[6,14,18] One important aspect to consider for $Ge_{1-x}Sn_x$ thin film growth, which is not very significant for nanowire or any other nanostructure growth, is the role of compressive strain from the substrate (Ge virtual substrate/Ge) underneath. The substrate underneath can affect the crystal quality, Sn incorporation and band structure of the alloy films. Epitaxy of fully strained $Ge_{1-x}Sn_x$ thin film growth on Ge or strain relaxed virtual Ge substrate leads to high bi-axial compressive strain ($\sim 0.15\%$ per 1 at.% Sn)[63,72–74] ,which negates the effect of alloying Sn with Ge for direct bandgap conversion. The presence of compressive strain causes the fundamental energy gap to blue-shift to lower wavelengths, thus more Sn incorporation ($\approx$ 17 at.%)[75] is necessary to achieve a direct bandgap.[13,14,73,74] However, due the incredibly low equilibrium solubility of Sn in Ge (< 1 at. %) and the tendency for Sn to segregate at high growth temperatures, this task becomes increasingly difficult.[76,77] The usual approach to achieve strain relaxation is to increase the $Ge_{1-x}Sn_x$ epilayer thickness much beyond the critical thickness for strain relaxation as the epilayer plastically relax via the formation of misfit dislocations for larger thicknesses.[6,18,19,69,78,79] However, this approach for strain relaxation is mostly reported for CVD grown thin films with limited success for MBE grown layers[80]. Other methods such as using a relaxed $In_yGa_{1-y}P$ buffer layer or compositionally graded $Ge_{1-x}Sn_x$ buffer have been reported to result in strain relaxation and large uniform Sn incorporation.[81–83] One concern for

a strain relaxed $Ge_{1-x}Sn_x$ layer is the possible appearance of large amount of misfit dislocations in the $Ge_{1-x}Sn_x$ epilayer. These dislocations, particularly threading dislocations, can propagate through the entire epitaxial layer and severely deteriorate material quality by acting as non-radiative recombination centers. Regarding strain relaxation, formation of core/shell Ge/GeSn nanowires; which will be discussed in Section 3.2.1; is a promising solution, as fully elastic strain relaxation can be achieved, both due to the highly elastic compliance of a thin Ge core and to the effect of the free facets at the sidewalls.[20]

3.2. $Ge_{1-x}Sn_x$ Nanostructures

Although research on $Ge_{1-x}Sn_x$ thin film has gained lots of interest in last decade, there have been no or minimal reports on the fabrication of group IV direct bandgap materials, *e.g.* nanowires or nanoparticles, until recently. The development of nanowires is essential to keep track with the miniaturization of Si-based nanoelectronics and to take advantage of their 1D geometry for new age transistors, *e.g.* finFET and gate-all-around (GAA) FET devices. A few advantages of nanowire growth over this films are: (i) strain due to epitaxial misfits between a substrate and $Ge_{1-x}Sn_x$ nanowire can be accommodated due to strain release at nanoscale dimensions, thus easing the generation of single crystalline lattices without crystal defects, (ii) utilization of a third party material (as catalyst) to encourage enhance Sn incorporation and (iii) employment of solution phase methods to take advantage of the vast range of available liquid phase precursors. Additionally, $Ge_{1-x}Sn_x$ nanowires and nanoparticles are also of interest as they provide opportunities for additional bandgap tuning, useful in optoelectronic, electronic and energy storage applications.

3.2.1. $Ge_{1-x}Sn_x$ Nanowires

Despite the first reported fabrication of $Ge_{1-x}Sn_x$ nanowires in 2003,[21] the surge in popularity of $Ge_{1-x}Sn_x$ nanowires is a recent development. The first convincing report on the synthesis of $Ge_{1-x}Sn_x$ nanowires via bottom-up growth was by Barth *et al.*[84], and expanded upon by Seifner *et al.*,[22] detailing the fabrication of nanowires with $x = 0.125$ by a solution-based, microwave-assisted approach. These nanowires, grown using Sn as a growth catalyst had non-uniform diameters and an increasing Sn content along the lengths of the wires. A three-stage solution-liquid-solution (SLS) growth regime was proposed for the $Ge_{1-x}Sn_x$ nanowires synthesized (Figure 2), with the metallic Sn seed consumed as the reaction progressed. A mixture of pure Ge and heterometallic Sn–Ge imido cubane precursors was used for nucleating $Ge_{1-x}Sn_x$ nanowires with high tin content. Seifner *et al.*[85] expanded their study by pushing the limit of Sn incorporation in the nanowires grown via the microwave assisted method, achieving $Ge_{1-x}Sn_x$ nanowires with $x = 0.28$. These nanowires, grown with a modified microwave approach at 140 ºC, exploited a thermal treatment to induce further Sn incorporation into their as-grown $Ge_{1-x}Sn_x$ ($x = 0.17$) nanowires. The formation of a Ge-stabilized α-Sn intermediate was proposed for the growth of Sn rich $Ge_{1-x}Sn_x$ nanowires upon considering a "phase map" with the nanowire phases and compositions formed under specific experimental conditions. Although growth temperature and kinetics play an important role in obtaining a high Sn incorporation, impurity incorporation via a kinetic dependent "solute trapping" mechanism [86] was not considered for $Ge_{1-x}Sn_x$ nanowires with a high Sn inclusion due to the relatively low growth temperature and the absence of sharp metal-nanowire interface. The thermal stability of the $Ge_{1-x}Sn_x$ nanowires with and without the presence of the Sn seed was also investigated, revealing the diffusion of metallic Sn clusters through the $Ge_{1-x}Sn_x$ nanowires at high temperatures where the material composition was non-homogeneous. In the quest to achieve further control over the growth of $Ge_{1-x}Sn_x$ nanowires with colossal Sn incorporation, both in-

plane $Ge_{1-x}Sn_x$ (x=0.22) nanowires[87] and epitaxial vertical growth of $Ge_{1-x}Sn_x$ (x=0.19) nanowires[88] on Ge (111) substrates were successfully depicted. In-plane nanowires were also produced by an innovative solid-liquid-solid (SLS) growth process using SnO_2 as catalyst precursor and a-Ge:H as the Ge source, whereas vertical $Ge_{1-x}Sn_x$ nanowires were grown via a self-seeded VLS growth where Sn seeds acted as both nucleation promoter and a source of Sn in GeSn nanowires. Unlike other bottom-up grown $Ge_{1-x}Sn_x$ nanowires, in-plane nanowires grown on silicon substrates accommodate a large amount of compressive strain similar to $Ge_{1-x}Sn_x$.thin films.

We have reported the, CVD growth of $Ge_{1-x}Sn_x$ nanowires at a relatively high growth temperature (440 °C) with a high Sn content ($x > 0.09$) via conventional vapor-liquid-solid (VLS) growth using commercially available Ge and Sn precursors.[89] Using Au and $Au_{1-x}Ag_x$ metal catalysts and employing a post-growth step anneal at the bulk Ge-Sn eutectic temperature (~230 °C), $Ge_{0.91}Sn_{0.09}$ nanowires were fabricated. The non-equilibrium induction of Sn in the Ge host was explained by the "solute trapping"[86] of Sn atoms at a finite growth velocity in the emerging Ge nanowire lattice. Kinetic dependent incorporation of Sn in the nanowire lattice was aided by the negligible diffusion of Sn in Ge at the growth conditions employed, the epitaxial mismatch between Sn and Ge resulting in elastic strain and the lack of truncating side facets at the catalyst-particle interface.

The uniform and relatively ordered distribution of Sn impurities in a 1D alloy lattice during the VLS nanowire growth can be achieved via this kinetic driven "solute trapping" process, where the impurities are incorporated by solute redistribution at the catalyst-nanowire interface via an increase of chemical potential and deviation of the partition coefficient.[86] Growth kinetics

of semiconductor nanowires can be modified by influencing the concentration of the growth species, *e.g.* by using high temperatures to induce fast cracking of precursors or by using precursors with high catalytic decomposition rates. These parameters directly influence the supersaturation ($\Delta\mu$), *i.e.* the chemical potential difference in the vapor phase and liquid eutectic phase; allowing the growth rate of the nanowires to be manipulated. Increased supersaturation and hence the nanowire growth rate can also be achieved by lowering the equilibrium concentration (C_e) of growth species in the liquid seeds formed during VLS growth, with the use of bi-metallic growth catalysts such as AuAg alloys.[90] To attain a high Sn content in $Ge_{1-x}Sn_x$ nanowires in conventional single step VLS growth, the growth parameters were altered to increase the nanowire growth rate.[91] Faster growth kinetics, obtained with a particular set of growth constrains such as temperature, precursor type and catalyst type, resulted in the formation of $Ge_{1-x}Sn_x$ nanowires with a high Sn incorporation, i.e. ~9 at. % Sn (Figure 3). The incorporation of a substantial amount of Sn ($x > 0.09$) in Ge is desirable into the 1D Ge host lattice to achieve direct band gap. However, how these Sn impurities is ordered in Ge can provide an additional engineering of freedom and can influence physical properties of the alloy material. Ordering of Sn in Ge is associated with the engineering of electronic band structure such as reduction of band gap, degeneracy at the valence band and their emission characteristics of $Ge_{1-x}Sn_x$ nanowires such as emission width and lifetime. We observed that $Ge_{1-x}Sn_x$ grown in a single step CVD process displayed increased atomic ordering when compared to nanowires with a similar Sn content, grown by a two-step VLS process[89]; as determined by Raman, TEM and photoluminescence analysis. For a better understanding of the influence of "solute trapping" on Sn inclusion in the $Ge_{1-x}Sn_x$ nanowire, AuSn alloy catalysts with varying Sn content were directly utilized as growth promoters.[92] Similar to the observation shown in the Au catalyzed growth of $Ge_{1-x}Sn_x$ nanowires, high Sn concentration in the AuSn catalyst resulted larger Sn inclusion in the

crystallinity of the GeSn nanowire; up to 5 at.% with 86 at.% Sn in the catalyst. This observation suggests "solute trapping" as the mechanism for Sn incorporation in $Ge_{1-x}Sn_x$ nanowires as Ge supersaturation and step-flow kinetics is greatly enhanced by the presence of large content of Sn in the catalyst seed, resulting larger intake of Sn in the nanowire. Kinetic dependent Sn incorporation was also observed in this growth process, where a "dimer insertion model" was used to explain the high Sn incorporation. In this growth, the nucleation of Ge in GeSn is achieved via Ge pairs or dimers (Ge−Ge), and the incorporation of Sn atoms is realized via Ge−Sn dimers.

CVD parameters have also been tailored to grow branched $Ge_{1-x}Sn_x$ nanostructures, consisting of nanowire branches, with a Sn concentration of ~8.0 at.% epitaxially grown from nanowire branches, with a Sn concentration of ~4.4 at.%[93] These branched GeSn nanostructures could have potential uses in optoelectronic, nanoelectronic and energy storage applications, due to their unique morphology, high surface areas. The greatly enhanced numbers of junctions in the branched alloy nanostructures could also potentially act as semiconductor heterojunctions, where the bandgap between different segments could be controlled *via* manipulation of alloy composition in different segments. These novel heterostructures (Figure 4) were grown via a VLS process employing $Au_{0.80}Ag_{0.20}$ nanoparticles as catalyst seeds. Excess Sn on the sidewalls of the nanowire 'trunks' (diameter ~200 nm) subsequently catalyzed the secondary growth of 'branches' (diameter ~ 50 nm), ordered along the length of the trunks. These branch nanowire segments were ordered in the <111> direction along the nanowire trunks at an angle of ~ 70 º. The wetting of the nanowire 'trunks' by Sn, originating from the alloy formed between Sn with the $Au_{0.80}Ag_{0.20}$ nanoparticles seeds, were pinpointed as the primary source of Sn. The formation of these novel 3D $Ge_{1-x}Sn_x$ nanostructures, can potentially trigger different electron band transitions in a single structure.

The growth of Ge/$Ge_{1-x}Sn_x$ core/shell nanowires have also been reported since 2016[20,94–98] These $Ge_{1-x}Sn_x$ /Ge dual nanowire heterostructure can effectively release the compressive strain in $Ge_{1-x}Sn_x$, while introducing tensile strain in Ge simultaneously.[94] The nanowires typically comprise of a Sn-rich $Ge_{1-x}Sn_x$ shell surrounding a pure Ge nanowire or a $Ge_{1-x}Sn_x$ nanowire with low Sn content. Ge/$Ge_{1-x}Sn_x$ core/shell nanowires with Sn rich $Ge_{1-x}Sn_x$ shell often have increasing Sn content radially outwards from the Ge core. One noticeable difference between the growth of pure $Ge_{1-x}Sn_x$ nanowires to the growth of Ge/$Ge_{1-x}Sn_x$ core/shell nanowires is the choice of precursors. Traditional gas phase CVD reactions involving popular thin film precursors, *e.g.* GeH_4, $SnCl_4$ result in Ge/$Ge_{1-x}Sn_x$ core/shell nanowires whereas solution phase growth involving liquid phase precursors, *e.g.* diphenyl germane, tetraethyl tin leads to pure $Ge_{1-x}Sn_x$ nanowires. As per standard VLS growth, Au nanoparticle catalysts and germane (GeH_4) and tin(IV) chloride ($SnCl_4$) precursors were used for the growth of either phase pure Ge/$Ge_{1-x}Sn_x$ core shell nanowires (Figure 5)[94] or $Ge_{1-x}Sn_x$ nanowire with low Sn content (1 at.%) at the core and high Sn content (10 at.%) in the shell segment.[96] These core/shell nanowires usually display tapering near their tips and inverse tapering along the lengths of nanowires (Figure 5), with a majority of nanowires (60 %) growing in the <111> direction. The nanowires had 7 at. % Sn incorporated into the $Ge_{1-x}Sn_x$ shell, while the Ge core had a small amount of Sn incorporation (~ 1 at. %).[96] In another report on Ge/$Ge_{1-x}Sn_x$ core/shell nanowires, Assali *et al.*[95] utilized EDX measurements, correlated with atom probe tomography (APT) of the cross sectional areas of nanowires to determine the Sn distribution in the shell (Figure 6). Using a similar growth process to Meng *et al.*[94], with identical catalysts and precursor, Ge/$Ge_{1-x}Sn_x$ core/shell nanowires with 13 at. % Sn were produced. The EDX and APT analysis displayed a "sunburst-like" geometry of Sn rich areas in the $Ge_{1-x}Sn_x$ shells along the {112} side facets compared to the {110} facets. This Sn-rich region increased sharply from

the Ge core to 8 at. % in the shell (near the core-shell interface), which gradually increased to 13 at. % toward the outer edge of the shell. A linear profile of this change in Sn content can be seen in Figure 6(f). To achieve better control over the quality and yield of the GeSn core–shell nanowires, a better understanding of the nanowire growth mechanisms is critical. For this purpose, Wang *et al.* [99] systematically studied the radial growth of core–shell Ge/$Ge_{1-x}Sn_x$ nanowires, using a phase field model coupled with elasticity. The model successfully captured several important features such as sidewall facets and elastic energy distributions of the nanowires during its growth process and predicted the minimization of chemical potentials as the trigger for initiating the shell growth at given tin concentrations.

The critical strain for these core/shell nanowires with sunburst geometry was further explore by Albani *et al.*[20] on nanowires with 10.5 at.% Sn incorporation in the outmost region of the $Ge_{1-x}Sn_x$ shell. Increased Sn content in thick Ge layers has been reported to induce further strain relaxation. [20] A recent study on core–shell structure demonstrates the growth of epitaxial $Ge_{1-x}Sn_x$ active material on Ge nanowire core for additional band structure engineering and optical property manipulation in the Ge core nanowire due to strain from core–shell lattice mismatching.[98] Spatially resolved strain analysis, using 4D-STEM of Ge-core/$Ge_{0.96}Sn_{0.04}$-shell nanowires showed significant axial tensile strain in the Ge core (~0.56 %) and almost no strain in the $Ge_{0.96}Sn_{0.04}$ shell. The effect of strain on the growth of GeSn alloys in a Ge/GeSn core/shell nanowire geometry was also explored by controlling the Ge core diameter.[100] A regular and homogeneous $Ge_{1-x}Sn_x$ shell formation was observed for smaller core, whereas larger cores lead to the formation of multifaceted sidewalls and broadened segregation domains, inducing the nucleation of defects. Therefore, the growth of $Ge_{1-x}Sn_x$ alloys in a core/shell nanowire geometry is beneficial when the strain in the shell is kept below the threshold for plastic relaxation and hence when using thinner (50 nm) Ge cores.[100] In contrary,

a reverse $Ge_{1-x}Sn_x$/Ge core/shell structure with 30 at.% Sn in the core was successfully fabricated below the GeSn eutectic temperature via a plasma assisted solid-liquid-solid growth with Sn nanoparticle catalyst.[101] The presence of GeH_4 plasma resulted the deposition of crystalline Ge on the $Ge_{1-x}Sn_x$ to form a core−shell nanowire structure.

While all of the above $Ge_{1-x}Sn_x$ nanowire growth techniques make use of bottom-up growth regimes, it is important to note that $Ge_{1-x}Sn_x$ nanowires have also been fabricated by top-down methods.[102–106] The top-down fabrication of $Ge_{1-x}Sn_x$ nanowires typically involves the bottom-up growth of a $Ge_{1-x}Sn_x$ layer on a Ge buffer layer. The presence of this Ge buffer layer presents a unique opportunity to create $Ge_{1-x}Sn_x$/Ge nanowire heterostructures with a precisely controlled interface. This precise control is as of yet under-developed, however selective dry etching of Ge over $Ge_{1-x}Sn_x$ has been demonstrated by Gupta *et al.*[105] (Figure 7). Dry etching of the Ge buffer substrate was used to achieve a strain free, direct bandgap $Ge_{1-x}Sn_x$ layer (x = 0.08). A combination of wet and dry etching has also recently shown promise as a route to the top-down fabrication of $Ge_{1-x}Sn_x$ nanowires, however, the dry etch is significantly dependent on the Sn content of the $Ge_{1-x}Sn_x$ layer.[104] Hence, detailed calibration of this technique is required for future reproducible, tuneable $Ge_{1-x}Sn_x$ nanowire production.

3.2.2 $Ge_{1-x}Sn_x$ Nanoparticles & other nanocrystals

Nanocrystals of $Ge_{1-x}Sn_x$ have recently been investigated by several research groups, as these nanostructures can allow effective relaxation of lattice strain, potentially leading to a reduction in the amount of Sn needed to achieve a direct bandgap. Additionally, at small dimensions, quantum confinement effects can widen the material's bandgap into the visible solar region which is useful for implementation in solar cells, optical detectors and biosensors.[107–109] In this

regard, the growth of $Ge_{1-x}Sn_x$ nanocrystals has been reported using a number of synthetic techniques. A cost-effective solution based approach has recently gained more interest in the synthesis of $Ge_{1-x}Sn_x$ nanocrystals compared to traditional deposition based approach such as molecular beam epitaxy, CVD, sputtering etc., though the co-deposition (of Sn and Ge) method can result in epitaxial growth of $Ge_{1-x}Sn_x$ nanocrystals on desired substrates.[110] A solution based approached has been detailed by Ramasamy *et al.*[107] utilising a host of readily available precursors. They determined that a highly reactive Ge precursor and a relatively inert Sn precursor, which can form an in-situ complex that can be reduced to form $Ge_{1-x}Sn_x$ nanocrystals, is a prerequisite to synthesize non-trivial amounts of $Ge_{1-x}Sn_x$ nanocrystals. The resulting $Ge_{1-x}Sn_x$ nanocrystals formed were found to be quasi-spherical in shape, with mean diameters between 5 – 15 nm. Sn incorporation in these nanoparticles was much larger (x = 0.42) than has been reported for GeSn thin films or nanowires. This colossal Sn incorporation could be necessary in $Ge_{1-x}Sn_x$ nanocrystals to induce a direct bandgap, as quantum confinement effects may inhibit a crossover to direct-gap behavior. The tunability of the bandgaps in $Ge_{1-x}Sn_x$ nanoparticles has been explored by Esteves *et al.*[109], where $Ge_{1-x}Sn_x$ nanocrystals were fabricated by a solution-based process as illustrated in the scheme shown in Figure 8, with germanium diiodide and tin dichloride used as the Ge and Sn precursors respectively. By holding the mixture at a temperature of 300 °C for between 0 and 10 minutes, post growth, $Ge_{1-x}Sn_x$ nanocrystals of varying sizes were produced (4.1 – 4.6 nm for 0 minutes and 15 – 17 nm for 10 minutes). The resulting 15 – 17 nm $Ge_{1-x}Sn_x$ nanocrystals, $0.05 \leq x \leq 0.279$ were not shown to contain any metallic Sn clustering, despite their high Sn impurity. The smaller $Ge_{1-x}Sn_x$ nanocrystals, 4.1 – 4.6 nm were synthesized to explore confinement effects. These $Ge_{1-x}Sn_x$ nanocrystals, however, were not as Sn rich as their larger counterparts, with $x \leq 0.116$. While this Sn content was markedly lower than in the larger nanocrystals, it was nonetheless a substantial Sn inclusion compared to the bulkier GeSn alloy system.

The optical properties of $Ge_{1-x}Sn_x$ alloy quantum dots, with diameters between 1-12 nm and different levels of Sn incorporation, have been shown to exhibit tunable bandgaps between 0.72-2.16 eV.[111–114] A novel, low temperature (60-180 °C) colloidal method to prepare monodisperse $Ge_{1-x}Sn_x$ (x= 0.18) alloy nanoparticles, by reacting uniform Sn nanocrystals with a GeI_2-TOP (tri-n-octylphosphine) precursor solution under reducing conditions, has recently been reported.[114] The mean nanoparticle diameter and Sn content could be engineered in this approach by changing the dimension of the Sn nanoparticle template in the reaction process. The size effects on the optical properties of these $Ge_{1-x}Sn_x$ nanocrystals will be discussed later in this review article.

Apart from the solution phase method, alternative method using gas phase deposition and reaction for synthesising $Ge_{1-x}Sn_x$ nanocrystals has also been reported. Cho *et al.*[108] describe the use of gas-phase laser photolysis to produce $Ge_{1-x}Sn_x$ nanocrystals with $x = 0.05 – 0.4$. The $Ge_{1-x}Sn_x$ nanocrystals with a high Sn content ($x \geq 0.1$) were found to contain significant amounts of tetragonal phase metallic Sn. The $Ge_{1-x}Sn_x$ nanocrystals were produced by focussing a Nd:YAG pulsed laser into a reactor containing tetramethyl germanium and tetramethyl tin under vacuum. The presence of an increasing amount of metallic Sn was noted for the increasing Sn content, as determined by X-ray diffraction (XRD) measurements; the larger the value of x, the larger the observed β-phase Sn peak. These $Ge_{1-x}Sn_x$ nanocrystals with $x = 0.05$ were explored as anode materials for Li-ion batteries, which will be discussed later in the article. $Ge_{1-x}Sn_x$ nanocrystals (x = 0.09-0.22) with a mean diameter of 6 nm embedded in a SiO_2 matrix were also fabricated by thermal treatment of amorphous $Ge_{1-x}Sn_x/SiO_2$ layers.[115] The temperature range was however limited for growing high Sn content alloy nanocrystals in SiO_2 matrix. Segregation of β-Sn phase at temperature between 400-600

°C in the bulk alloy[116], depending on the Sn content and the strain in the alloy, can have consequence in diminishing the Sn concentration in the nanocrystals. Also, using a similar vapor phase deposition of Ge and Sn and further thermal treatment at the Ge-Sn eutectic temperature, high density $Ge_{1-x}Sn_x$ ($x > 0.10$) nanodots on Ge substrate were formed.[117] Interestingly, these nanodots; both in SiO_2 matrix and Ge substrate; had the shape of a hemispherical dome, which is quite different from that of nanodots formed by the usual Stranski–Krastanov (SK) mode epitaxy. One noticeable aspect of $Ge_{1-x}Sn_x$ nanoparticle growth is the achievement of very high Sn content (x=0.10-0.40) compared to GeSn films and nanowires. Usually, depending on the growth method, small or large nanoparticles facilitates larger amount of Sn in the Ge lattice. For example, high Sn incorporation was observed for large nanoparticles for GeSn nanoparticles produced via the formation of an initial Sn nanoparticle template and subsequent diffusion of Ge in them in solution phase.[114] An opposite trend was observed in Sn incorporation with nanoparticle size for the colloidal synthesized GeSn nanoparticles produced by in-situ reduction of Ge-Sn complexes.[107]

As with $Ge_{1-x}Sn_x$ nanowires, there are far fewer reports on the top-down fabrication-of $Ge_{1-x}Sn_x$ nanocrystals compared to bottom-up growth methods. Bartolomeo *et al.*[118] detailed the bottom-up growth of $Ge_{1-x}Sn_x$ nanocrystals on top-down patterned Si nanopillars.[119] These $Ge_{1-x}Sn_x$ nanocrystals, grown by MBE, were reported to have Sn contents roughly in line with the expected equilibrium solubility of 1 at. %, but this may be an overestimation due to the propensity of Sn to segregate into metallic Sn at the high growth temperature of 750 °C employed. Despite this low Sn incorporation, these $Ge_{1-x}Sn_x$ nanocrystals displayed field emission currents with good stability.

One important aspect to consider for in $Ge_{1-x}Sn_x$ nanostructure (and for thin films) is the accuracy of the compositional analysis, i.e. the stoichiometry, Sn impurity distribution etc., of this binary alloy nanomaterial as this influences the interpretation of the physical properties ,e.g. optical, electrical properties, of the nanostructure. Continued advancement of in $Ge_{1-x}Sn_x$ (or even SiGeSn) nanoscale materials and devices will depend critically on the knowledge of their atomic-scale structure because very small compositional fluctuations or relative ordering of impurities can alter the optical and electronic properties of these materials. For crystalline GeSn thin films, the compositions are usually measured using Rutherford backscattering (RBS), X-ray photoelectron spectroscopy (XPS) and X-ray diffraction (XRD).[9] The spatial resolution of secondary ion mass spectroscopy (SIMS) has also been sparsely used for compositional analysis of in $Ge_{1-x}Sn_x$ films. However, the nanowire/nanoparticle length-scales of interest are too small for accurate measurements using many of the techniques mentioned above. Transmission electron microscopy (TEM) and the elemental analysis, *e.g.* EDX, EELS, based on high resolution microscopy can estimate the qualitative and quantitative inclusion of Sn in nanostructures. XRD and Vegard's law is extensively used for the determination of Sn concentration in nanostructures along with SEM-EDX analysis. However, these measurements do not allow accurate qualitative analysis of Sn distribution in a Ge lattice at the nanoscale. For example, in an ideal random alloy a linear change in the lattice parameter with alloy composition, as predicted by Vegard's law, may not be obeyed for different crystal structures. Also changes in lattice parameters due to nanoscale dimensions also need to be account for when estimating Sn at. % from lattice parameter shifts due to alloying. Also, the very local distribution of Sn in the lattice (such as formation of Sn-Sn dimers) cannot be verified from bulk analysis techniques. The formation of local metallic Sn segments and Sn-Sn dimers could quench efficient emission from $Ge_{1-x}Sn_x$ nanomaterials due to the creation of dark trapping

sites for charge carriers. Thus, to confirm the sparse distribution of Sn in a very localized volume of a Ge lattice, the determination of the spatial arrangement of Sn through high resolution mappings, *e.g.* EELS is critical. However, the delocalized Sn EELS M-edge makes it very difficult to resolve Sn as part of a Ge-Sn dumb-bell, especially when the Sn atoms are buried deep inside the lattice. So the proximity effect of Sn atoms in the lattice may represent as Sn clusters in high resolution EELS mapping.[89] Also, the elemental mapping in TEM is limited for the volumetric mapping of low-concentration elements (such as Sn in $Ge_{1-x}Sn_x$) in nanostructures. For example, the Sn composition measured by EDS is significantly higher than that predicted by XRD in case of Ge/ $Ge_{1-x}Sn_x$ core shell nanowires[94], due to the incorporation of Sn rich phases in the nanowires that are not detected by XRD. The key factor to accurately estimate Sn in $Ge_{1-x}Sn_x$ binary nanostructure alloys is to use different complementary techniques such as microscopic, spectroscopic and diffraction techniques. Also, apart from the amount of Sn inclusion, the Sn impurity ordering in $Ge_{1-x}Sn_x$ nanowires has a profound effect on the quality of light emission obtained and on the directness of the band gap. Thus, the important challenge of incorporating Sn atoms into the "bulk" of Ge nanowires and nanocrystals while avoiding surface segregation and estimation of very localized distribution of Sn, *e.g.* ordering, with Ge "bulk" further emphasizes the need for localized and three-dimensional composition characterization in these nanostructures such as atom probe tomography (APT).[120]

4. PHYSICAL PROPERTIES OF $Ge_{1-x}Sn_x$ NANOMATERIALS

4.1. Optical properties of $Ge_{1-x}Sn_x$ Nanomaterials

Incorporating Sn into the Ge lattice has been predicted to show enhanced absorption in the near infrared region. There are many theoretical and experimental reports regarding the predicted

optical properties of $Ge_{1-x}Sn_x$ alloys with varying Sn content and strain incorporation.[34,44,45,121,122] In this review we will primarily focus on the optical properties of $Ge_{1-x}Sn_x$ nanocrystals highlighting the evolution of bandgap with Sn content in the nanostructures. The experimental verification of the nature of the bandgap, specifically indirect-to-direct crossover, in $Ge_{1-x}Sn_x$ alloys, for both bulk and thin films, has proven to be very difficult; with different techniques have been used to determine the nature of the bandgap in $Ge_{1-x}Sn_x$ alloys and its dependence on Sn composition. For MBE grown alloy films optical absorbance studies were used to determine the nature of the band gap in the alloy. These studies showed significant bowing in the compositional dependence of the direct band gap, with less pronounced bowing for the indirect band gap[37] However, optical absorbance spectroscopy is limited in terms of accurate determination of the indirect gap in $Ge_{1-x}Sn_x$ alloys due to weak indirect signals compared to the direct gap, the proximity of indirect and direct band gap for $Ge_{1-x}Sn_x$ alloys and alloy broadening.

Photoluminescence (PL) is the most common method used for determining the band structure of $Ge_{1-x}Sn_x$ alloys, for both bulk and nanoscale $Ge_{1-x}Sn_x$ alloys. PL allows the observation of distinct direct and indirect peaks, especially for thin films and materials below a micron in size, making PL a superior alternative to absorption measurements for band gap determination. PL studies are useful in resolving the size of a bandgap, transitions from indirect to direct states, as well as defining if band-to-band transitions are direct, indirect or mixed.[13,74] The linewidths and shape of PL spectra, as well as peak position, give invaluable insight into the nature of electronic transitions. Accurate PL line[35] shape and width analysis is critical, especially for the indirect-to-direct gap crossover determination as small changes in the slope of either gap can affect the predicted crossover value. Extrapolating room temperature PL data for $Ge_{1-x}Sn_x$ alloys ($x \leq 0.06$), a crossover at $x = 0.073$ is predicted for CVD grown $Ge_{1-x}Sn_x$ alloys.[35] In

notable work by Gallagher *et al*., who obtained direct and indirect bands gap for $Ge_{1-x}Sn_x$ thin films at room temperature from PL data. Using a band gap bowing model, by assuming composition-dependent band gap bowing, they were able to obtain a Sn crossover concentration (from indirect to direct transition) of 13 at.% was obtained for $Ge_{1-x}Sn_x$ (x exceeding 0.10) alloys.[36] As any compositional dependence of bowing parameters can change the predicted crossover composition in a significant way, assuming a constant bowing parameters resulted in much lower crossover point (x = 0.073) for GeSn alloys with sa mall compositional range ($x \leq 0.06$).[35]

Temperature dependent PL studies have also proved to be critical to determine the nature of band transitions in $Ge_{1-x}Sn_x$ alloys. There is a distinct change in the relationship between the PL intensity and temperature in changing from an indirect to direct bandgap material. A direct bandgap alloy results in an inverse relationship between temperature and intensity, with increasing temperature leading to a decrease in the PL intensity.[14,74,89,91] This is attributed to a reduced transfer of electrons from the Γ to L valleys by thermal activation.[123] Thus, the increase in the intensity of the PL peak with decreasing temperature for direct bandgap $Ge_{1-x}Sn_x$ is attributed to the higher population of the Γ valley. A monotonical decrease in the PL intensity with increasing temperature, which is typical behavior seen in direct bandgap semiconductors,[6,74,89,124,125] can therefore be used to confirm a direct bandgap transition for $Ge_{1-x}Sn_x$. However, it has been suggested that due to the pivotal role of dislocations on the recombination dynamics, the steady-state temperature dependent PL measurements need to be complemented by direct measurements of the carrier lifetime in order to precisely resolve the directness of the electronic band structure.[125]

Due to the gradual transition of $Ge_{1-x}Sn_x$ alloys from an indirect to a direct bandgap, a certain degree of band mixing can also be observed for $Ge_{1-x}Sn_x$ alloys through PL studies. Unusually, broad PL line-widths for $Ge_{1-x}Sn_x$ alloys can sometimes be observed, which can be attributed to band mixing participation from both direct and indirect transitions resulting in an overlap of their PL peaks, as the indirect transition is shifted to lower energies.[14] Recent pressure-dependent optical characterization of $Ge_{1-x}Sn_x$ photodiodes[42] has provided the first significant evidence of the hybridized nature of the $Ge_{1-x}Sn_x$ alloy band gap by demonstrating that the band gap pressure coefficient evolves continuously between that of the indirect towards that associated with the direct band gap (for Sn ~ 10 at.%). The determination of the activation energy for non-radiative transitions from low temperature PL is also possible, with typical values for the activation energy of $Ge_{1-x}Sn_x$ dependent on both x, and the relative atomistic order.[91] PL studies have also been employed to investigate the difference in bandgap energies between doped and undoped $Ge_{1-x}Sn_x$.[13] Doped $Ge_{1-x}Sn_x$ demonstrates a band transition with a decreased energy separation compared to undoped $Ge_{1-x}Sn_x$ with the same Sn incorporation, for both direct and indirect samples.

Spectroscopic ellipsometry is another technique that has been used to characterize the interband transition and compositional dependence of band gap, refractive index, extinction coefficients and the dielectric properties of $Ge_{1-x}Sn_x$ thin films (or substrates densely covered in nanostructures).[3,28,51,126] The technique can be employed for both crystalline and amorphous materials and can be used to examine any difference in the optical properties upon crystallization of the material. For example, Lieten *et al.* [127] used spectroscopic ellipsometry to explore the differences in refractive index and extinction coefficient for amorphous and crystalline $Ge_{1-x}Sn_x$ thin films (x = 0.045). Ellipsometric studies of the near-band gap optical properties in $Ge_{1-x}Sn_x$ alloys (x = 0.02) showed that excitonic effects to play a strong role in

enhancing the near-band gap absorption.[128] A clear monotonical shift in the absorption edges, corresponding to the interband transitions at the direct gap with increased Sn concentration reaching 8 μm for $x \sim 0.3$, was observed for $Ge_{1-x}Sn_x$ alloys grown directly on Si.[129]

4.1.1. Optical properties of $Ge_{1-x}Sn_x$ Nanowires. A Recent flurry of activities on $Ge_{1-x}Sn_x$ nanomaterials, such as nanowires have triggered research activities on their physical properties, especially their optical properties. In the optical measurements of nanomaterials, such as nanowires, light with wavelengths longer than the diameter of the nanowires, but shorter than their lengths are typically employed. The probing light used in optical measurement is difficult to be confined within a single nanowire or nanoparticles due to its small dimension. Thus, the effect of the surrounding such as the substrate material, grain boundaries etc. can prominently influence the measurement of optical properties. In PL measurements, the effect of the substrate can be negated by the use of non-light emitting substrates, or if the substrate does not absorbs light in the frequency range of the probing light. However, for the measurement of reflection and transmission, even though the substrate does not absorb light, the measurement data can be impacted. Also, due to the scattering from grain boundaries present in the nanostructures, mean free path decreases and the free electron absorption and interband absorption of light is modified by the by grain boundary scattering, thus affecting the optical absorption. Surface quality is also an important issue to consider for $Ge_{1-x}Sn_x$ nanowires. For example, pure Ge nanowires with a native oxide coating do not exhibit indirect-gap PL due to surface recombination, while core-shell Ge/SiGe nanowires exhibit both direct and indirect-gap emission because confinement in the Ge core effectively separates photogenerated carriers from surface defects.[130] It is not known whether similar effects occur for $Ge_{1-x}Sn_x$ nanowires or nanoparticles functionalized with different organic ligands. Another factor which could influence the PL and the intensity of the PL emission from $Ge_{1-x}Sn_x$ nanowires is the usual

presence of metallic growth promoters, *e.g.* Sn and Au. The presence of these metallic components in the nanowires, usually at their tips, could result in low emission intensity due to luminescence quenching from the metallic impurities. Also, the high surface-to-volume ratio of nanowires compared to thin films can account for the lower luminescence intensity.

In the case of pure $Ge_{1-x}Sn_x$ nanowires, low-temperature PL (7 -300 K) and power-dependent PL measurements have been used to determine the energy gap, nature of the bandgap and quality of light emission from nanowires with a Sn content between 6 to 9 at.% [64,91]. The bandgap of the nanowires (diameter ≈ 50 nm) was tuned between 0.6-0.7 eV at 77 K depending on the amount of Sn inclusion in the alloy. The nature of the bandgap in the $Ge_{1-x}Sn_x$ nanowires changed significantly, from near direct to direct, with an increasing amount of Sn in the alloy from 7.4 to 9.1 at.%. This is contrary to the recent theoretical calculation[50] of band structure which depicted much higher concentration of Sn (x = 0.14) to achieve a direct band gap for $Ge_{1-x}Sn_x$ NWs of diameter 12 nm and 24 nm. However, it has been stated that the direct-band-gap of $Ge_{1-x}Sn_x$ nanowires can be easily obtained with a lower Sn concentration for large diameter nanowires. This transition from an indirect to a direct bandgap was deemed as gradual rather than abrupt, due to a degree of band overlap resulting from the narrow energy difference between the direct and indirect bands. With increasing excitation (up to 16 P_0) spectral broadening was also observed, coupled with a blue-shift of the PL peak position for the alloy nanowires at 9 at.% Sn incorporation. This shift was not observed for phase pure Ge nanowires and was attributed to carrier filling of closely spaced Γ and L energy bands. A significant recent development was the ability to achieve mid-infrared emission (0.3 eV) at room temperature from epitaxial $Ge_{1-x}Sn_x$ (x = 0.19) nanowires grown on Ge (111) substrates.[131] The position of the maximum in the direct energy emission and other

characteristics, such as activation energy from the $Ge_{1-x}Sn_x$ (x = 0.19) nanowires matched well with the reported emission from alloy thin films of similar composition where an emission peak was observed at 0.36 eV for x = 0.179.[132] Also, a significant increase in the activation energy from 16 to 37 meV for the non-radiative process was observed for $Ge_{1-x}Sn_x$ (x = 0.19)[91] compared to $Ge_{1-x}Sn_x$ (x = 0.09) nanowires[88], implying prominent direct bandgap recombination in the nanowires at large Sn concentrations. Although the steady state PL measurements gave an indication as to the nature of the band gap for the $Ge_{1-x}Sn_x$ nanowires in this study, direct measurements of the carrier lifetime are required in order to precisely resolve the directness of the electronic band structure.

The optical properties of $Ge_{1-x}Sn_x$ alloys can be enhanced further by shaping them in nanoscale heterostructured forms, such as core-shell nanowires. Core-shell nanowire structures, *e.g.* $Ge/Ge_{1-x}Sn_x$, provides confinement of two-dimensional electron gases at the semiconductor heterojunction interface which can enhance carrier recombination. Core/shell $Ge/Ge_{1-x}Sn_x$ nanowires can also incorporate strain from epitaxial mismatch to achieve a direct bandgap in these heterostructure materials. The nature of the band gap and the band gap energy in arrays of $Ge/Ge_{1-x}Sn_x$ nanowires were determined mainly by absorption and PL measurements. Some of these core/shell nanowires demonstrated very high absorption of light, close to 100 %, which was assigned to the tapered nanowire geometry and the direct bandgap of $Ge_{1-x}Sn_x$ (x = 0.13) shell.[95] The temperature dependent PL study confirmed the nature of the bandgap as direct, where the lowest Γ-minimum was far enough below the L-minimum to prevent intervalley tunneling. Core-shell nanowires showed slightly higher emission energy (0.465 eV) at room temperature compared to state-of-the-art bulk $Ge_{1-x}Sn_x$ with similar Sn contents, due to the residual compressive strain in the $Ge_{1-x}Sn_x$ shell. Possibly, this compressive strain also increases the amount of Sn required, from 9 to 10.5 at.%, to obtain a direct band gap in the

core-shell nanowires compared to strain free $Ge_{1-x}Sn_x$ nanowires.[91,95] Infrared reflectance and transmittance measurements of core/shell $Ge/Ge_{0.96}Sn_{0.04}$ nanowires indicated that fewer long wavelength photons were reflected and transmitted for these core-shell structures, thus showing an increased absorption even for core-shell nanowires with lower Sn incorporation (4 at. %).[98] The lattice coherency strain at the $Ge/Ge_{0.96}Sn_{0.04}$ interface changes the band structure of the Ge by decreasing the Γ valley transition energy, making a direct gap transition more favorable (Figure 9). In this $Ge/Ge_{0.96}Sn_{0.04}$ system strain improves the optical properties of the Ge core, which when photoexcited, provides carriers that enhance light emission from the $Ge_{0.96}Sn_{0.04}$ shell. Core-shell $Ge_{1-x}Sn_x$ alloy nanowires have also demonstrated a strong PL signal at room temperature compared to Ge nanowires,[94] indicating that radiative recombination of photogenerated carriers in the Ge core is strongly enhanced, similar to Ge/SiGe nanowires[130], in the core-shell wires compared to Ge nanowires coated with native oxide. Placing the Ge nanowire cores in the $Ge/Ge_{1-x}Sn_x$ nanowires under tension enhances their PL by decreasing the energy of the Γ-valley relative to the L-valley. At the same time, significantly enhanced PL intensity is observed in the largely unstrained shells compared to the tensile-strained Ge cores, indicating the promise of $Ge_{1-x}Sn_x$ nanowires for photonic applications. In addition, the effect of strain and Sn segregation in the optical emission of the $Ge_{1-x}Sn_x$ shell for Ge/ $Ge_{1-x}Sn_x$ core/shell nanowires of different Ge core thickness was also determined with low-temperature PL study.[133] Temperature dependent PL measurements showed a quenching of the emission above 100 K for thicker core, while in the thinner core band-to-band recombination was observed at room temperature. All these findings clearly show that minimizing strain and segregation in the $Ge/Ge_{1-x}Sn_x$ core-shell system is of paramount importance to preserve the high optical quality of these nanowires.

4.1.2. Optical properties of $Ge_{1-x}Sn_x$ Nanoparticles. Introducing Sn into Ge nanocrystals to form $Ge_{1-x}Sn_x$ alloy nanoparticles is a feasible way to obtain a tunable bandgap material in the near-infrared region. The incorporation of Sn significantly reduces the energy gaps (0.35–0.80 eV for x = 15.0–0.00 at.%) and promotes the metallic character of the direct-gap $Ge_{1-x}Sn_x$ alloys, eliminating any potential application in visible to near-IR optoelectronics. To promote direct-gap behavior in $Ge_{1-x}Sn_x$ alloys and expand the optical range, quantum confinement effects were utilized by producing low-dimensional nanostructured $Ge_{1-x}Sn_x$ alloys. In this regard, nanoparticles or quantum dots have been reported both in strongly-confined and weakly-confined size regimes that promote wider direct energy gaps from the visible to near-IR spectrum.[109,113,134,135]

Solid-state diffuse reflectance NIR spectroscopy, in conjunction with the Kubelka-Munk (KM) remission function (to obtain pseudo-absorption from reflectance) to determine bandgaps from reflectance data, has been carried out on $Ge_{1-x}Sn_x$ nanocrystals of varying Sn content and sizes ($0.00 \leq x \leq 0.116$ and 3.4 – 4.6 nm respectively) by Esteves *et al.*[109] This investigation provided a deeper understanding of the impact of confinement effects on $Ge_{1-x}Sn_x$ (Figure 10).[109] The bandgaps obtained from KM analysis were indicative of the strong effect of quantum confinement in $Ge_{1-x}Sn_x$ nanocrystals; an energy gap of 0.95 eV was observed for $Ge_{1-x}Sn_x$ nanocrystals (x = 0.116) which was a 0.15 eV increase when compared to the fundamental direct bandgap of bulk Ge (0.80 eV). This blue shift towards higher energies was expected upon dramatically decreasing the size of the nanostructure. The same research group have also successfully produced ultra-small (≈2 nm) $Ge_{1-x}Sn_x$ quantum dots with a Sn content up to 23 at.%, from which they have obtained tunable visible (orange-red) emission.[112] PL spectra from nanoparticles of different Sn concentration indicated both strong confinement effects and a redshift in emission energy with increasing the Sn content. A clear redshift for $Ge_{1-x}Sn_x$ quantum dots of x

= 0.018 to 0.236 was observed with the PL maximum shifting from 620 to 720 nm. In such, they have successfully expanded the optical window of $Ge_{1-x}Sn_x$ alloys into the visible spectrum allowing for applications in bio-imaging and chemical sensing. A large direct bandgap of 0.8 eV, compared to bulk GeSn of similar composition, was also observed via room temperature PL measurements for $Ge_{0.864}Sn_{0.136}$ quantum dots embedded in a GeSn matrix due to quantum confinement effects.[136] The room temperature PL at 1.55 μm (0.8 eV) fell in the range of optical communication wavelengths, and consolidates its potential applications in near infrared optoelectronics. In general, the larger $Ge_{1-x}Sn_x$ alloy nanoparticles (15-23 nm) exhibited minimum or no confinement effects and absorption energy gaps (0.2–0.4 eV) that were red-shifted from bulk Ge. [109] This is similar to those reported for bulk $Ge_{1-x}Sn_x$ thin film alloys and $Ge_{1-x}Sn_x$ nanowires. In contrast, smaller $Ge_{1-x}Sn_x$ alloy quantum dots (~2–5 nm) showed strong confinement effects with composition-tunable absorption onsets in the near infra-red region and visible PL exclusively for ultra-small quantum dots (1.8–2.2 nm).[113,135,137] Figure 11 compares the bandgap of nanoparticles and nanowires with bulk $Ge_{1-x}Sn_x$for similar Sn incorporation, derived from the room temperature PL measurements.

Esteves *et al.*[137] also reported tunable visible luminescence in $Ge_{1-x}Sn_x$ (x = 0.055-0.236) quantum dots of similar diameters (~2 nm). Using time-resolved PL spectroscopy the authors revealed slowly decaying emission (3-27 μs) which they assigned to the recombination of spin-forbidden dark excitons and the recombination of carriers trapped at surface states. Increasing the Sn concentration and temperature resulted in faster PL decay kinetics due to thermal activation of spin-allowed bright excitons and carrier detrapping from surface states. Time-resolved PL spectroscopy also revealed similar microsecond and nanosecond timescale decays at 15 and 295 K, respectively, for $Ge_{1-x}Sn_x$ alloy quantum dots with a narrow size dispersity (3.3 ± 0.5–5.9 ± 0.8 nm) and up to 20.5 at.% Sn composition.[113] This decay was assigned to the radiative

recombination of dark and bright excitons as well as the interplay of surface traps and core electronic states. In this case, the quantum confinement effects resulted in tunable energy gaps in the near-IR region that were significantly blue-shifted compared to bulk with absorption onsets at 1.72-0.84 eV for $x = 0.015$-0.20 and PL peaks at 1.62-1.31 eV, for $x = 0.015$-0.056 for the $Ge_{1-x}Sn_x$ alloys (Figure 12). Comparing with pure Ge quantum dots where the dark versus bright exciton transitions are very distinct, the addition of Sn in Ge introduces mixing of excitonic states, smearing the dark-bright exciton distinction and bright/dark excitons oscillator strength ratio decreases to a few hundred.[128,134] Excitonic effects have been shown to play a strong role in enhancing the near-band gap absorption for both $Ge_{1-x}Sn_x$ quantum dots and thin films[134], although in quantum dots the effective dielectric screening might be reduced to enhance excitonic effects.

4.2. Electrical properties of $Ge_{1-x}Sn_x$ Nanomaterials

The incorporation of Sn into a Ge lattice results in changes in the electrical properties of the material. Theoretical studies of the electrical properties of $Ge_{1-x}Sn_x$ show some similar or enhanced values of electron mobilities and concentrations compared with doped Ge counterparts.[51] Reported high hole mobilities in $Ge_{1-x}Sn_x$ thin films ($x = 0.02$), in the order of $> 10^{18}$ cm^{-3}, make this alloy a promising candidate as a channel material for MOSFET devices.[51] However, despite the extensive studies and the continuous improvement of $Ge_{1-x}Sn_x$ as a material there are only few reports on the electronic properties of $Ge_{1-x}Sn_x$ nanostructures. In the context of a bottom-up growth approach, there are limited reports on the implementation of the bottom-up grown nanowires in FET-like devices. Only recently, $Ge_{0.81}Sn_{0.19}$ nanowires were shown to have higher conductivity compared to pure Ge nanowires by fabricating simple two and four terminal devices from an individual nanowire. In contrast, top-down fabricated nanostructures, based on the etching and doping of thin films, a few reports are present in the literature that show promising features of $Ge_{1-x}Sn_x$ fin-like structures as FET devices.[138,139] In

one of the first reports of nanoscale $Ge_{1-x}Sn_x$ FET devices, by forming nanostructures from the passivated $Ge_{1-x}Sn_x$ films, Lei *et al.* successfully produced the world's first $Ge_{1-x}Sn_x$ p-FinFET on $Ge_{1-x}Sn_x$-on-insulator (GSOI), with channel lengths down to 50 nm and fin widths down to 20 nm. In comparison with other reported $Ge_{1-x}Sn_x$ p-FETs, a low subthreshold slope (SS) of 79 mV/decade at V_{DS} = -0.5 V was achieved[139,140].

GeSn nanowire-MOSFET devices can borrow considerably from the thin film devices in terms of surface passivation. High-mobility was observed in strained $Ge_{0.958}Sn_{0.042}$ p-channel MOSFETs with ammonium sulphide surface passivation.[141] A ~10 nm thick fully-strained single crystalline $Ge_{1-x}Sn_x$ layer was epitaxially grown on Ge (100) as the channel layer. Ammonium sulfide surface passivation was performed for the $Ge_{1-x}Sn_x$ surface, followed by gate stack formation. This $Ge_{0.958}Sn_{0.042}$ devices had a peak effective mobility of 509 cm^2/Vs.[141] Lei *et al.* [142] also assessed the impact of sulfur passivation on the gate stack quality in $Ge_{1-x}Sn_x$ devices. At a high inversion carrier density (N_{inv} of 1×10^{13} cm^{-2}), sulfur passivation increased the effective mobility by 25 % in $Ge_{0.83}Sn_{0.17}$ p-MOSFETs.[142] In another passivation technique, O_2 plasma treatments were used on solid phase epitaxially grown $Ge_{1-x}Sn_x$ films to assess the effectiveness for passivating GeSn n-MOSFETs[143](Figure 13). The O_2 plasma treatment formed a $Ge_{1-x}Sn_xO_n$ film on the surface of the alloy which was subsequently covered in-situ by Al_2O_3 for the gate stack in the $Ge_{1-x}Sn_x$ MOS devices. The benefit of the surface passivation was evidenced by the low interface trap density of 1.62×10^{11} $cm^{-2}eV^{-1}$ obtained, resulting in $Ge_{1-x}Sn_x$ N-MOSFETs with a peak electron mobility of 518 cm^2/Vs[143].

Another critical aspect for consideration in the formation of $Ge_{1-x}Sn_x$ nanowire FET devices is the choice of source-drain contact metals. In this regard, recent knowledge on the GeSn thin

film devices can be helpful for the successful fabrication of efficient GeSn nanowire transistors. High-k gate stacks and NiGeSn source and drain metallic contacts have been characterized for $Ge_{1-x}Sn_x$ alloys over a Sn content range between 0 - 14.5 at. % in n-FETs devices.[5] Wirths *et al.*[144] also investigated Ni(SiGeSn) metal contact formation for Sn compositions from 6 to 9 at.% and quaternary NiSiGeSn alloys, formed on SiGeSn ternaries with large Si/Sn compositions ratios.

$Ge_{1-x}Sn_x$ is also promising material for TFET devices. Han *et al.* [145] fabricated $Ge_{1-x}Sn_x$ quantum well (QW) p-type tunnel-FETs (TFETs) and pMOSFETs on Si(111) substrates. These devices demonstrated a high effective hole mobility of 505 cm^2/Vs, related to the high crystallinity of the $Ge_{1-x}Sn_x$ material produced. They also reported these QW pTFETs on Si(111) outperformed devices produced on Si(001) substrates, both in term of their subthreshold swing (SS) and ON-state current. By characterizing vertical Ge and GeSn heterojunction TFETs, Schulze *et al.*[146] observed that by incorporating a $Ge_{1-x}Sn_x$ layer only at the source/channel junction and limiting the transistor size was a promising strategy to increase the on-current in TFETs; a high on-current of I_{ON} = 88.4 μA/μm at $V_{DS} = V_G = -2$ V was obtained for a GeSn-TFET. Cong *et al.*[147] fabricated a multilayer graphene and $Ge_{1-x}Sn_x$/Ge QW heterostructure as a Si-based light source. Specially designed $Ge_{0.9}Sn_{0.1}$/Ge QWs were used as the active layer, which achieved a PL peak at 2050 nm. Huang *et al.*[138] also fabricated compressively strained $Ge_{1-x}Sn_x$ QW channels sandwiched by Ge sacrificial layers grown using CVD. The stacked $Ge_{0.93}Sn_{0.07}$ -channel p-gate-all-around FET had a record high I_{ON} current of 1975 μA/μm at −1 V for a $Ge_{1-x}Sn_x$ pFETs. Although the electrical properties of $Ge_{1-x}Sn_x$ thin films have been experimentally well explored, in-depth studies on the electrical property on bottom-up fabricated $Ge_{1-x}Sn_x$ nanostructures, such as nanowires, is very limited. Semiconductor nanowires are particularly attractive for TFET research, as they allow for

heteroepitaxy of lattice mismatched materials. Nanowire-TFETs are predicted to provide improved device performance over their planar counterparts as nanowire devices have a circular geometry and a confined-volume body and a gate that wraps around the nanowire, potentially providing excellent electrostatic control over the channel. This improved channel control is expected to both reduce the SS value and improve the on-current of nanowire-TFETs. Moreover, confinement effects such as the volume inversion of carriers and the reduction of transverse momentum conservation requirements may further enhance tunnelling probabilities in nanowire systems.

As a side note, the mechanical properties of $Ge_{1-x}Sn_x$ nanowires (x = 7.1–9.7 at.%) were reported recently to assess their suitability as nanoelectromechanical (NEM) switches.[148] Young's moduli of 61 ± 24 GPa and 59 ± 30 GPa were obtained by resonance and bending methods respectively for $Ge_{1-x}Sn_x$ nanowires with diameters >30 nm. As expected, these values were lower than experimentally obtained Young's moduli values obtained for Ge nanowires with similar diameters by resonance ((106 ± 19 GPa[149] and bending (112 ± 43 GPa[150] experiments, but close to the theoretical value of 82 GPa calculated for GeSn.[151] Significantly, the bending stresses measured at the fracture point for the nanowires was 8-12 % of the theoretical limit, making them promising future materials for NEMs devices.

5. APPLICATIONS OF $Ge_{1-x}Sn_x$ ALLOYS including NANOMATERIALS

With the unique, and often remarkable qualities that $Ge_{1-x}Sn_x$ alloys possess, their integration into many varied devices is possible. The direct bandgap alloy is beneficial for implementation in optoelectronic and photonic devices such as lasers and photodetectors;[6,7,152–154] and the high carrier mobility of $Ge_{1-x}Sn_x$ over Ge or Si is beneficial for integration into electronic devices

such as FET and TFETs.[10,155,156] Additionally, the integration of different functional materials in the alloy and high carrier mobility characteristics of $Ge_{1-x}Sn_x$ nanostructures discussed in the previous sections makes them a probable candidate for energy storage applications. As the application of $Ge_{1-x}Sn_x$ nanostructures including nanowire devices is still in its infancy, we have tried to summarize few recent initiatives on applying $Ge_{1-x}Sn_x$ alloys; including thin films and bulk; in electronic, optoelectronic and photonic devices.

5.1 $Ge_{1-x}Sn_x$ in electronic devices

A multitude of semiconductor applications for $Ge_{1-x}Sn_x$ materials have recently been reported. For example, negative-capacitance FETs (NC-FETs) for steep slope switches have been studied by Zhou *et al.* [157], who explored the negative differential resistance and hysteresis reduction in planar Ge pFETs[158,159] using a $HfZrO_x$ gate stack. The same group produced a highly impressive $Ge_{1-x}Sn_x$ (4 at.% Sn) based ferroelectric NC-FET with a sub-20 mV/dec subthreshold slope. The stack in this case was comprised of a metal-ferroelectric-metal-insulator[157]. Liu *et al.* [160] designed a heterojunction-enhanced n-channel tunnelling field-effect-transistor with a $Ge_{1-x}Sn_x/Ge_{1-y}Sn_y$ ($x > y$) heterojunction located in the channel region. At a supply voltage of 0.3 V, a >300 % ON-state current enhancement was demonstrated in a $Ge_{0.92}Sn_{0.08}/Ge_{0.94}Sn_{0.06}$ FET, compared to a $Ge_{0.92}Sn_{0.08}$ homogeneous structured FET, due to a steeper average subthreshold slope[160]. High-performance $Ge_{1-x}Sn_x$ metal-semiconductor-metal photodetectors and $Ge_{1-x}Sn_x$ pFinFETs on an advanced $Ge_{1-x}Sn_x$-on-insulator platform was also demonstrated. The detection range of the $Ge_{1-x}Sn_x$ photodetector was beyond 2 μm, with responsivities of 0.39 and 0.10 A/W at 1550 nm and 2003 nm, respectively. $Ge_{1-x}Sn_x$ pFinFETs with fin width scaled down to 15 nm were also fabricated on GSOI platforms, exhibiting a small SS of 93 mV/decade and a high drive current of 176 μA/μm[161]. Other examples of impressive process module development have included the work by Buca *et al.* [162] who recently studied gate stack and Ni(SiGeSn) metal contact formation on low bandgap

strained (Si)Ge(Sn) semiconductors. Quintero *et al.*[163] also studied the stanogermanide system, involving Ni-$Ge_{1-x}Sn_x$ based materials. They evaluated the impact of the addition of 10 at. % of Pt in Ni thin films. At an alloy formation temperature of 360 °C, a stable $(Ni_{1-y}Pt_y)(Ge_{1-x}Sn_x)$ phase was obtained. For further reading on the electronic properties and application of GeSn materials Gupta *et al.*[164] presented a comprehensive overview of the state of the art in Ge and $Ge_{1-x}Sn_x$ transistor research in their 2014 review article. Key material challenges involved in fabrication, such as gate stack formation and achieving low-resistance contacts to transistor source/drain regions were reviewed.

5.2. $Ge_{1-x}Sn_x$ in optoelectronic devices

The tunability of the bandgap in $Ge_{1-x}Sn_x$, and its compatibility with Si platforms, allows for the facile implementation of $Ge_{1-x}Sn_x$ nanomaterials into optoelectronic devices. Photoresponse and photoconductivity measurements are imperative to determine the optoelectronic properties of $Ge_{1-x}Sn_x$. Unsurprisingly, the addition of Sn results in the photoresponse of $Ge_{1-x}Sn_x$ alloys to shift to lower energies (longer wavelengths) than their pure Ge counterparts.[77,165,166] The direct bandgap of Ge is approximately 0.8 eV, indicating that Ge film photodetectors have low responsivities as wavelengths exceed 1550 nm, whereas $Ge_{1-x}Sn_x$ photodetectors have a broad detection spectrum (extending to 1800 nm) covering the entire telecommunication range. Naturally, this can be predicted as the lower energies are expected due to the reducing energy of the Γ valley. Due to the presence of band mixing, $Ge_{1-x}Sn_x$ alloys also have a broad spectral response, across all telecommunications bands.[57,167,168] A strong spectral response has been observed for $Ge_{1-x}Sn_x$ thin films ($0.045 < x < 0.052$) compared to pure Ge thin films, or indeed, for samples with $x > 0.052$ which showed similar magnitudes at 1550 nm[169]. This consistency of responsivity of $Ge_{1-x}Sn_x$ devices with increasing x indicates that a photodetector comprised of $Ge_{1-x}Sn_x$ will be of equal, or greater, quality than a Ge

photodetector. Hart *et al.*[169] reported that their $Ge_{1-x}Sn_x$ layer (x = 0.113) displayed a dark conductivity three times higher than their Ge reference. In fact, it was noted that at room temperature, the dark conductance increased with increasing Sn content. The induction of Sn is also expected to result in increased carrier mobilities for both Ge and Si[1,170] and increased photoresponsivity in $Ge_{1-x}Sn_x$ photodetectors, compared to Ge has been reported[12,57,77,171 6,14,74,85,89,91] All of these aspects potential enable the co-integration of infrared optoelectronics and nanoelctronic platforms based solely on group IV materials.

The use of $Ge_{1-x}Sn_x$ thin films in photodetectors[77,153,165,172,173] and photodiodes[152] has become increasingly popular during recent years. The use of $Ge_{1-x}Sn_x$ detectors has escalated in last few years due to: (i) broad operation wavelength coverage (1.55 to 12 μm) with varying Sn compositions, (ii) direct bandgap allowing for enhanced band-to-band light absorption and (iii) a full compatibility with Si micro/nanoelectronics.[174] $Ge_{1-x}Sn_x$ thin films are expected to have increased photoconductivity and a broader photoresponse than their pure Ge counterparts,[122] and have been predicted to exhibit greater carrier mobilities.[51,170] $Ge_{1-x}Sn_x$ p-i-n photodetectors have been demonstrated using $Ge_{1-x}Sn_x$ thin films with varying Sn amounts, exhibiting a shift to lower energies with Sn addition, as well as increased dark conductivity.[152,154,165,167,173] Essentially, GeSn p-i-n photodetectors can be fabricated by doping different segments of the same $Ge_{1-x}Sn_x$ structure, *i.e.* a homo-structure, or by fabricating a heterostructure comprised of a $Ge_{1-x}Sn_x$ intrinsic layer (or the intrinsic layer and one of the doped layer) and epitaxial materials, such as Ge or Si, which contribute to the doped part of the device. Most photodiodes from $Ge_{1-x}Sn_x$ are based on the formation of heterostruture, *e.g.* n-i-$Ge_{1-x}Sn_x$/p-Si , n-Ge/p-$Ge_{1-x}Sn_x$/n-$Ge_{1-x}Sn_x$,[175,176] which show higher quantum efficiencies than comparable pure-Ge device designs even at low Sn concentrations. Specifically, several $Ge_{1-x}Sn_x$ photodetector devices (both in p-i-n and in photoconductor structure) have showed relatively high

responsivity ranging from 0.2 to 0.38 A/W at wavelengths between 1.5 to 2 μm.[165,177,178] A nice summary of the GeSn based photodetectors reported to 2019 can be found in a recent paper by Tran *et al.*[174] where they have investigated $Ge_{1-x}Sn_x$ photodetector devices with Sn concentrations varying from10.5 to 22.3 at.%. However, due to the lattice mismatch between Ge and Sn, thin films often experience large amounts of strain. Compressive strain shifts the energy gap to lower wavelengths, which requires a higher Sn incorporation to achieve a direct bandgap.[13,14]

A promising solution to the strain induction in $Ge_{1-x}Sn_x$ thin films is the move towards 1D $Ge_{1-x}Sn_x$ nanostructures; a nanowire morphology allows for increased strain relaxation over thin films due to the free sidewall facets.[20] The large surface to volume ratio and Debye length comparable to its small size resulting in superior light sensitivity, shape and size dependent optical and electronic properties make $Ge_{1-x}Sn_x$ nanostructures, especially nanowires, great candidates for efficient photodetectors. Although there has been significant progress in fabricating and characterizing $Ge_{1-x}Sn_x$ thin film photodetectors, to the best of our knowledge, there are only few reports on photodetection from $Ge_{1-x}Sn_x$ nanostructures with no reports on nanowires. Nanowires usually shows low optical reflectance and light trapping compared to thin films, thus achieving a high absorption of light with from a reduced amount of material, which is beneficial for photodetector devices. Apart from this, $Ge_{1-x}Sn_x$ nanowires can be accommodated easily with lattice mismatched materials (III-V, graphene etc.) in a radial core-shell or axial heterojunction structure, thus allowing easy fabrication of photodiode or photoconductor architecture. In some recent work, $Ge_{1-x}Sn_x$ nanocrystals embedded in a SiO_2 matrix were used as short-wave infrared photosensitive layers. Extension of the IR detection up to 2.4 μm was demonstrated in samples containing $Ge_{1-x}Sn_x$ nanocrystals with 15 at.% Sn by measuring the photovoltaic current in SiO_2 embedded $Ge_{1-x}Sn_x$ nanocrystals/p-Si

heterojunctions diodes.[115] Although $Ge_{1-x}Sn_x$ based p-i-n photodiodes are much more explored as photodetectors, $Ge_{1-x}Sn_x$ based photoconductors with different Sn contents have also been reported to operate at low temperatures.[179,180] In a recent work[174], considerable improvement on the peak responsivity (1.61 A/W at 2.0 μm), wavelength detection range (up to 3.65 μm) and specific defectivity (1.1×10^{10} $cm \cdot Hz^{1/2} \cdot W^{-1}$) was achieved with a $Ge_{1-x}Sn_x$ photoconductor with Sn incorporation up to 22.3 at.%. For more details on $Ge_{1-x}Sn_x$ photodetector devices we recommend a review by Zheng *et al.*[181] $Ge_{1-x}Sn_x$ nanowires directly grown on relevant substrate, *e.g.* doped Si, can positively contribute to responsivity and photoconductive gain as large surface to volume ratios result in the long lifetime of surface state trapped electrons.

5.3. $Ge_{1-x}Sn_x$ in Photonic devices

Direct bandgap $Ge_{1-x}Sn_x$ has been put forward as a suitable gain material in lasing applications [34,121,182] and recently there have been several reports on $Ge_{1-x}Sn_x$ lasers.[6,7,183] Wirths *et al.*[6] demonstrated lasing in partially strain-relaxed $Ge_{1-x}Sn_x$ ($x = 0.126$) thin films; the use of power dependent PL studies and a Fabry-Perot waveguide were employed to observe clear lasing under optical pumping. The $Ge_{1-x}Sn_x$ films were fabricated by CVD on virtual Ge substrates to increase strain relaxation. A threshold excitation density of ~325 kW/cm^2 at 100 K was observed. Von den Driesch *et al.*[184] explored $Ge_{1-x}Sn_x/Si_yGe_{1-x}Sn_x$ group IV heterostructure lasers, where different types of double heterostructures and multi-quantum wells were epitaxially grown with varying well thicknesses and barriers. Al-Kabi *et al.*[7] and Stange *et al.*[183] each reported the fabrication of $Ge_{1-x}Sn_x$ lasers in 2016.[7,183] The laser produced by Al-Kabi *et al.*,[7] utilising a strain relaxed $Ge_{1-x}Sn_x$ ($x = 0.0895$) thin film grown on a Ge buffer layer, was fabricated in a low cost regime with commercially available precursors, *i.e.* a "manufacture ready" process.[7] This process development is of significant importance for the

future of $Ge_{1-x}Sn_x$ and its place in photonic devices. Stange *et al.*[183] sought to improve the lasing temperature and threshold of $Ge_{1-x}Sn_x$ lasers by fabricating $Ge_{1-x}Sn_x$ microdisks (x = 0.125). These microdisks were produced by forming a $Ge_{1-x}Sn_x$ layer on a Ge buffer layer; the buffer was then selectively etched to manufacture a $Ge_{1-x}Sn_x$ microdisk on a Ge pedestal (Figure 14). This etching of the Ge buffer layer was crucial in increasing the optical confinement in the $Ge_{1-x}Sn_x$ laser, as the large refractive index contrast between $Ge_{1-x}Sn_x$ and air results in an improvement of the optical properties. This unique approach resulted in a $Ge_{1-x}Sn_x$ laser which was usable up to temperatures of 130 K; the highest temperature reported to-date.

5.4 $Ge_{1-x}Sn_x$ for energy storage

The high mobility of $Ge_{1-x}Sn_x$ alloys means that they can be utilised for energy storage devices, such as batteries. $Ge_{1-x}Sn_x$ nanostructures have shown promise as anode materials for Li-ion batteries using nanoparticles[108,185,186], nanorods[124], nanowires[187] and branched nanostructures.[93] The incorporation of just 5 at. % Sn in $Ge_{1-x}Sn_x$ nanocrystals resulted in a non-trivial increase in specific capacities in Li-ion battery.[108] The $Ge_{1-x}Sn_x$ nanocrystals maintained a capacity of 1010 mA h g^{-1} and a coulombic efficiency of 96.8 %, compared to capacities of 800 mA h g^{-1} for pure Ge nanocrystals of comparable size and structure (Figure 15). However, the increasing Sn composition resulted in a decrease in capacities due to the tendency of metallic Sn to segregate. Further to $Ge_{1-x}Sn_x$ nanocrystals, $Ge_{1-x}Sn_x$ nanowires and branched nanostructures have also been explored as anode materials for Li-ion batteries.[93,187] The open continuous channel along the axis of a nanowire could result in an increase in capacity and retention due to a decrease in sidewall reactions. Also, the relative cost of the Ge anode materials could be also reduced by alloying it with the cheaper and more abundant Sn. $Ge_{1-x}Sn_x$ branched nanostructures revealed themselves to be capable anode materials for Li-ion batteries.

Particularly, the unique combination of the morphology of $Ge_{1-x}Sn_x$ branched nanostructures resulted in exceptionally high specific capacity (≈1000 mAh/g) with a high retention (94 %) because of the increased charge carrier pathways and surface area, and the incorporation of Sn into the nanostructure. In general, $Ge_{1-x}Sn_x$ nanowires behaved as a dual alloying mode anode material as reduction/oxidation peaks for both Ge and Sn were observed. However, the reversible lithiation of Ge was responsible for most of the charge stored due to the relatively low amount of Sn present within the alloy nanowires. A future goal would be to find the Sn based group IV binary and ternary (including Si) alloy nanomaterials with critical composition as the highly efficient anode material for Li-ion battery.

6. CONCLUSION AND OUTLOOK

To address the drive to create Si compatible, direct bandgap materials for implementation in CMOS and beyond CMOS devices, Ge and Sn based group IV alloys have gained increasing interest. Alloying of Ge with Sn represents a novel solution to the lack of light emission in group IV compounds, with an indirect to direct bandgap transition predicted for Sn incorporation greater than 6.5 at. %. With a focus on the recent shift in interest toward $Ge_{1-x}Sn_x$ nanostructures, this review has reported recent advances in the growth and characterization of $Ge_{1-x}Sn_x$ materials. Of note, nanostructures such as $Ge_{1-x}Sn_x$ nanowires can incorporate large amounts of Sn with minimal strain compared to thin films. Both vapor and solution-based three-phase growth methods have been utilized to fabricate these nanowires, but the key is to employ a kinetically driven non-equilibrium growth regime. Three phase catalytic bottom-up growth has been demonstrated as a feasible pathway, via the catalyst-crystal interface, to incorporate large amount of Sn impurities in Ge nanowires. Primarily, kinetic driven solute trapping process influenced colossal injection of Sn in Ge nanowires.

In addition to conventional $Ge_{1-x}Sn_x$ nanowires, core-shell structures incorporating a Ge core and $Ge_{1-x}Sn_x$ alloy shell have also been fabricated which offer enhanced optical properties due to the presence of both the tensile strained Ge core and $Ge_{1-x}Sn_x$ shell. $Ge_{1-x}Sn_x$ quantum dots have also grabbed the interest of research community due to the possibility of attaining tunable direct bandgaps ranging from the visible to near infrared region. With the demonstration of epitaxial growth, room temperature light emission, tunable direct bandgap, optical gain and broad photoresponse across the mid-IR, $Ge_{1-x}Sn_x$ nanostructures are ideal for implementation in group IV photonics and optoelectronics.

The implementation of $Ge_{1-x}Sn_x$ nanostructures in photonic, optoelectronic, electronic and energy storage devices needs the development of high quality, uniform and stable $Ge_{1-x}Sn_x$ alloy nanoforms. Although there are now several reports on $Ge_{1-x}Sn_x$ alloy nanostructures, there are still gaps of knowledge in terms of their fabrication, *e.g.* localized growth, doping, heterostructure formation, growth mechanisms, scale-up, surface functionalization *etc*. Also, taking account of the variability factor, *e.g.* surface quality, alloy ordering, Sn migration *etc*., in these alloy nanostructures, in-depth correlation of the optical, electrical and mechanical properties with the structural/morphological variables of the alloys are required. Specifically, the electronic properties of $Ge_{1-x}Sn_x$ nanostructures have not been studied in detail. For nanostructured MOSFET devices knowledge on device architecture, stability and the important transistor parameters (*e.g.* drive current (I_{ON}), off current (I_{OFF}), I_{ON}/I_{OFF} ratio, threshold voltage, subthreshold slope) is crucial. Exploring the key parameters as a function of nanostructure dimension, crystal structure, alloy compositions, doping concentration, dopant distribution, gate architecture is also crucial to its successful implementation in large scale

applications. Specifically, the doping of $Ge_{1-x}Sn_x$ nanoscale materials need to be explored extensively for proper implementation of these materials in nanoelectronic devices. In this regard, in-situ method where the dopant atom is incorporated during the nanowire growth could play a crucial role as ex-situ doping methods (*e.g.* ion implantation, molecular-layer-doping etc.) are limited for $Ge_{1-x}Sn_x$ nanostructure due to the need of additional perturbation (*e.g.* rapid thermal annealing, laser annealing etc.). This additional processing may influence the Sn distribution in the Ge lattice by the surface or bulk segregation of Sn.

Parallel initiatives on improving the processing aspects with simulation analysis is crucial to achieve breakthrough results in future for $Ge_{1-x}Sn_x$ nanostructure electronic, optoelectronic and photonic devices. Also, another critical factor to investigate is the maximum process temperature from materials to device fabrication. This should be compatible with back-end-of-line integration schemes in nano/optoelectronic chip production. Going forward, future focus could also be on the development of ternary nanoscale alloy materials in group IV regime to decouple strain and band-structure, like III-V quaternary semiconductors.

Author Contribution

J.D and S.B. contributed equally in writing this review.

Acknowledgements

This research was funded by Science Foundation Ireland (Grant No: 14/IA/2513), and by the Irish Research Council through a Postgraduate Scholarship to JD (Grant No.: GOIPG/2015/2772).

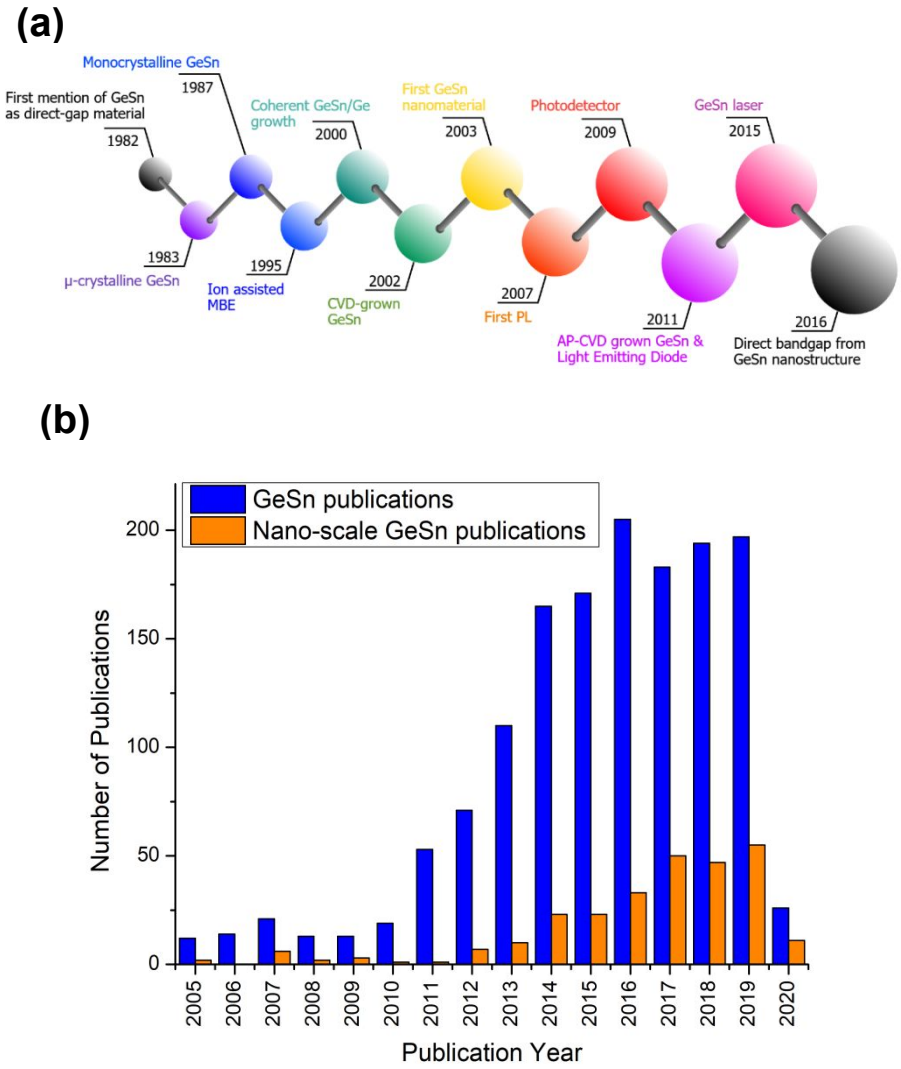

Figure 1: Recent advances in $Ge_{1-x}Sn_x$ and increase in popularity. (a) Timeline of historical $Ge_{1-x}Sn_x$ benchmarks including development on nanomaterials. (b) Google Scholar results for publications on $Ge_{1-x}Sn_x$ per calendar year showing recent increase in number of publications on nanostructure.

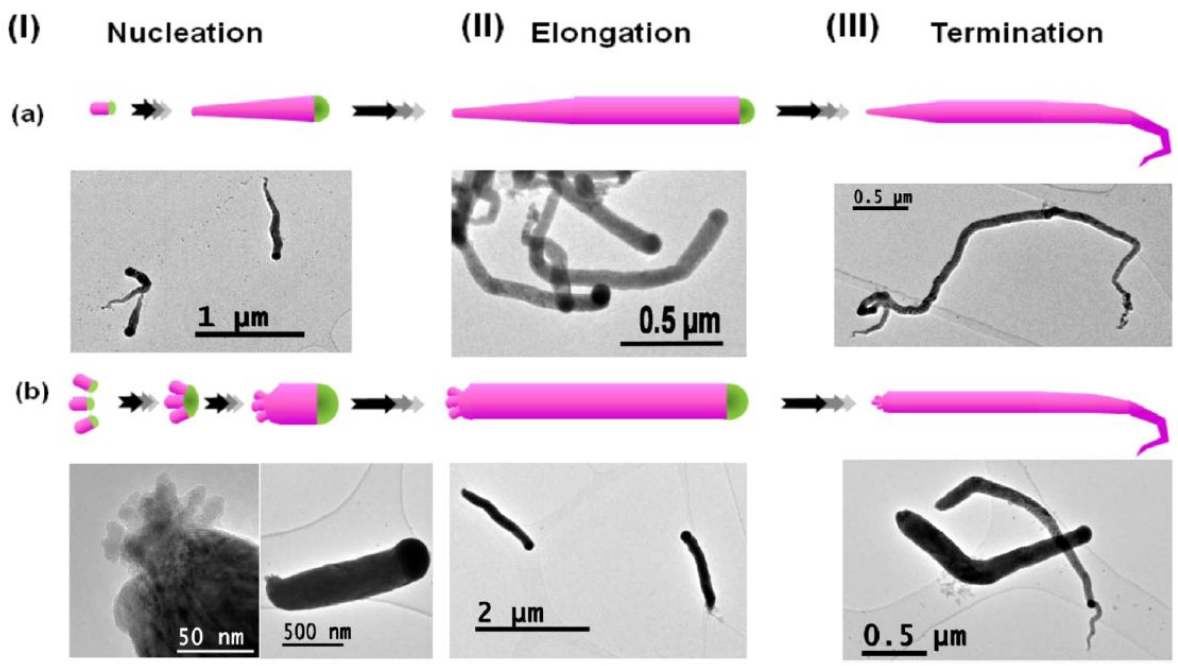

Figure 2: Schematic for microwave-assisted growth of $Ge_{1-x}Sn_x$ nanowires ($x = 0.125$ and TEM images to illustrate the structural features (Ge in purple; Sn in green). (a) Describes the growth via homogeneous nucleation with diameter expansion and accumulation of Sn at the growth front. (b) Represents the pre-nucleation of $Ge_{1-x}Sn_x$ nanowires by an additional heat treatment and nucleus formation via oriented attachment leading to a quickly settling nanowire diameter at the nucleation (I) stage. The elongation (II) is a phase where the nanowire grows along its axis with a constant diameter due to constant Sn supply and consumption caused by incorporation in the Ge matrix. The termination (III) includes shrinkage in nanowire diameter and the consumption of the tin growth seed. Reprinted with permission from M. Seifner *et al.*[22] Copyright (2015) American Chemical Society.

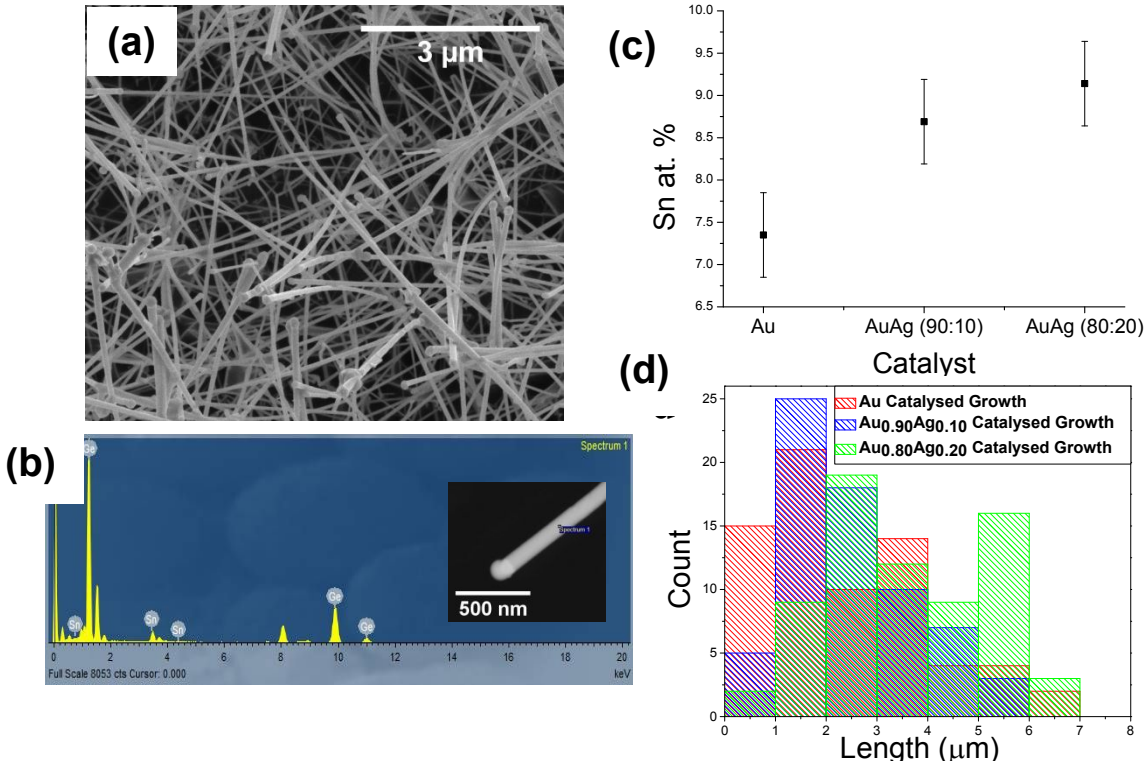

Figure 3: Investigation of the impact of growth kinetics on Sn incorporation in $Ge_{1-x}Sn_x$ nanowires. (a) SEM image of $x = 0.09$ $Ge_{1-x}Sn_x$ nanowires, displaying negligible Sn clusters. (b) Energy dispersive X-ray (EDX) spectrum showing high Sn incorporation and the absence of Au or Ag impurities from the $Au_{0.80}Ag_{0.20}$ nanoparticle catalysts. (c) and (d) display the relationship between growth kinetics and Sn incorporation; with the faster growth rate resulting in both longer nanowires and an increased Sn content. Republished with permission of Royal Society of Chemistry, from J. Doherty *et al.*[91]; permission conveyed through Copyright Clearance Center, Inc.

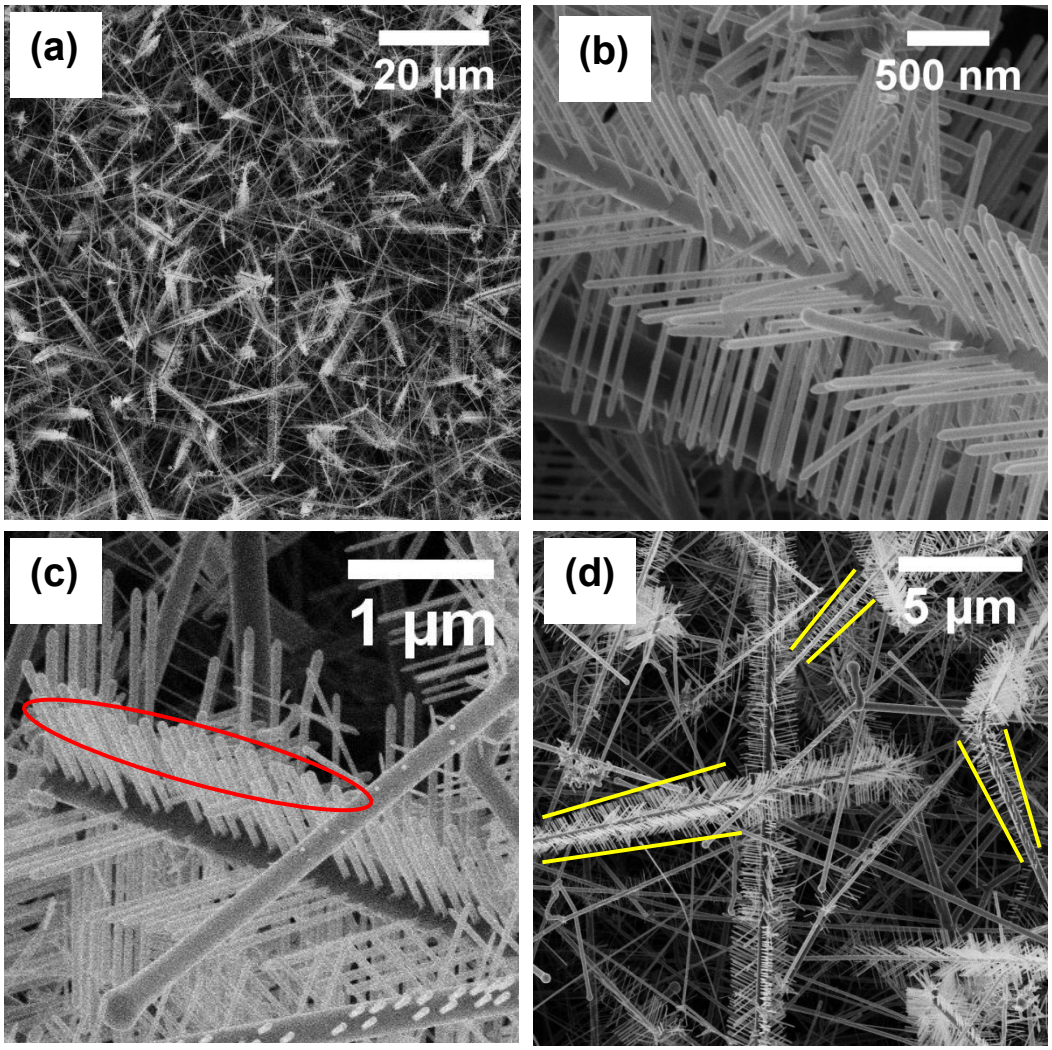

Figure 4: SEM images of $Ge_{1-x}Sn_x$ branched nanostructures. The high yield of branched nanostructures with respect to conventional nanowires is apparent in (a), and the uniformity is clearly apparent in (b). The presence of nanoparticle seeds on the branched nanowires is not clear in all cases (b), however nanoparticle seeds on the tips of the branched nanowires is clearly visible in (c). The changing length of branched nanowires along the main nanowire trunk is observed in (d), with longer branches seen toward the end of the nanowire trunk and shorter branches closer to the nanowire tip. The yellow lines are provided as a guides for the eye. Reprinted with permission form J. Doherty *et al*.[93] Copyright (2019) American Chemical Society.

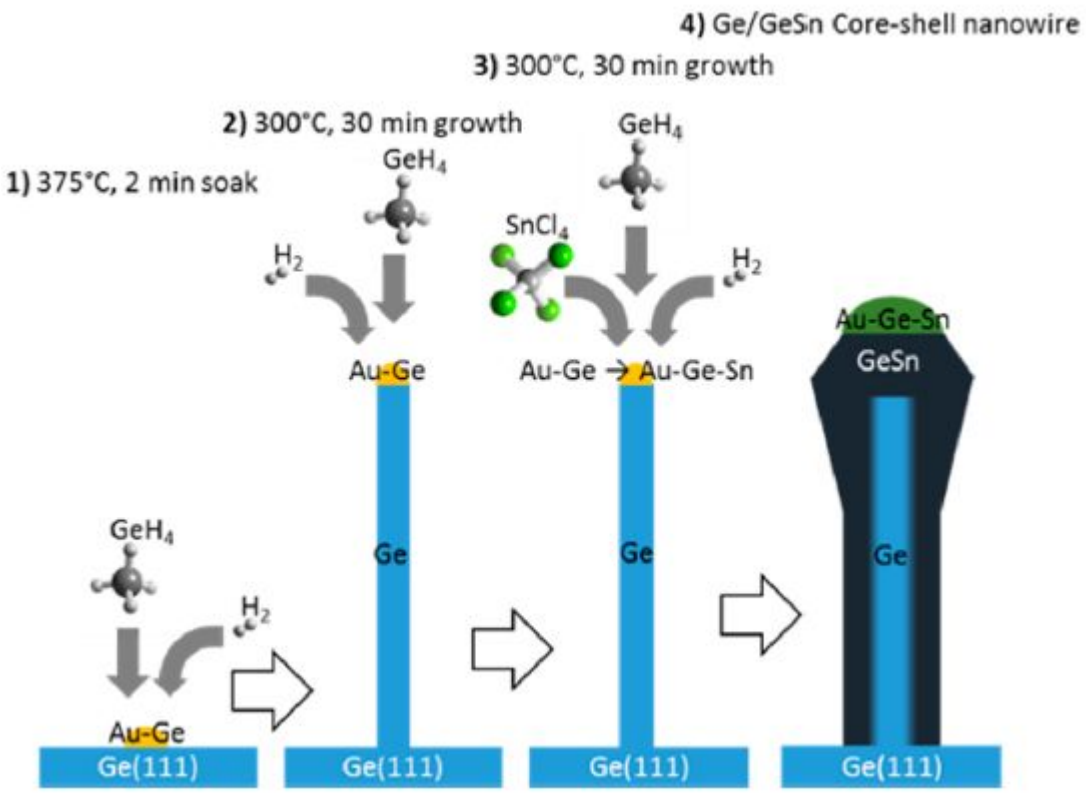

Figure 5: Growth schematic for core/shell nanowires at four different growth stages. Reprinted with permission from A. Meng *et al.*[94] Copyright (2018) American Chemical Society.

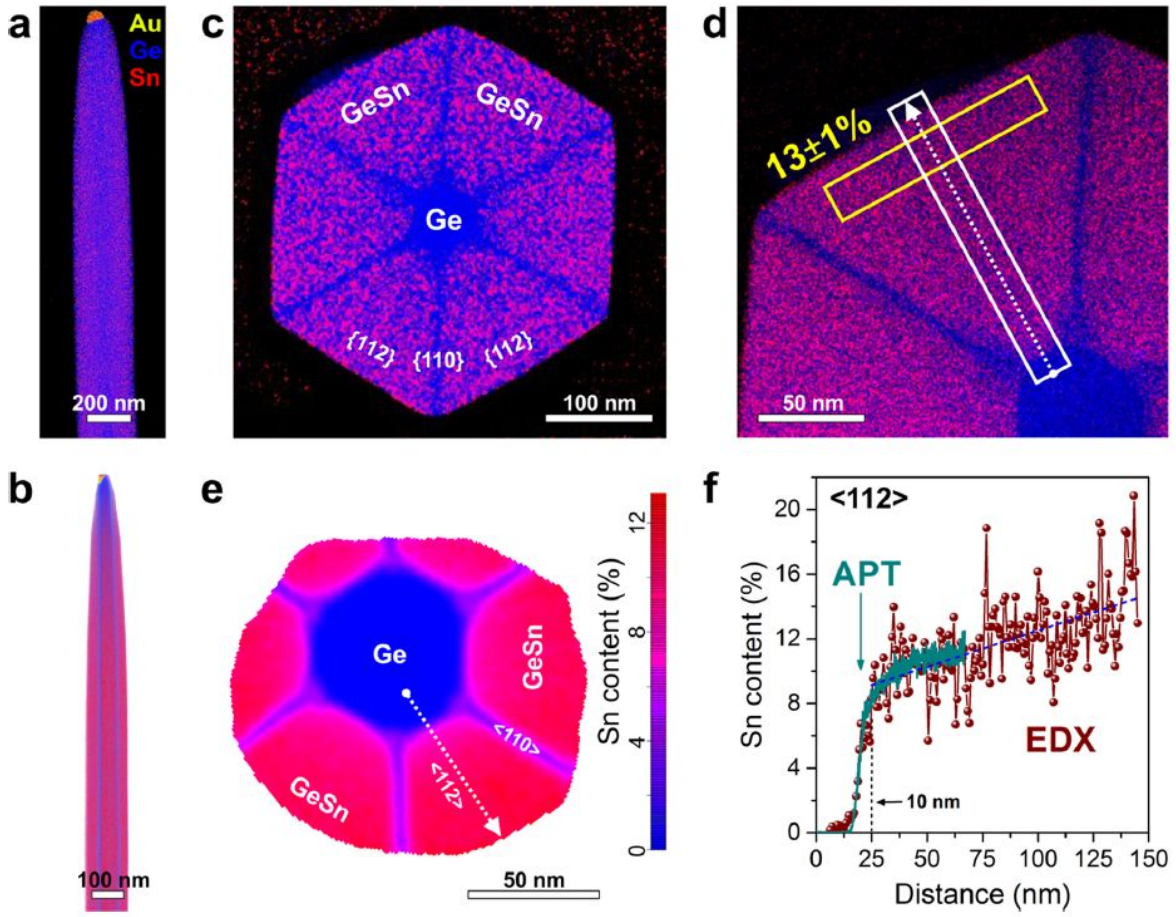

Figure 6: Radial Sn incorporation in a Ge/$Ge_{1-x}Sn_x$ core-shell nanowire. (a) EDX compositional map and (b) APT image showing the Ge/$Ge_{0.87}Sn_{0.13}$ core/shell structure. A uniform Sn distribution is observed in the $Ge_{1-x}Sn_x$ shell along the NW growth axis, while no axial growth of $Ge_{1-x}Sn_x$ is present. (c) and (d) Cross-sectional EDX compositional maps showing a ~120 nm thick $Ge_{1-x}Sn_x$ shell, with enhanced Sn incorporation on the {112} side-facets compared to the {110} facets. The integrated tangential composition profile in the yellow rectangle provides an average Sn content of 13 ± 1 %, while the radial line-profile (white dashed arrow) is shown in (f). (e) APT measurements showing the Ge core and the inner portion of the $Ge_{1-x}Sn_x$ shell. The line-profile (dashed arrow) is shown in (f). (f) Plot of the Sn content as a function of the distance along the radial direction for EDX and APT measurements. After a 10 nm transition region from the Ge core into the $Ge_{1-x}Sn_x$ shell, the Sn

content gradually increases toward the outer portion of the shell. The blue dashed line is the linear fit of the EDX profile. Reprinted with permission from S. Assali *et al.*[95] Copyright (2017) American Chemical Society.

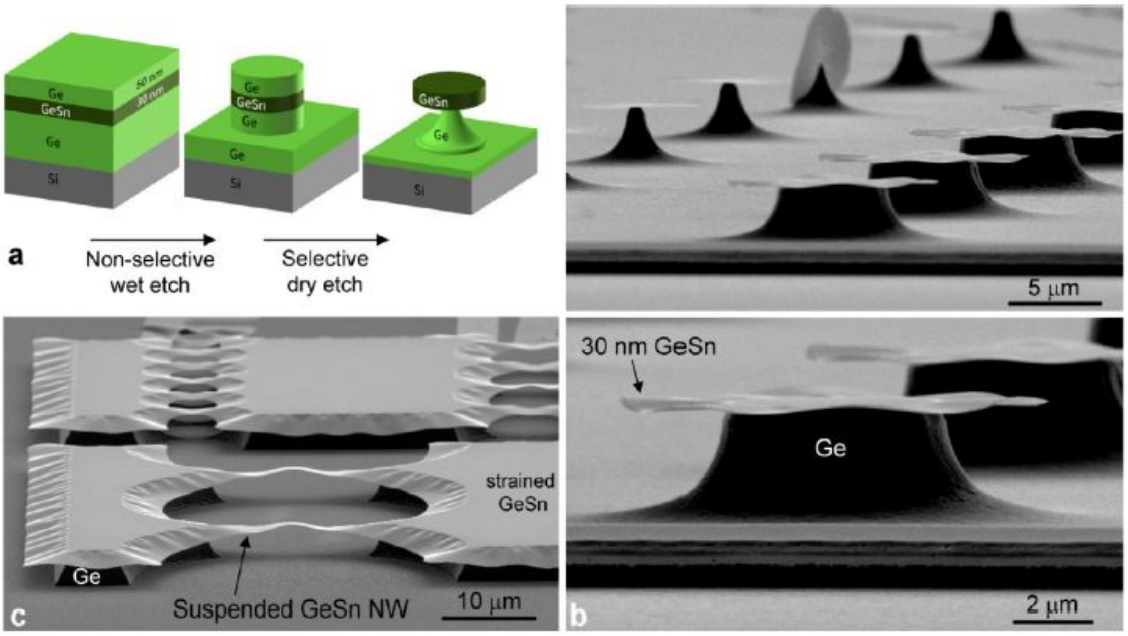

Figure 7: (a) Key steps in the process flow for fabrication of $Ge_{1-x}Sn_x$ undercut structures on sample B. (b) SEM images of $Ge_{1-x}Sn_x$ microdisks fabricated on sample B using the process flow shown in (a). Note that the $Ge_{1-x}Sn_x$ layer is only 30 nm thick. (c) SEM image of suspended $Ge_{1-x}Sn_x$ nanowires. Even though the length of the suspended region is greater than 15 μm, the wires do not collapse onto the substrate. These SEM images prove the high resistance of $Ge_{1-x}Sn_x$ to CF_4 plasma etching. Reprinted with permission from S. Gupta *et al.*[105] Copyright (2013) American Chemical Society.

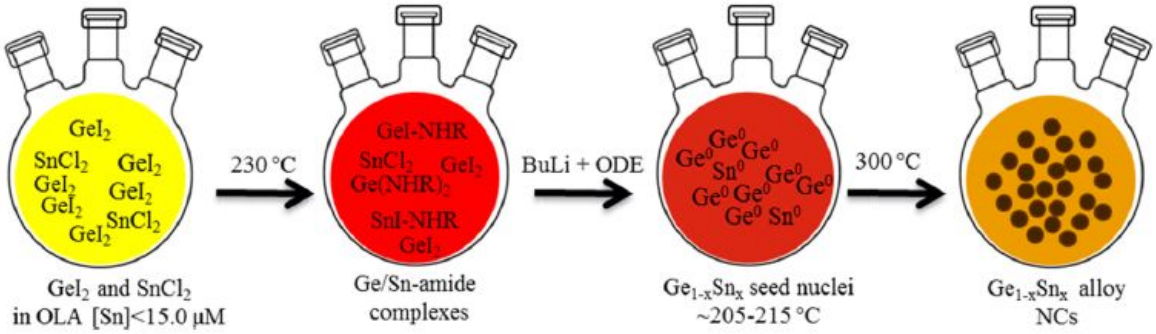

Figure 8: An Illustration of the synthesis of $Ge_{1-x}Sn_x$ alloy nanocrystals. Fast chemical co-reduction of precursor halides dissolved in oleylamine (OLA), followed by the growth of resulting alloy nuclei at 300 °C has been successfully utilised to produce homogeneous $Ge_{1-x}Sn_x$ nanoalloys. Reprinted with permission from R. Esteves *et al.*[109] Copyright (2015) American Chemical Society.

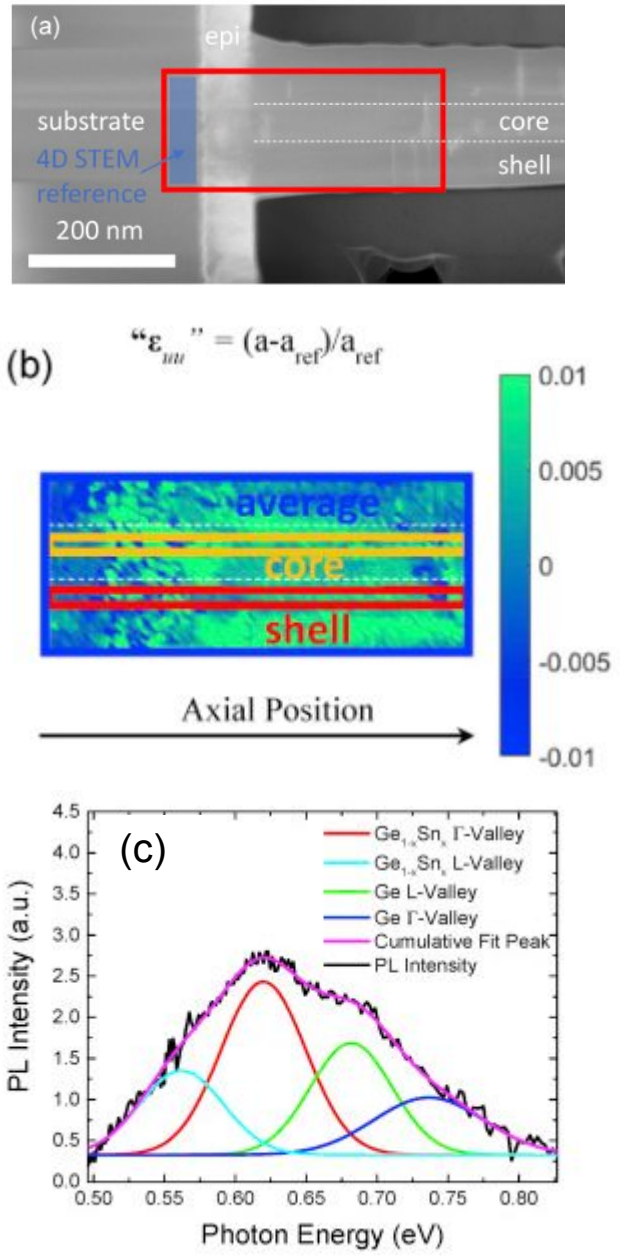

Figure 9: (a) STEM image and (b) corresponding 4D STEM strain map of Ge/$Ge_{0.96}Sn_{0.04}$ core/shell nanowires. (c) PL spectra of Ge/$Ge_{0.96}Sn_{0.04}$ core/shell nanowires. Reprinted from Meng *et al*. [98] Copyright (2019) with permission from Elsevier.

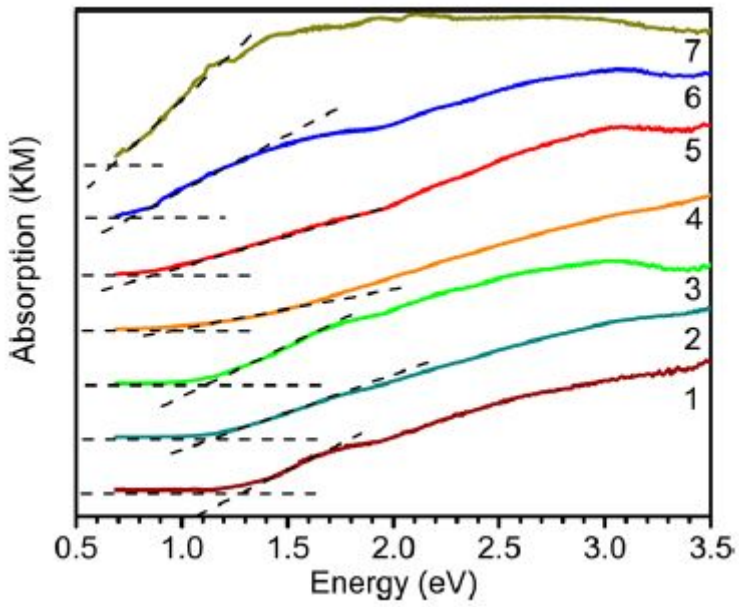

Figure 10: Diffuse reflectance spectra (converted to absorbance using the Kubelka−Munk (KM) remission function) of 3.6−4.3 nm $Ge_{1-x}Sn_x$ alloy nanocrystals as a function of Sn composition: x = 0.000 (spectrum 1), x = 0.033 (spectrum 2), x = 0.056 (spectrum 3), x = 0.077 (spectrum 4), x = 0.088 (spectrum 5), x = 0.092 (spectrum 6), and x = 0.116 (spectrum 7). Reprinted with permission from R. Esteves *et al.*[109] Copyright (2015) American Chemical Society.

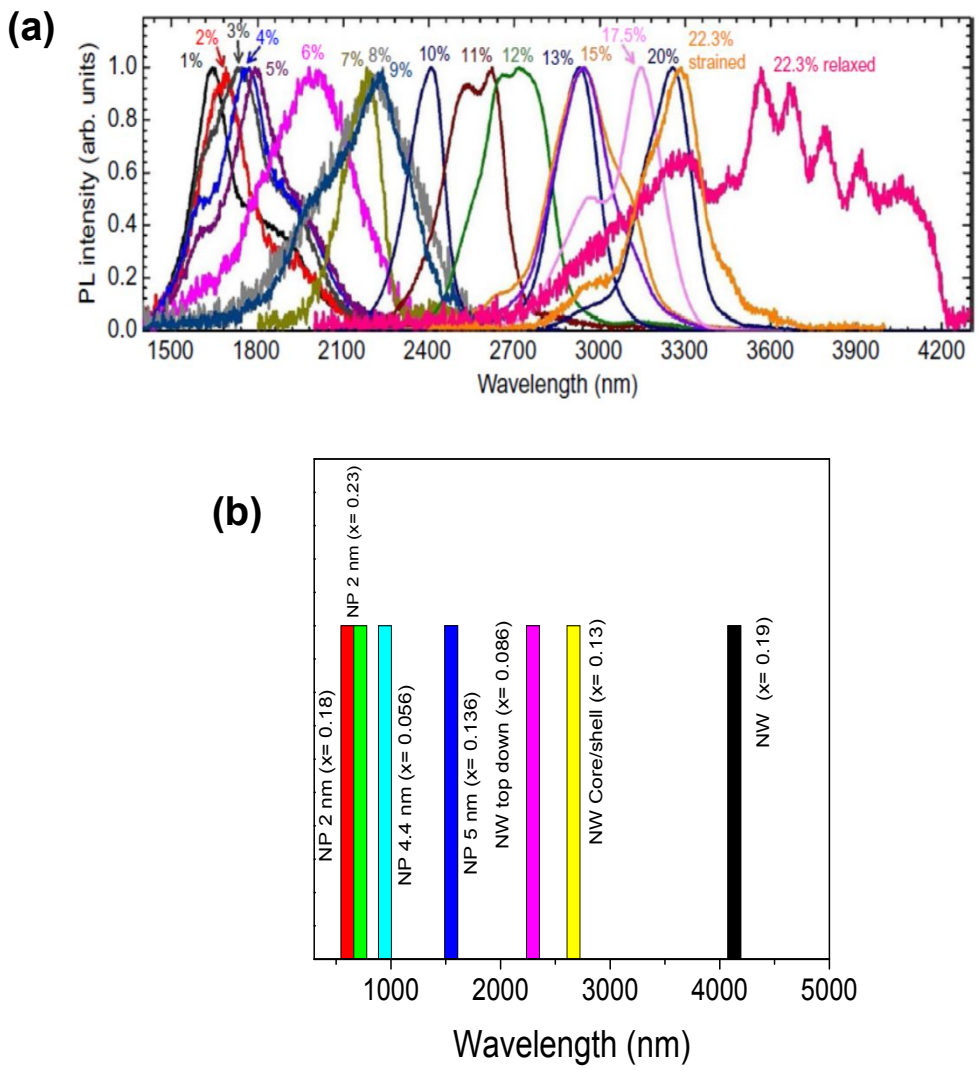

Figure 11: (a) Room temperature PL emissions from unintentionally doped GeSn samples with Sn compositions from 1% to 22.3%. Reprinted from Du *et al.*[188] Copyright (2020) with permission from Elsevier. (b) Peak position of the maximum PL emission at room temperature for nanoscale materials.

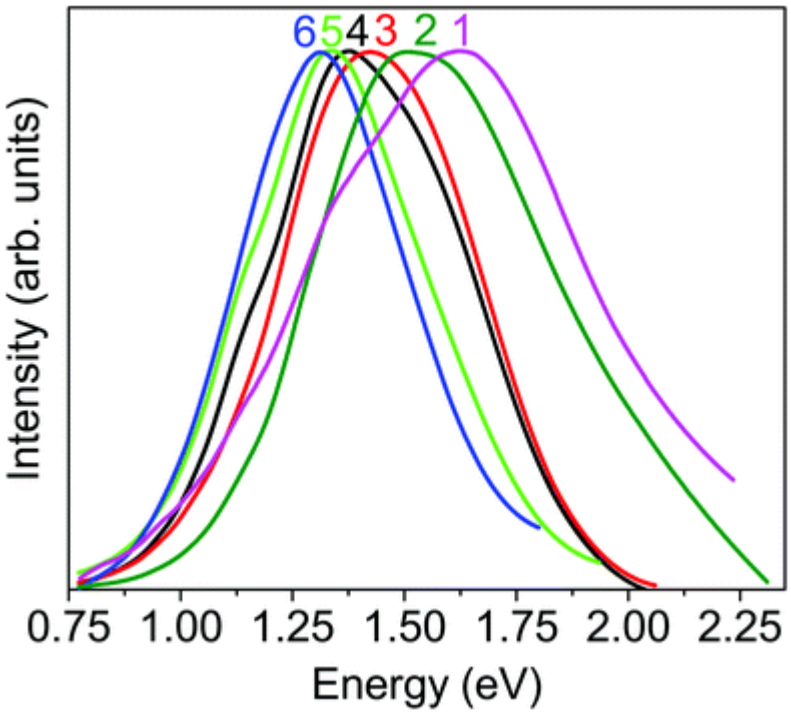

Figure 12: Room-temperature solid-state PL spectra of the $Ge_{1-x}Sn_x$ alloy QDs with varying Sn compositions: (1) x = 1.5% (1.62 eV), (2) x = 1.9% (1.52 eV), (3) x = 2.7% (1.43 eV), (4) x = 3.4% (1.38 eV), (5) x = 4.2% (1.34 eV), and (6) x = 5.6% (1.31 eV) showing red shift. Republished with permission of Royal Society of Chemistry, from Tallapally *et al* [113]; permission conveyed through Copyright Clearance Center, Inc.

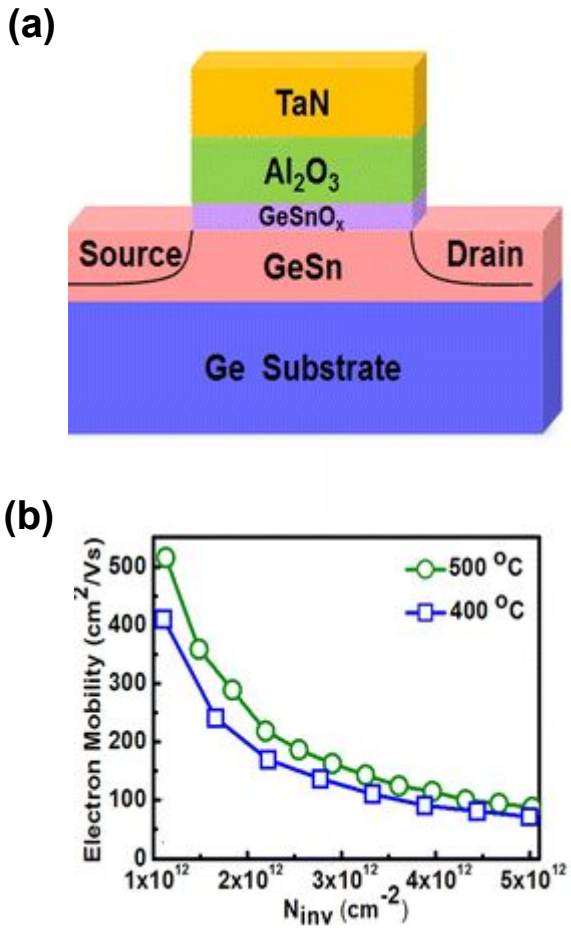

Figure 13: (a) Stacked GeSn n-MOSFETs device with O_2 plasma passivation. (b) Electron mobility versus inversion charge (N_{inv}) shows high electron mobility of greater than 500 cm^2/Vs. Reprinted with permission from Fang *et al.*[143] Copyright (2015) American Chemical Society.

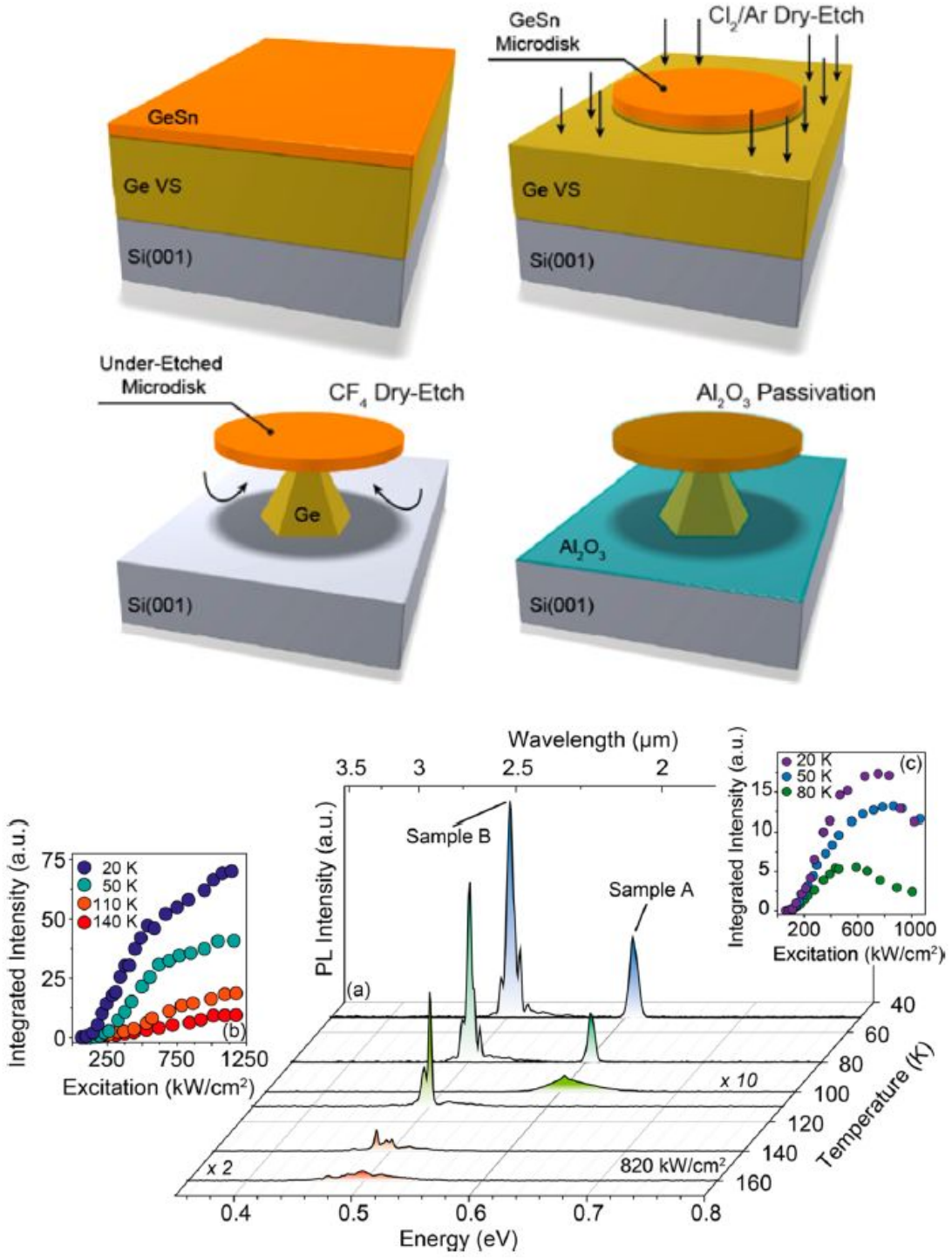

Figure 14: $Ge_{1-x}Sn_x$ microdisk lasers. (Top) Fabrication of $Ge_{1-x}Sn_x$ microdisks, schematic representation of the fabrication flow and of 8 μm diameter $Ge_{0.875}Sn_{0.125}$ microdisks with the underlying Ge virtual substrate (VS) undercut by 3.6 μm. (Bottom) Power and temperature dependence for different Sn contents. (a) Temperature-dependent spectra of 8 μm diameter microdisks from samples A (x = 0.085) and B (x = 0.125) at 820 kW/cm². Light-in and light-

out curves at different temperatures for (b) sample B and (c) sample A. Reprinted with permission from D. Stange *et al.*[183] Copyright (2016) American Chemical Society.

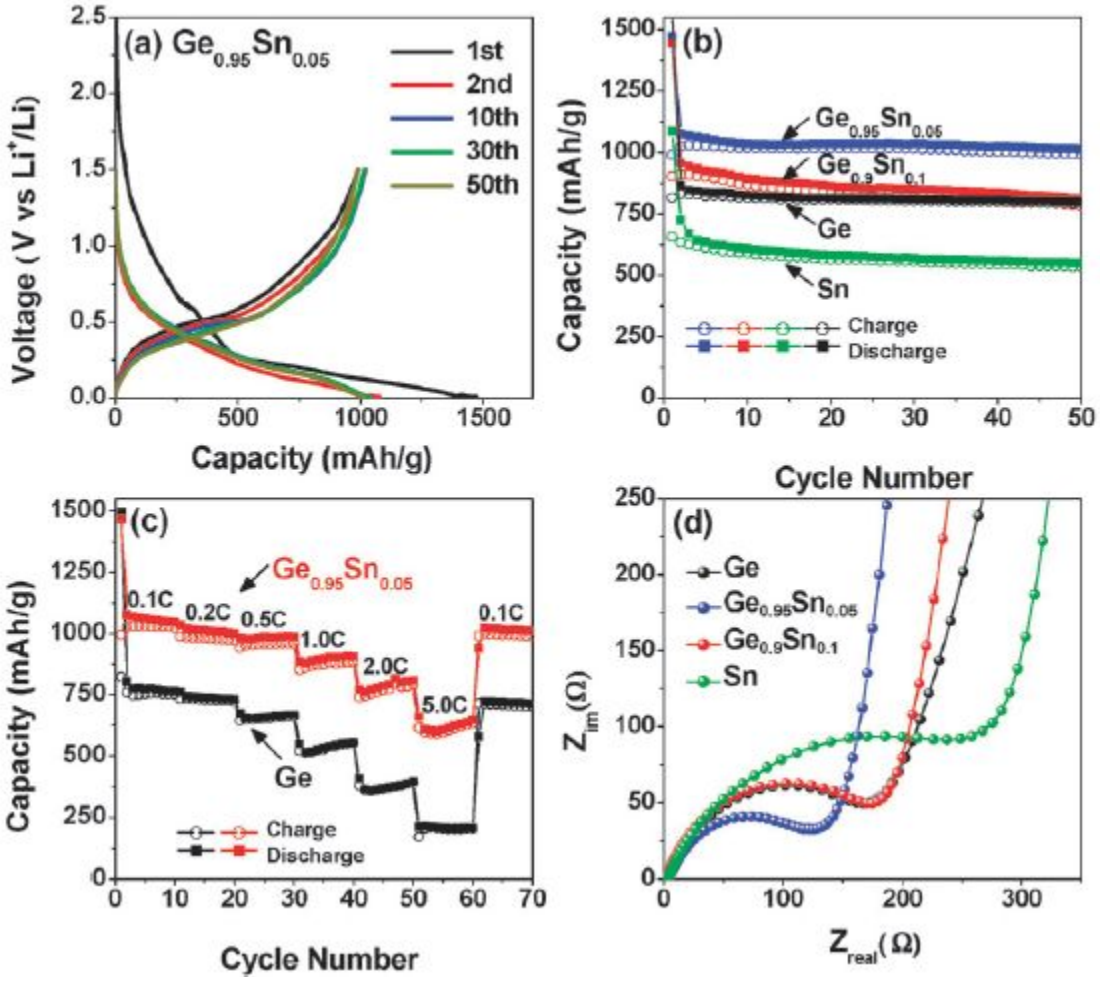

Figure 15: Charge and discharge voltage profiles of a half cell using $Ge_{0.95}Sn_{0.05}$ nanocrystals for 1, 2, 10, 30, and 50 cycles tested between 0.01 and 1.5 V, at a rate of 0.1 C. (b) Charge–discharge capacity vs. cycle number for half cells of Ge (ref. 15), $Ge_{0.95}Sn_{0.05}$, $Ge_{0.9}Sn_{0.1}$, and Sn nanocrystals at a rate of 0.1 C. (c) Cycling performance of Ge and $Ge_{0.95}Sn_{0.05}$ NCs as the rate is increased from 0.1 C to 5.0 C. (d) Nyquist plots of Ge, $Ge_{0.95}Sn_{0.05}$, $Ge_{0.9}Sn_{0.1}$, and Sn nanocrystals. Republished with permission of Royal Society of Chemistry, from Y. Cho *et al.*[108]; permission conveyed through Copyright Clearance Center, Inc.

References

(1) Sau, J. D.; Cohen, M. L. Possibility of Increased Mobility in Ge-Sn Alloy System. *Phys. Rev. B - Condens. Matter Mater. Phys.* **2007**, *75*, 045208.

(2) Jenkins, D. W.; Dow, J. D. Electronic Properties of Metastable GexSn1-x Alloys. *Phys. Rev. B* **1987**, *36* , 7994–8000.

(3) Richard D'Costa, V.; Wang, W.; Zhou, Q.; Soon Tok, E.; Yeo, Y. C. Above-Bandgap Optical Properties of Biaxially Strained GeSn Alloys Grown by Molecular Beam Epitaxy. *Appl. Phys. Lett.* **2014**, *104*, 022111.

(4) Ionescu, A. M.; Riel, H. Tunnel Field-Effect Transistors as Energy-Efficient Electronic Switches. *Nature* **2011**, *479* , 329–337.

(5) Schulte-Braucks, C.; Glass, S.; Hofmann, E.; Stange, D.; von den Driesch, N.; Hartmann, J. M.; Ikonic, Z.; Zhao, Q. T.; Buca, D.; Mantl, S. Process Modules for GeSn Nanoelectronics with High Sn-Contents. *Solid. State. Electron.* **2017**, *128*, 54–59.

(6) Wirths, S.; Geiger, R.; Driesch, N. V. Den; Mussler, G.; Stoica, T.; Mantl, S.; Ikonic, Z.; Luysberg, M.; Chiussi, S.; Hartmann, J. M.; Sigg, H.; Faist, J.; Buca, D.; Grützmacher, D. Lasing in Direct-Bandgap GeSn Alloy Grown on Si. *Nat. Photonics* **2015**, *9*, 88–92.

(7) Al-Kabi, S.; Ghetmiri, S. A.; Margetis, J.; Pham, T.; Zhou, Y.; Dou, W.; Collier, B.; Quinde, R.; Du, W.; Mosleh, A.; Liu, J.; Sun, G.; Soref, R. A.; Tolle, J.; Li, B.; Mortazavi, M.; Naseem, H. A.; Yu, S. Q. An Optically Pumped 2.5 Um GeSn Laser on Si Operating at 110 K. *Appl. Phys. Lett.* **2016**, *109*, 171105.

(8) Soref, R. Mid-Infrared Photonics in Silicon and Germanium. *Nat. Photonics* **2010**, *4*, 495–497.

(9) Wirths, S.; Buca, D.; Mantl, S. Si–Ge–Sn Alloys: From Growth to Applications. *Prog. Cryst. Growth Charact. Mater.* **2016**, *62*, 1–39.

(10) Wang, H.; Liu, Y.; Han, G.; Shao, Y.; Zhang, C.; Feng, Q.; Zhang, J.; Hao, Y. Performance Enhancement in Uniaxially Strained Germanium-Tin FinTFET: Fin Direction Dependence. *IEEE Trans. Electron Devices* **2017**, *64*, 2804–2811.

(11) Peng, Y.-H.; Cheng, H. H.; Mashanov, V. I.; Chang, G.-E. GeSn P-i-n Waveguide Photodetectors on Silicon Substrates. *Appl. Phys. Lett.* **2014**, *105*, 231109.

(12) Werner, J.; Oehme, M.; Schmid, M.; Kaschel, M.; Schirmer, A.; Kasper, E.; Schulze, J. Germanium-Tin p-i-n Photodetectors Integrated on Silicon Grown by Molecular Beam Epitaxy. *Appl. Phys. Lett.* **2011**, *98*, 061108.

(13) Al-Kabi, S.; Ghetmiri, S. A.; Margetis, J.; Du, W.; Mosleh, A.; Alher, M.; Dou, W.; Grant, J. M.; Sun, G.; Soref, R. A.; Tolle, J.; Li, B.; Mortazavi, M.; Naseem, H. A.; Yu, S. Q. Optical Characterization of Si-Based Ge1−xSnxAlloys with Sn Compositions up to 12%. *J. Electron. Mater.* **2016**, *45*, 2133–2141.

(14) Ghetmiri, S. A.; Du, W.; Margetis, J.; Mosleh, A.; Cousar, L.; Conley, B. R.; Nazzal, A.; Sun, G.; Soref, R. a; Tolle, J.; Li, B.; Naseem, H. a; Ghetmiri, S. A.; Du, W.; Margetis, J.; Mosleh, A.; Cousar, L.; Tolle, J.; Li, B.; Naseem, H. a; Yu, S. Direct-

Bandgap GeSn Grown on Silicon with 2230nm Photoluminescence. *Appl. Phys. Lett.* **2014**, *105*, 151109.

(15) Su, S.; Cheng, B.; Xue, C.; Wang, W.; Cao, Q.; Xue, H.; Hu, W.; Zhang, G.; Zuo, Y.; Wang, Q. GeSn P-i-n Photodetector for All Telecommunication Bands Detection. *Opt. Express* **2011**, *19*, 6400–6405.

(16) Kouvetakis, J.; Menendez, J.; Chizmeshya, A. V. G. TIN-BASED GROUP IV SEMICONDUCTORS: New Platforms for Opto- and Microelectronics on Silicon. *Annu. Rev. Mater. Res.* **2006**, *36*, 497–554.

(17) Zaima, S.; Nakatsuka, O.; Taoka, N.; Kurosawa, M.; Takeuchi, W.; Sakashita, M. Growth and Applications of GeSn-Related Group-IV Semiconductor Materials. *Sci. Technol. Adv. Mater.* **2015**, *16*, 043502.

(18) Yu, I. S.; Wu, T. H.; Wu, K. Y.; Cheng, H. H.; Mashanov, V. I.; Nikiforov, A. I.; Pchelyakov, O. P.; Wu, X. S. Investigation of Ge1-XSnx/Ge with High Sn Composition Grown at Low-Temperature. *AIP Adv.* **2011**, *1*, 042118.

(19) Wang, W.; Zhou, Q.; Dong, Y.; Tok, E. S.; Yeo, Y.-C. Critical Thickness for Strain Relaxation of $Ge_{1-x}Sn_x$ ($x \leq 0.17$) Grown by Molecular Beam Epitaxy on Ge(001). *Appl. Phys. Lett.* **2015**, *106*, 232106.

(20) Albani, M.; Assali, S.; Verheijen, M. A.; Koelling, S.; Bergamaschini, R.; Pezzoli, F.; Bakkers, E. P. A. M.; Miglio, L. Critical Strain for Sn Incorporation into Spontaneously Graded Ge/GeSn Core/Shell Nanowires. *Nanoscale* **2018**, *10*, 7250–7256.

(21) Ragan, R.; Ahn, C. C.; Atwater, H. a. Nonlithographic Epitaxial SnxGe1-x Dense Nanowire Arrays Grown on Ge(001). *Appl. Phys. Lett.* **2003**, *82*, 3439–3441.

(22) Seifner, M. S.; Biegger, F.; Lugstein, A.; Bernardi, J.; Barth, S. Microwave-Assisted Ge1-XSnx Nanowire Synthesis: Precursor Species and Growth Regimes. *Chem. Mater.* **2015**, *27*, 6125–6130.

(23) Goodman, P. C. H. L. Direct-Gap Group IV Semiconductors Based on Tin. *IEE PROC.* **1982**, *129*, 189–192.

(24) Mäder, K. A.; Baldereschi, A.; von Känel, H. Band Structure and Instability of Ge1-XSnx Alloys. *Solid State Commun.* **1989**, *69*, 1123–1126.

(25) Oguz, S.; Paul, W.; Deutsch, T. F.; Tsaur, B. Y.; Murphy, D. V. Synthesis of Metastable, Semiconducting Ge-Sn Alloys by Pulsed UV Laser Crystallization. *Appl. Phys. Lett.* **1983**, *43*, 848–850.

(26) Shah, S. I.; Greene, J. E.; Abels, L. L.; Yao, Q.; Raccah, P. M. Growth of Single-Crystal Metastable Ge1-XSnxalloys on Ge(100) and GaAs(100) Substrates. *J. Cryst. Growth* **1987**, *83*, 3–10.

(27) Bauer, M. R.; Tolle, J.; Bungay, C.; Chizmeshya, A. V. G.; Smith, D. J.; Menéndez, J.; Kouvetakis, J. Tunable Band Structure in Diamond-Cubic Tin-Germanium Alloys Grown on Silicon Substrates. *Solid State Commun.* **2003**, *127*, 355–359.

(28) Bauer, M.; Taraci, J.; Tolle, J.; Chizmeshya, A. V. G.; Zollner, S.; Smith, D. J.; Menendez, J.; Hu, C.; Kouvetakis, J. Ge-Sn Semiconductors for Band-Gap and Lattice Engineering. *Appl. Phys. Lett.* **2002**, *81*, 2992–2994.

(29) Liu, J.; Sun, X.; Pan, D.; Wang, X.; Kimerling, L. C.; Koch, T. L.; Michel, J. Tensile-Strained, n-Type Ge as a Gain Medium for Monolithic Laser Integration on Si. *Opt. Express* **2007**, *15*, 11272–11277.

(30) Zhang, F.; Crespi, V. H.; Zhang, P. Prediction That Uniaxial Tension along 111 Produces a Direct Band Gap in Germanium. *Phys. Rev. Lett.* **2009**, *102*, 156401.

(31) Moontragoon, P.; Ikonić, Z.; Harrison, P. Band Structure Calculations of Si-Ge-Sn Alloys: Achieving Direct Band Gap Materials. *Semicond. Sci. Technol.* **2007**, *22*, 742–748.

(32) Attiaoui, A.; Moutanabbir, O. Indirect-to-Direct Band Gap Transition in Relaxed and Strained Ge 1-x-YSixSny Ternary Alloys. *J. Appl. Phys.* **2014**, *116*, 063712.

(33) Lu Low, K.; Yang, Y.; Han, G.; Fan, W.; Yeo, Y. C. Electronic Band Structure and Effective Mass Parameters of Ge 1-XSnx Alloys. *J. Appl. Phys.* **2012**, *112*, 103715.

(34) Dutt, B.; Lin, H.; Sukhdeo, D. S.; Vulovic, B. M.; Gupta, S.; Nam, D.; Saraswat, K. C.; Harris, J. S. Theoretical Analysis of GeSn Alloys as a Gain Medium for a Si-Compatible Laser. *IEEE J. Sel. Top. Quantum Electron.* **2013**, *19*, 1502706.

(35) Jiang, L.; Gallagher, J. D.; Senaratne, C. L.; Aoki, T.; Mathews, J.; Kouvetakis, J.; Menéndez, J. Compositional Dependence of the Direct and Indirect Band Gaps in Ge1-YSny Alloys from Room Temperature Photoluminescence: Implications for the Indirect to Direct Gap Crossover in Intrinsic and n-Type Materials. *Semicond. Sci. Technol.* **2014**, *29*, 115028.

(36) Gallagher, J. D.; Senaratne, C. L.; Kouvetakis, J.; Menéndez, J. Compositional Dependence of the Bowing Parameter for the Direct and Indirect Band Gaps in Ge1-YSny Alloys. *Appl. Phys. Lett.* **2014**, *105*, 142102.

(37) He, G.; Atwater, H. A. Interband Transitions in Snx Ge1 − x Alloys. *Phys. Rev. Lett.* **1997**, *79*, 1937.

(38) Eckhardt, C.; Hummer, K.; Kresse, G. Indirect-to-Direct Gap Transition in Strained and Unstrained SnxGe1-x Alloys. *Phys. Rev. B - Condens. Matter Mater. Phys.* **2014**, *89*, 165201.

(39) Huang, W.; Cheng, B.; Xue, C.; Liu, Z. Comparative Studies of Band Structures for Biaxial (100)-, (110)-, and (111)-Strained GeSn: A First-Principles Calculation with GGA+U Approach. *J. Appl. Phys.* **2015**, *118*, 165704.

(40) Freitas, F. L.; Furthmüller, J.; Bechstedt, F.; Marques, M.; Teles, L. K. Influence of the Composition Fluctuations and Decomposition on the Tunable Direct Gap and Oscillator Strength of Ge1-XSnx Alloys. *Appl. Phys. Lett.* **2016**, *108*, 092101.

(41) Polak, M. P.; Scharoch, P.; Kudrawiec, R. The Electronic Band Structure of $Ge_{1-x}Sn_x$ in the Full Composition Range: Indirect, Direct, and Inverted Gaps Regimes, Band Offsets, and the Burstein–Moss Effect. *J. Phys. D. Appl. Phys.* **2017**, *50*, 195103.

(42) Eales, T. D.; Marko, I. P.; Schulz, S.; O'Halloran, E.; Ghetmiri, S.; Du, W.; Zhou, Y.; Yu, S. Q.; Margetis, J.; Tolle, J.; O'Reilly, E. P.; Sweeney, S. J. Ge1−xSnx Alloys: Consequences of Band Mixing Effects for the Evolution of the Band Gap Γ-Character with Sn Concentration. *Sci. Rep.* **2019**, *9*, 14077.

(43) O'Halloran, E. J.; Broderick, C. A.; Tanner, D. S. P.; Schulz, S.; O'Reilly, E. P.

Comparison of First Principles and Semi-Empirical Models of the Structural and Electronic Properties of Ge 1-XSn x Alloys. *Opt. Quantum Electron.* **2019**, *51*, 314.

(44) Zaoui, A.; Ferhat, M.; Certier, M.; Khelifa, B.; Aourag, H. Optical Properties of SiSn and GeSn. *Infrared Phys. Technol.* **1996**, *37*, 483–488.

(45) Gupta, S.; Magyari-Köpe, B.; Nishi, Y.; Saraswat, K. C. Achieving Direct Band Gap in Germanium through Integration of Sn Alloying and External Strain. *J. Appl. Phys.* **2013**, *113*, 073707.

(46) Yin, W. J.; Gong, X. G.; Wei, S. H. Origin of the Unusually Large Band-Gap Bowing and the Breakdown of the Band-Edge Distribution Rule in the Snx Ge1-x Alloys. *Phys. Rev. B - Condens. Matter Mater. Phys.* **2008**, *78*, 161203.

(47) Chang, G.-E.; Chang, S.-W.; Chuang, S. L. Theory for N-Type Doped, Tensile-Strained Ge–SixGeySn1−x−y Quantum-Well Lasers at Telecom Wavelength. *Opt. Express* **2009**, *17*, 11246.

(48) Zhu, Y. H.; Xu, Q.; Fan, W. J.; Wang, J. W. Theoretical Gain of Strained GeSn0.02/Ge1-x-Y′ SixSny′ Quantum Well Laser. *J. Appl. Phys.* **2010**, *107*, 073108.

(49) Rainko, D.; Ikonic, Z.; Vukmirović, N.; Stange, D.; von den Driesch, N.; Grützmacher, D.; Buca, D. Investigation of Carrier Confinement in Direct Bandgap GeSn/SiGeSn 2D and 0D Heterostructures. *Sci. Rep.* **2018**, *8*, 15557.

(50) Xiong, W.; Fan, W. J.; Song, Z. G.; Tan, C. S. The Theoretical Optical Gain of Ge1−xSnx Nanowires. *Phys. Status Solidi - Rapid Res. Lett.* **2020**, *14*, 1900704.

(51) D'Costa, V. R.; Tolle, J.; Xie, J.; Menéndez, J.; Kouvetakis, J. Transport Properties of Doped GeSn Alloys. *AIP Conf. Proc.* **2009**, *1199*, 57–58.

(52) Paul, J.; Mondal, C.; Biswas, A. Subthreshold Modeling of Nanoscale Germanium-Tin (GeSn)-on-Insulator MOSFETs Including Quantum Effects. *Mater. Sci. Semicond. Process.* **2019**, *94*, 128–135.

(53) Wang, H.; Han, G.; Liu, Y.; Hu, S.; Zhang, C.; Zhang, J.; Hao, Y. Theoretical Investigation of Performance Enhancement in GeSn/SiGeSn Type-II Staggered Heterojunction Tunneling FET. *IEEE Trans. Electron Devices* **2016**, *63*, 303–310.

(54) Sant, S.; Schenk, A. Band-Offset Engineering for GeSn-SiGeSn Hetero Tunnel FETs and the Role of Strain. *IEEE J. Electron Devices Soc.* **2015**, *3*, 164–175.

(55) Haehnel, D.; Fischer, I. A.; Hornung, A.; Koellner, A. Tuning the Ge (Sn) Tunneling FET : Influence of Drain Doping , Short Channel , and Sn Content. **2014**, *62*, 36-43.

(56) Vincent, B.; Gencarelli, F.; Bender, H.; Merckling, C.; Douhard, B.; Petersen, D. H.; Hansen, O.; Henrichsen, H. H.; Meersschaut, J.; Vandervorst, W.; Heyns, M.; Loo, R.; Caymax, M. Undoped and In-Situ B Doped GeSn Epitaxial Growth on Ge by Atmospheric Pressure-Chemical Vapor Deposition. *Appl. Phys. Lett.* **2011**, *99*, 2–5.

(57) Kim, S.; Bhargava, N.; Gupta, J.; Coppinger, M.; Kolodzey, J. Infrared Photoresponse of GeSn/n-Ge Heterojunctions Grown by Molecular Beam Epitaxy. *Opt. Express* **2014**, *22*, 11029.

(58) Pérez Ladrón De Guevara, H.; Rodríguez, A. G.; Navarro-Contreras, H.; Vidal, M. A. Ge1-XSnxalloys Pseudomorphically Grown on Ge(001). *Appl. Phys. Lett.* **2003**, *83*,

4942–4944.

(59) Lieten, R. R.; Seo, J. W.; Decoster, S.; Vantomme, A.; Peters, S.; Bustillo, K. C.; Haller, E. E.; Menghini, M.; Locquet, J. P. Tensile Strained GeSn on Si by Solid Phase Epitaxy. *Appl. Phys. Lett.* **2013**, *102*, 052106.

(60) Kim, M.; Fan, W.; Seo, J. H.; Cho, N.; Liu, S. C.; Geng, D.; Liu, Y.; Gong, S.; Wang, X.; Zhou, W.; Ma, Z. Polycrystalline GeSn Thin Films on Si Formed by Alloy Evaporation. *Appl. Phys. Express* **2015**, *8*, 061301.

(61) Mahmodi, H.; Hashim, M. R.; Kim, M.; Fan, W.; Seo, J.-H.; Liu, Z.; Wen, J.; Zhang, X.; Maeda, T.; Jevasuwan, W.; Hattori, H.; Xi, H. Z.; Man, B. Y.; Chen, C. S.; Yoshimine, R.; Toko, K.; Suemasu, T.; Chen, N.; Lin, G.; Zhang, L.; Li, C.; Chen, S.; Huang, W.; Xu, J.; Wang, J. Low-Temperature Formation of GeSn Nanocrystallite Thin Films by Sputtering Ge on Self- Assembled Sn Nanodots on SiO 2 /Si Substrate. *Jpn. J. Appl. Phys* **2017**, *56*, 050301.

(62) Kringhoj, P.; Elliman, R. G. Diffusion of Ion Implanted Sn in Si, Si1-XGex, and Ge. *Appl. Phys. Lett.* **1994**, *65*, 324–326.

(63) Mosleh, A.; Ghetmiri, S. A.; Conley, B. R.; Hawkridge, M.; Benamara, M.; Nazzal, A.; Tolle, J.; Yu, S.-Q.; Naseem, H. A. Material Characterization of Ge1−x Sn x Alloys Grown by a Commercial CVD System for Optoelectronic Device Applications. *J. Electron. Mater.* **2014**, *43*, 938–946.

(64) S. Wirths, D. Buca, A.T. Tiedemann, B. Holländer, P. Bernardy, T. S.; D. Grützmacher, and S. M. Epitaxial Growth of Ge1-XSnx by Reduced Pressure CVD Using SnCl4 and Ge2H6. *ECS Trans.* **2012**, *50*, 885–893.

(65) Zollner, S.; Edwards, N. V.; Duda, E.; Tolle, J.; Taraci, J.; McCartney, M. R.; Menendez, J.; Wolf, G.; Smith, D. J.; Kouvetakis, J. Optical, Vibrational, and Structural Properties of GeSn Alloys on Si. *Mat. Res. Soc. Symp. Proc.* **2002**, *1*, 8010.

(66) Bauer, M. R.; Cook, C. S.; Aella, P.; Tolle, J.; Kouvetakis, J.; Crozier, P. a.; Chizmeshya, a. V. G.; Smith, D. J.; Zollner, S. SnGe Superstructure Materials for Si-Based Infrared Optoelectronics. *Appl. Phys. Lett.* **2003**, *83*, 3489–3491.

(67) Margetis, J.; Ghetmiri, S. A.; Du, W.; Conley, B. R.; Mosleh, A.; Soref, R.; Sun, G.; Domulevicz, L.; Naseem, H. A.; Yu, S.-Q.; Tolle, J. Growth and Characterization of Epitaxial Ge1-XSnx Alloys and Heterostructures Using a Commercial CVD System. *ECS Trans.* **2014**, *6*, 711–720.

(68) Roucka, R.; Tolle, J.; Cook, C.; Chizmeshya, A. V. G.; Kouvetakis, J.; D'Costa, V.; Menendez, J.; Chen, Z. D.; Zollner, S. Versatile Buffer Layer Architectures Based on Ge 1- x Sn x Alloys. *Appl. Phys. Lett.* **2005**, *86*, 191912.

(69) Margetis, J.; Mosleh, A.; Al-Kabi, S.; Ghetmiri, S. A.; Du, W.; Dou, W.; Benamara, M.; Li, B.; Mortazavi, M.; Naseem, H. A.; Yu, S. Q.; Tolle, J. Study of Low-Defect and Strain-Relaxed GeSn Growth via Reduced Pressure CVD in H2 and N2 Carrier Gas. *J. Cryst. Growth* **2017**, *463*, 128–133.

(70) Margetis, J.; Al-Kabi, S.; Du, W.; Dou, W.; Zhou, Y.; Pham, T.; Grant, P.; Ghetmiri, S.; Mosleh, A.; Li, B.; Liu, J.; Sun, G.; Soref, R.; Tolle, J.; Mortazavi, M.; Yu, S. Q. Si-Based GeSn Lasers with Wavelength Coverage of 2-3 Mm and Operating Temperatures up to 180 K. *ACS Photonics* **2018**, *5*, 827–833.

(71) Grzybowski, G.; Beeler, R. T.; Jiang, L.; Smith, D. J.; Kouvetakis, J.; Menéndez, J. Next Generation of Ge 1-YSn y (y = 0.01-0.09) Alloys Grown on Si(100) via Ge 3H 8 and SnD 4: Reaction Kinetics and Tunable Emission. *Appl. Phys. Lett.* **2012**, *101*, 072105.

(72) Su, S.; Zhang, D.; Xue, C.; Cheng, B. Influence of Growth and Annealing Temperature on the Strain and Surface Morphology of Ge0.995Sn0.005 Epilayer. *Appl. Surf. Sci.* **2015**, *340*, 132–137.

(73) Zhou, Y.; Dou, W.; Du, W.; Pham, T.; Ghetmiri, S. A.; Al-Kabi, S.; Mosleh, A.; Alher, M.; Margetis, J.; Tolle, J.; Sun, G.; Soref, R.; Li, B.; Mortazavi, M.; Naseem, H.; Yu, S. Q. Systematic Study of GeSn Heterostructure-Based Light-Emitting Diodes towards Mid-Infrared Applications. *J. Appl. Phys.* **2016**, *120*, 023102.

(74) Stange, D.; Wirths, S.; Von Den Driesch, N.; Mussler, G.; Stoica, T.; Ikonic, Z.; Hartmann, J. M.; Mantl, S.; Grützmacher, D.; Buca, D. Optical Transitions in Direct-Bandgap Ge1-XSnxAlloys. *ACS Photonics* **2015**, *2*, 1539–1545.

(75) Tonkikh, A. A.; Eisenschmidt, C.; Talalaev, V. G.; Zakharov, N. D.; Schilling, J.; Schmidt, G.; Werner, P. Pseudomorphic GeSn/Ge(001) Quantum Wells: Examining Indirect Band Gap Bowing. *Appl. Phys. Lett.* **2013**, *103*, 032106.

(76) Zaima, S.; Nakatsuka, O.; Asano, T.; Yamaha, T.; Ike, S.; Suzuki, A.; Takahashi, K.; Nagae, Y.; Kurosawa, M.; Takeuchi, W.; Shimura, Y.; Sakashita, M. Growth and Applications of GeSn-Related Group-IV Semiconductor Materials. *2016 IEEE Photonics Soc. Summer Top. Meet. Ser. SUM 2016* **2016**, *16*, 37–38.

(77) Su, S.; Cheng, B.; Xue, C.; Wang, W.; Cao, Q.; Xue, H.; Hu, W.; Zhang, G.; Zuo, Y.; Wang, Q. GeSn P-i-n Photodetector for All Telecommunication Bands Detection. *Opt. Express* **2011**, *19*, 6400–6405.

(78) Senaratne, C. L.; Gallagher, J. D.; Jiang, L.; Aoki, T.; Smith, D. J.; Menéndez, J.; Kouvetakis, J. Ge1-YSny (y = 0.01-0.10) Alloys on Ge-Buffered Si: Synthesis, Microstructure, and Optical Properties. *J. Appl. Phys.* **2014**, *116*, 133509.

(79) Conley, B. R.; Mosleh, A.; Ghetmiri, S. A.; Naseem, H. a; Tolle, J.; Yu, S. CVD Growth of Ge1-XSnx Using Large Scale Si Process for Higher Efficient Multi-Junction Solar Cells. *2013 IEEE 39th Photovolt. Spec. Conf.* **2013**, 1346–1349.

(80) Khiangte, K. R.; Rathore, J. S.; Sharma, V.; Laha, A.; Mahapatra, S. Engineering Strain Relaxation of GeSn Epilayers on Ge/Si(001) Substrates. *Solid State Commun.* **2018**, *284–286*, 88–92.

(81) Wang, W.; Loke, W. K.; Yin, T.; Zhang, Z.; D'Costa, V. R.; Dong, Y.; Liang, G.; Pan, J.; Shen, Z.; Yoon, S. F.; Tok, E. S.; Yeo, Y.-C. Growth and Characterization of Highly Tensile Strained Ge1−xSnx Formed on Relaxed InyGa1−yP Buffer Layers. *J. Appl. Phys.* **2016**, *119*, 125303.

(82) Assali, S.; Nicolas, J.; Moutanabbir, O. Enhanced Sn Incorporation in GeSn Epitaxial Semiconductors via Strain Relaxation. *J. Appl. Phys.* **2019**, *125*, 025304.

(83) Dou, W.; Benamara, M.; Mosleh, A.; Margetis, J.; Grant, P.; Zhou, Y.; Al-Kabi, S.; Du, W.; Tolle, J.; Li, B.; Mortazavi, M.; Yu, S. Q. Investigation of GeSn Strain Relaxation and Spontaneous Composition Gradient for Low-Defect and High-Sn Alloy Growth. *Sci. Rep.* **2018**, *8*, 5640.

(84) Barth, S.; Seifner, S.; Bernardi, J. Microwave-Assisted Solution–Liquid–Solid Growthof Ge1-XSnxnanowires with High Tin Content. *Chem. Commun.* **2015**, *51*, 12282–12285.

(85) Seifner, M. S.; Hernandez, S.; Bernardi, J.; Romano-Rodriguez, A.; Barth, S. Pushing the Composition Limit of Anisotropic Ge1−xSnx Nanostructures and Determination of Their Thermal Stability. *Chem. Mater.* **2017**, *29*, 9802–9813.

(86) Moutanabbir, O.; Isheim, D.; Blumtritt, H.; Senz, S.; Pippel, E.; Seidman, D. N. Colossal Injection of Catalyst Atoms into Silicon Nanowires. *Nature* **2013**, *496*, 78–82.

(87) Azrak, E.; Chen, W.; Moldovan, S.; Gao, S.; Duguay, S.; Pareige, P.; Roca I Cabarrocas, P. Growth of In-Plane Ge1- XSnx Nanowires with 22 at. % Sn Using a Solid-Liquid-Solid Mechanism. *J. Phys. Chem. C* **2018**, *122*, 26236–26242.

(88) Seifner, M. S.; Dijkstra, A.; Bernardi, J.; Steiger-Thirsfeld, A.; Sistani, M.; Lugstein, A.; Haverkort, J. E. M.; Barth, S. Epitaxial Ge0.81Sn0.19 Nanowires for Nanoscale Mid-Infrared Emitters. *ACS Nano* **2019**, *13*, 8047–8054.

(89) Biswas, S.; Doherty, J.; Saladukha, D.; Ramasse, Q.; Majumdar, D.; Upmanyu, M.; Singha, A.; Ochalski, T.; Morris, M. A.; Holmes, J. D. Non-Equilibrium Induction of Tin in Germanium: Towards Direct Bandgap Ge 1-XSnx Nanowires. *Nat. Commun.* **2016**, *7*, 114005.

(90) Biswas, S.; O'Regan, C.; Petkov, N.; Morris, M. a.; Holmes, J. D. Manipulating the Growth Kinetics of Vapor-Liquid-Solid Propagated Ge Nanowires. *Nano Lett.* **2013**, *13*, 4044–4052.

(91) Doherty, J.; Biswas, S.; Saladukha, D.; Ramasse, Q.; Bhattacharya, T. S.; Singha, A.; Ochalski, T. J.; Holmes, J. D. Influence of Growth Kinetics on Sn Incorporation in Direct Band Gap Ge 1−x Sn x Nanowires. *J. Mater. Chem. C* **2018**, *6*, 8738–8750.

(92) Sun, Y. L.; Matsumura, R.; Jevasuwan, W.; Fukata, N. Au-Sn Catalyzed Growth of Ge1- XSnx Nanowires: Growth Direction, Crystallinity, and Sn Incorporation. *Nano Lett.* **2019**, *19*, 6270–6277.

(93) Doherty, J.; Biswas, S.; Mcnulty, D.; Downing, C.; Raha, S.; Regan, C. O.; Singha, A.; Dwyer, C. O.; Holmes, J. D. One-Step Fabrication of GeSn Branched Nanowires. *Chem. Mater.* **2019**, *31*, 4016–4024.

(94) Meng, A. C.; Fenrich, C. S.; Braun, M. R.; McVittie, J. P.; Marshall, A. F.; Harris, J. S.; McIntyre, P. C. Core-Shell Germanium/Germanium-Tin Nanowires Exhibiting Room-Temperature Direct- and Indirect-Gap Photoluminescence. *Nano Lett.* **2016**, *16* , 7521–7529.

(95) Assali, S.; Dijkstra, A.; Li, A.; Koelling, S.; Verheijen, M. A.; Gagliano, L.; von den Driesch, N.; Buca, D.; Koenraad, P. M.; Haverkort, J. E. M.; Bakkers, E. P. A. M. Growth and Optical Properties of Direct Band Gap Ge/Ge $_{0.87}$ Sn $_{0.13}$ Core/Shell Nanowire Arrays. *Nano Lett.* **2017**, *17*, 1538–1544.

(96) Haffner, T.; Zeghouane, M.; Bassani, F.; Gentile, P.; Gassenq, A.; Chouchane, F.; Pauc, N.; Martinez, E.; Robin, E.; David, S.; Baron, T.; Salem, B. Growth of Ge $_{1-x}$ Sn $_{x}$ Nanowires by Chemical Vapor Deposition via Vapor-Liquid-Solid Mechanism Using GeH $_4$ and SnCl $_4$. *Phys. Status Solidi* **2017**, *215*, 1700743.

(97) Han, D.; Ye, H.; Song, Y.; Zhu, Z.; Yang, Y.; Yu, Z.; Liu, Y.; Wang, S.; Di, Z. Analysis of Raman Scattering from Inclined GeSn/Ge Dual-Nanowire Heterostructure on Ge(111) Substrate. *Appl. Surf. Sci.* **2018**, *463*, 581–586.

(98) Meng, A. C.; Braun, M. R.; Wang, Y.; Fenrich, C. S.; Xue, M.; Diercks, D. R.; Gorman, B. P.; Richard, M.; Marshall, A. F.; Cai, W.; Harris, J. S.; Mcintyre, P. C. Coupling of Coherent Misfit Strain and Composition Distributions in Core-Shell Ge/Ge1-XSnx Nanowire Light Emitters. *Mater. Today Nano* **2019**, *5*, 100026.

(99) Wang, Y.; Meng, A. C.; McIntyre, P. C.; Cai, W. Phase-Field Investigation of the Stages in Radial Growth of Core-Shell Ge/Ge1-: XSnx Nanowires. *Nanoscale* **2019**, *11*, 21974.

(100) Assali, S.; Albani, M.; Bergamaschini, R.; Verheijen, M. A.; Li, A.; Kölling, S.; Gagliano, L.; Bakkers, E. P. A. M.; Miglio, L. Strain Engineering in Ge/GeSn Core/Shell Nanowires. *Appl. Phys. Lett.* **2019**, *115*, 113102.

(101) Azrak, E.; Chen, W.; Moldovan, S.; Duguay, S.; Pareige, P.; Roca Cabarrocas, P. Low-Temperature Plasma-Assisted Growth of Core-Shell GeSn Nanowires with 30% Sn. *J. Phys. Chem. C* **2020**, *124*, 1220–1226.

(102) Gong, X.; Han, G.; Su, S.; Cheng, R.; Guo, P.; Bai, F.; Yang, Y.; Zhou, Q.; Liu, B.; Goh, K. H. Uniaxially Strained Germanium-Tin (GeSn) Gate-All-Around Nanowire PFETs Enabled by a Novel Top-Down Nanowire Formation Technology. *2013 Symp. VLSI Circuits* **2013**, 34–35.

(103) Noroozi, M.; Hamawandi, B.; Toprak, M. S.; Radamson, H. H. Fabrication and Thermoelectric Characterization of GeSn Nanowires. *ULIS 2014 - 2014 15th Int. Conf. Ultim. Integr. Silicon* **2014**, 125–128.

(104) Shang, C. K.; Wang, V.; Chen, R.; Gupta, S.; Huang, Y. C.; Pao, J. J.; Huo, Y.; Sanchez, E.; Kim, Y.; Kamins, T. I.; Harris, J. S. Dry-Wet Digital Etching of Ge1-XSnx. *Appl. Phys. Lett.* **2016**, *108*, 063110.

(105) Gupta, S.; Chen, R.; Huang, Y. C.; Kim, Y.; Sanchez, E.; Harris, J. S.; Saraswat, K. C. Highly Selective Dry Etching of Germanium over Germanium-Tin (Ge1-XSnx): A Novel Route for Ge1-XSnxnanostructure Fabrication. *Nano Lett.* **2013**, *13*, 3783–3790.

(106) Xu, X.; Lei, D.; Wang, W.; Dong, Y.; Gong, X.; Yeo, Y. C. Formation of Vertically Stacked Germanium-Tin (Ge1-XSn x) Nanowires Using a Selective Dry Etch Technique. *2014 7th Int. Silicon-Germanium Technol. Device Meet. ISTDM 2014* **2014**, 167–168.

(107) Ramasamy, K.; Kotula, P. G.; Fidler, A. F.; Brumbach, M. T.; Pietryga, J. M.; Ivanov, S. A. SnxGe1-XAlloy Nanocrystals: A First Step toward Solution-Processed Group IV Photovoltaics. *Chem. Mater.* **2015**, *27*, 4640–4649.

(108) Cho, Y. J.; Kim, C. H.; Im, H. S.; Myung, Y.; Kim, H. S.; Back, S. H.; Lim, Y. R.; Jung, C. S.; Jang, D. M.; Park, J.; Lim, S. H.; Cha, E. H.; Bae, K. Y.; Song, M. S.; Cho, W. Il. Germanium-Tin Alloy Nanocrystals for High-Performance Lithium Ion Batteries. *Phys. Chem. Chem. Phys.* **2013**, *15*, 11691–11695.

(109) Esteves, R. J. A.; Ho, M. Q.; Arachchige, I. U. Nanocrystalline Group IV Alloy Semiconductors: Synthesis and Characterization of Ge1- XSnxquantum Dots for

Tunable Bandgaps. *Chem. Mater.* **2015**, *27*, 1559–1568.

(110) Nakamura, Y.; Masada, A.; Cho, S. P.; Tanaka, N.; Ichikawa, M. Epitaxial Growth of Ultrahigh Density Ge1-XSnx Quantum Dots on Si (111) Substrates by Codeposition of Ge and Sn on Ultrathin SiO2 Films. *J. Appl. Phys.* **2007**, *102*, 124302.

(111) Abdel-Rahim, M. A.; Hafiz, M. M.; Alwany, A. E. B. The Effect of Composition on Structural and Optical Properties of ZnSe Alloys. *Opt. Laser Technol.* **2013**, *47*, 88–94.

(112) Alan Esteves, R. J.; Hafiz, S.; Demchenko, D. O.; Özgür, Ü.; Arachchige, I. U. Ultra-Small Ge1-XSnx Quantum Dots with Visible Photoluminescence. *Chem. Commun.* **2016**, *52*, 11665–11668.

(113) Tallapally, V.; Nakagawara, T. A.; Demchenko, D. O.; Özgür, Ü.; Arachchige, I. U. Ge1−xSnx Alloy Quantum Dots with Composition-Tunable Energy Gaps and near-Infrared Photoluminescence. *Nanoscale* **2018**, *10*, 20296–20305.

(114) Yang, Q.; Zhao, X.; Wu, X.; Li, M.; Di, Q.; Fan, X.; Zhu, J.; Song, X.; Li, Q.; Quan, Z. Facile Synthesis of Uniform Sn 1- x Ge x Alloy Nanocrystals with Tunable Bandgap. *Chem. Mater.* **2019**, *31*, 2248–2252.

(115) Slav, A.; Palade, C.; Logofatu, C.; Dascalescu, I.; Lepadatu, A. M.; Stavarache, I.; Comanescu, F.; Iftimie, S.; Antohe, S.; Lazanu, S.; Teodorescu, V. S.; Buca, D.; Ciurea, M. L.; Braic, M.; Stoica, T. GeSn Nanocrystals in GeSnSiO 2 by Magnetron Sputtering for Short- Wave Infrared Detection. *ACS Appl. Nano Mater.* **2019**, *2*, 3626–3635.

(116) Zaumseil, P.; Hou, Y.; Schubert, M. A.; Von Den Driesch, N.; Stange, D.; Rainko, D.; Virgilio, M.; Buca, D.; Capellini, G. The Thermal Stability of Epitaxial GeSn Layers. *APL Mater.* **2018**, *6*, 076108.

(117) Okamoto, H.; Takita, K.; Tsushima, K.; Tawara, T.; Tateno, K.; Zhang, G.; Gotoh, H. Low-Temperature Formation of GeSn Nanodots by Sn Mediation. *Jpn. J. Appl. Phys.* **2019**, *58*, SDDG09.

(118) Di Bartolomeo, A.; Passacantando, M.; Niu, G.; Schlykow, V.; Lupina, G.; Giubileo, F.; Schroeder, T. Observation of Field Emission from GeSn Nanoparticles Epitaxially Grown on Silicon Nanopillar Arrays. *Nanotechnology* **2016**, *27*, 5707.

(119) Bauer, J.; Yamamoto, Y.; Zaumseil, P.; Fursenko, O.; Schulz, K.; Kozlowski, G.; Schubert, M. A.; Schroeder, T.; Tillack, B. Nanostructured Silicon for Ge Nanoheteroepitaxy. *Microelectron. Eng.* **2012**, *97*, 169–172.

(120) Mukherjee, S.; Kodali, N.; Isheim, D.; Wirths, S.; Hartmann, J. M.; Buca, D.; Seidman, D. N.; Moutanabbir, O. Short-Range Atomic Ordering in Nonequilibrium Silicon-Germanium-Tin Semiconductors. *Phys. Rev. B* **2017**, *95*, 161402.

(121) Ranjan, R.; Das, M. K. Theoretical Estimation of Optical Gain in Tin-Incorporated Group IV Alloy Based Transistor Laser. *Opt. Quantum Electron.* **2016**, *48*, 201.

(122) Soref, R. A.; Friedman, L. Direct-Gap Ge/GeSn/Si and GeSn/Ge/Si Heterostructures. *Superlattices and Microstructures*. **1993**, *14*, 189–193.

(123) Saladukha, D.; Doherty, J.; Biswas, S.; Ochalski, T. J.; Holmes, J. D. Optical Study of Strain-Free GeSn Nanowires. *Silicon Photonics XII* **2017**, *10108*, 101081C.

(124) Ryu, M. Y.; Harris, T. R.; Yeo, Y. K.; Beeler, R. T.; Kouvetakis, J. Temperature-Dependent Photoluminescence of Ge/Si and Ge 1-YSny/Si, Indicating Possible Indirect-to-Direct Bandgap Transition at Lower Sn Content. *Appl. Phys. Lett.* **2013**, *102*, 171908.

(125) Pezzoli, F.; Giorgioni, A.; Patchett, D.; Myronov, M. Temperature-Dependent Photoluminescence Characteristics of GeSn Epitaxial Layers. *ACS Photonics* **2016**, *3*, 2004–2009.

(126) Tran, T. T.; Pastor, D.; Gandhi, H. H.; Smillie, L. A.; Akey, A. J.; Aziz, M. J.; Williams, J. S. Synthesis of Ge1-XSnx Alloys by Ion Implantation and Pulsed Laser Melting: Towards a Group IV Direct Bandgap Material. *J. Appl. Phys.* **2016**, *119*, 183102.

(127) Lieten, R. R.; Fleischmann, C.; Peters, S.; Santos, N. M.; Amorim, L. M.; Shimura, Y.; Uchida, N.; Maeda, T.; Nikitenko, S.; Conard, T.; Locquet, J.-P.; Temst, K.; Vantomme, a. Structural and Optical Properties of Amorphous and Crystalline GeSn Layers on Si. *ECS J. Solid State Sci. Technol.* **2014**, *3*, P403–P408.

(128) D'Costa, V. R.; Fang, Y.; Mathews, J.; Roucka, R.; Tolle, J.; Menéndez, J.; Kouvetakis, J. Sn-Alloying as a Means of Increasing the Optical Absorption of Ge at the C- and L-Telecommunication Bands. *Semicond. Sci. Technol.* **2009**, *24*, 115006.

(129) Xu, C.; Wallace, P. M.; Ringwala, D. A.; Chang, S. L. Y.; Poweleit, C. D.; Kouvetakis, J.; Menéndez, J. Mid-Infrared (3-8 μ m) Ge1-YSny Alloys ($0.15 < y < 0.30$): Synthesis, Structural, and Optical Properties. *Appl. Phys. Lett.* **2019**, *114*, 212104.

(130) Hu, S.; Kawamura, Y.; Huang, K. C. Y.; Li, Y.; Marshall, A. F.; Itoh, K. M.; Brongersma, M. L.; McIntyre, P. C. Thermal Stability and Surface Passivation of Ge Nanowires Coated by Epitaxial SiGe Shells. *Nano Lett.* **2012**, *12*, 1385–1391.

(131) Seifner, M. S.; Dijkstra, A.; Bernardi, J.; Steiger-Thirsfeld, A.; Sistani, M.; Lugstein, A.; Haverkort, J. E. M.; Barth, S. Epitaxial Ge0.81Sn0.19 Nanowires for Nanoscale Mid-Infrared Emitters. *ACS Nano* **2019**, *13*, 8047–8054.

(132) Assali, S.; Nicolas, J.; Mukherjee, S.; Dijkstra, A.; Moutanabbir, O. Atomically Uniform Sn-Rich GeSn Semiconductors with 3.0-3.5 μ m Room-Temperature Optical Emission. *Appl. Phys. Lett.* **2018**, *112*, 251903.

(133) Assali, S.; Bergamaschini, R.; Scalise, E.; Verheijen, M. A.; Albani, M.; Dijkstra, A.; Li, A.; Koelling, S.; Bakkers, E. P. A. M.; Montalenti, F.; Miglio, L. Kinetic Control of Morphology and Composition in Ge/GeSn Core/Shell Nanowires. *ACS Nano* **2020**, *14*, 2445–2455.

(134) Demchenko, D. O.; Tallapally, V.; Esteves, R. J. A.; Hafiz, S.; Nakagawara, T. A.; Arachchige, I. U.; Özgür, Ü. Optical Transitions and Excitonic Properties of Ge1-XSnx Alloy Quantum Dots. *J. Phys. Chem. C* **2017**, *121*, 18299–18306.

(135) Alan Esteves, R. J.; Hafiz, S.; Demchenko, D. O.; Özgür, Ü.; Arachchige, I. U. Ultra-Small Ge1-XSnx Quantum Dots with Visible Photoluminescence. *Chem. Commun.* **2016**, *52*, 11665–11668.

(136) Zhang, L.; Hong, H.; Li, C.; Chen, S.; Huang, W.; Wang, J.; Wang, H. High-Sn Fraction GeSn Quantum Dots for Si-Based Light Source at 1.55 Mm. *Appl. Phys.*

Express **2019**, *12*, 055504.

(137) Hafiz, S. A.; Esteves, R. J. A.; Demchenko, D. O.; Arachchige, I. U.; Özgür, Ü. Energy Gap Tuning and Carrier Dynamics in Colloidal Ge1-XSnx Quantum Dots. *J. Phys. Chem. Lett.* **2016**, *7*, 3295–3301.

(138) Huang, Y. S.; Lu, F. L.; Tsou, Y. J.; Ye, H. Y.; Lin, S. Y.; Huang, W. H.; Liu, C. W. Vertically Stacked Strained 3-GeSn-Nanosheet PGAAFETs on Si Using GeSn/Ge CVD Epitaxial Growth and the Optimum Selective Channel Release Process. *IEEE Electron Device Lett.* **2018**, *39*, 1274–1277.

(139) Lei, D., Lee, K.H., Bao, S., Wang, W., Masudy-Panah, S., Yadav, S., Kumar, A., Dong, Y., Kang, Y., Xu, S., Wu, Y., Huang, Y.-C., Chung, H., Chu, S.S., Kuppurao, S., Tan, C.S., Gong, X., Yeo, Y.-C. Germanium-Tin (GeSn) P-Channel Fin Field-Effect Transistor Fabricated on a Novel GeSn-on-Insulator Substrate. *IEEE Trans. Electron Devices* **2018**, *65*, 3754–3761.

(140) Lei, D.; Lee, K. H.; Bao, S.; Wang, W.; Masudy-panah, S.; Yadav, S.; Kumar, A.; Dong, Y.; Kang, Y.; Xu, S.; Wu, Y.; Huang, Y.; Chung, H.; Chu, S. S.; Kuppurao, S.; Tan, C. S.; Gong, X.; Yeo, Y. The First GeSn FinFET on a Novel GeSnOI Substrate Achieving Lowest S of 79 MV/Decade and Record High Gm, Int of 807 Ms/Mm for GeSn P-FETs. *Symp. VLSI Technol.* **2017**, T198–T199.

(141) Wang, L.; Su, S.; Wang, W.; Gong, X.; Yang, Y.; Guo, P.; Zhang, G.; Xue, C.; Cheng, B.; Han, G.; Yeo, Y. C. Strained Germanium-Tin (GeSn) p-Channel Metal-Oxide-Semiconductor Field-Effect-Transistors (p-MOSFETs) with Ammonium Sulfide Passivation. *Solid. State. Electron.* **2013**, *83*, 66–70.

(142) Lei, D.; Wang, W.; Zhang, Z.; Pan, J.; Gong, X.; Liang, G.; Tok, E. S.; Yeo, Y. C. Ge0.83Sn0.17p-Channel Metal-Oxide-Semiconductor Field-Effect Transistors: Impact of Sulfur Passivation on Gate Stack Quality. *J. Appl. Phys.* **2016**, *119*, 024502.

(143) Fang, Y. C.; Chen, K. Y.; Hsieh, C. H.; Su, C. C.; Wu, Y. H. N-MOSFETs Formed on Solid Phase Epitaxially Grown GeSn Film with Passivation by Oxygen Plasma Featuring High Mobility. *ACS Appl. Mater. Interfaces* **2015**, *7*, 26374–26380.

(144) Wirths, S., Troitsch, R., Mussler, G., Zaumseil, P., Hartmann, J.M., Schroeder, T., Mantl, S., Buca, D. Ni(SiGeSn) Metal Contact Formation on Low Bandgap Strained (Si)Ge(Sn) Semiconductors. *Trans. E C S Soc. Electrochem.* **2014**, *64*, 107–112.

(145) Han, G.; Wang, Y.; Liu, Y.; Zhang, C.; Feng, Q.; Liu, M.; Zhao, S.; Cheng, B.; Zhang, J.; Hao, Y. GeSn Quantum Well P-Channel Tunneling FETs Fabricated on Si(001) and (111) with Improved Subthreshold Swing. *IEEE Electron Device Lett.* **2016**, *37*, 701–704.

(146) Schulze, J.; Blech, A.; Datta, A.; Fischer, I. A.; Hähnel, D.; Naasz, S.; Rolseth, E.; Tropper, E. Solid-State Electronics Vertical Ge and GeSn Heterojunction Gate-All-around Tunneling Field Effect Transistors. *Solid State Electron.* **2015**, *110*, 59–64.

(147) Cong, H.; Yang, F.; Xue, C.; Yu, K.; Zhou, L.; Wang, N.; Cheng, B.; Wang, Q. Multilayer Graphene-GeSn Quantum Well Heterostructure SWIR Light Source. *Small* **2018**, *14*, 1704414.

(148) Kosmaca, J.; Meija, R.; Antsov, M.; Kunakova, G.; Sondors, R.; Iatsunskyi, I.; Coy, E.; Doherty, J.; Biswas, S.; Holmes, J. D.; Erts, D. Investigating the Mechanical

Properties of GeSn Nanowires. *Nanoscale* **2019**, *11*, 13612.

(149) Smith, D. A.; Holmberg, V. C.; Lee, D. C.; Korgel, B. A. Young's Modulus and Size-Dependent Mechanical Quality Factor of Nanoelectromechanical Germanium Nanowire Resonators. *J. Phys. Chem. C* **2008**, *112*, 10725–10729.

(150) Calahorra, Y.; Shtempluck, O.; Kotchetkov, V.; Yaish, Y. E. Young ' s Modulus, Residual Stress, and Crystal Orientation of Doubly Clamped Silicon Nanowire Beams. *Nano Lett.* **2015**, *15*, 2945–2950.

(151) Zhang, X.; Ying, C.; Li, Z.; Shi, G. First-Principles Calculations of Structural Stability , Elastic , Dynamical and Thermodynamic Properties of SiGe , SiSn , GeSn. *SUPERLATTICES Microstruct.* **2012**, *52*, 459–469.

(152) Pham, T.; Du, W.; Tran, H.; Margetis, J.; Tolle, J.; Sun, G.; Soref, R. A.; Naseem, H. A.; Li, B.; Yu, S.-Q. Systematic Study of Si-Based GeSn Photodiodes with 26 Mm Detector Cutoff for Short-Wave Infrared Detection. *Opt. Express* **2016**, *24*, 4519.

(153) Cong, H.; Xue, C.; Zheng, J.; Yang, F.; Yu, K.; Liu, Z.; Zhang, X.; Cheng, B.; Wang, Q. Silicon Based GeSn P-i-n Photodetector for SWIR Detection. *IEEE Photonics J.* **2016**, *8*, 6804706.

(154) Xu, S.; Huang, Y.-C.; Hong Lee, K.; Wang, W.; Dong, Y.; Lei, D.; Masudy-Panah, S.; Tan, C. S.; Gong, X.; Yeo, Y.-C. GeSn Lateral P-i-n Photodetector on Insulating Substrate. *Opt. Express* **2018**, *26*, 17312–17320.

(155) Gupta, S.; Chen, R.; Vincent, B.; Lin, D.; Magyari-Kope, B.; Caymax, M.; Dekoster, J.; Harris, J. S.; Nishi, Y.; Saraswat, K. C. (Invited) GeSn Channel n and p MOSFETs. *ECS Trans.* **2013**, *50*, 937–941.

(156) Yang, Y.; Lu Low, K.; Wang, W.; Guo, P.; Wang, L.; Han, G.; Yeo, Y. C. Germanium-Tin n-Channel Tunneling Field-Effect Transistor: Device Physics and Simulation Study. *J. Appl. Phys.* **2013**, *113*, 194507.

(157) Zhou, J.; Peng, Y.; Han, G.; Li, Q.; Liu, Y.; Zhang, J.; Liao, M.; Sun, Q. Q.; Zhang, D. W.; Zhou, Y.; Hao, Y. Hysteresis Reduction in Negative Capacitance Ge PFETs Enabled by Modulating Ferroelectric Properties in HfZrOx. *IEEE J. Electron Devices Soc.* **2017**, *6*, 41–48.

(158) Zhou, J.; Han, G.; Li, J.; Liu, Y.; Peng, Y.; Zhang, J.; Sun, Q. Q.; Zhang, D. W.; Hao, Y. Negative Differential Resistance in Negative Capacitance FETs. *IEEE Electron Device Lett.* **2018**, *39*, 622–625.

(159) Zhou, J.; Han, G.; Peng, Y.; Liu, Y.; Zhang, J.; Sun, Q. Q.; Zhang, D. W.; Hao, Y. Ferroelectric Negative Capacitance GeSn PFETs With Sub-20 MV/Decade Subthreshold Swing. *IEEE Electron Device Lett.* **2017**, *38*, 1157–1160.

(160) Liu, M.; Liu, Y.; Wang, H.; Zhang, Q.; Zhang, C.; Hu, S.; Hao, Y.; Han, G. Design of GeSn-Based Heterojunction-Enhanced N-Channel Tunneling FET with Improved Subthreshold Swing and ON-State Current. *IEEE Trans. Electron Devices* **2015**, *62*, 1262–1268.

(161) Wang, W.; Lei, D.; Huang, Y.; Lee, K. H.; Loke, W.; Dong, Y.; Xu, S.; Tan, C. S.; Wang, H.; Yoon, S.; Gong, X.; Yeo, Y. High-Performance GeSn Photodetector and Fin Field-Effect Transistor (FinFET) on an Advanced GeSn-on-Insulator Platform. *Opt. Express* **2018**, *26*, 10305.

(162) Buca, D.; Schulte-Braucks, C.; Von Den Driesch, N.; Tiedemann, A. T.; Breuer, U.; Hartmann, J. M.; Zaumseil, P.; Mantl, S.; Zhao, Q. T. Gate Stack and Ni(SiGeSn) Metal Contacts Formation on Low Bandgap Strained (Si)Ge(Sn) Semiconductors. *2018 18th Int. Work. Junction Technol. IWJT 2018* **2018**, 1–1.

(163) Quintero, A.; Gergaud, P.; Aubin, J.; Hartmann, J. M.; Chevalier, N.; Barnes, J. P.; Loup, V.; Reboud, V.; Nemouchi, F.; Rodriguez, P. Impact of Pt on the Phase Formation Sequence, Morphology, and Electrical Properties of Ni(Pt)/Ge0.9Sn0.1system during Solid-State Reaction. *J. Appl. Phys.* **2018**, *124*, 085305.

(164) Gupta, S.; Gong, X.; Zhang, R.; Yeo, Y. C.; Takagi, S.; Saraswat, K. C. New Materials for Post-Si Computing: Ge and GeSn Devices. *MRS Bull.* **2014**, *39*, 678–686.

(165) Zheng, J.; Wang, S.; Liu, Z.; Cong, H.; Xue, C.; Li, C.; Zuo, Y.; Cheng, B.; Wang, Q. GeSn P-i-n Photodetectors with GeSn Layer Grown by Magnetron Sputtering Epitaxy. *Appl. Phys. Lett.* **2016**, *108* ,033503.

(166) Roucka, R.; Beeler, R.; Mathews, J.; Ryu, M. Y.; Kee Yeo, Y.; Menéndez, J.; Kouvetakis, J. Complementary Metal-Oxide Semiconductor-Compatible Detector Materials with Enhanced 1550 Nm Responsivity via Sn-Doping of Ge/Si(100). *J. Appl. Phys.* **2011**, *109*, 103115.

(167) Su, S. J.; Xue, C. L.; Cheng, B. W.; Wang, W.; Zhang, G. Z.; Zuo, Y. H.; Wang, Q. M. GeSn on Si Photodetectors Grown by Molecular Beam Epitaxy. *IEEE Int. Conf. Gr. IV Photonics GFP* **2011**, 33–35.

(168) Zhang, D.; Xue, C.; Cheng, B.; Su, S.; Liu, Z.; Zhang, X.; Zhang, G.; Li, C.; Wang, Q. High-Responsivity GeSn Short-Wave Infrared p-i-n Photodetectors. *Appl. Phys. Lett.* **2013**, *102*, 98–102.

(169) Hart, J.; Adam, T.; Kim, Y.; Huang, Y. C.; Reznicek, A.; Hazbun, R.; Gupta, J.; Kolodzey, J. Temperature Varying Photoconductivity of GeSn Alloys Grown by Chemical Vapor Deposition with Sn Concentrations from 4% to 11%. *J. Appl. Phys.* **2016**, *119*, 093105.

(170) Zaumseil, P.; Nakatsuka, O.; Zaima, S.; Schroeder, T. Electrical and Optical Properties Improvement of GeSn Layers Formed at High Temperatures under Well-Controlled Sn Migration. *Mater. Sci. Semicond. Process.* **2017**, *57*, 48–53.

(171) Roucka, R.; Yu, S.-Q.; Tolle, J.; Fang, Y.-Y.; Wu, S.-N.; Menendez, J.; Kouvetakis, J. Photoresponse at 1.55 Mm in GeSn Epitaxial Films Grown on Si. *LEOS 2007 - IEEE Lasers Electro-Optics Soc. Annu. Meet. Conf. Proc.* **2007**, 178–179.

(172) Werner, J.; Oehme, M.; Schirmer, A.; Kasper, E.; Schulze, J. Molecular Beam Epitaxy Grown GeSn P-i-n Photodetectors Integrated on Si. *Thin Solid Films* **2012**, *520*, 3361–3364.

(173) Oehme, M.; Schmid, M.; Kaschel, M.; Gollhofer, M.; Widmann, D.; Kasper, E.; Schulze, J. GeSn P-i-n Detectors Integrated on Si with up to 4% Sn. *Appl. Phys. Lett.* **2012**, *101*, 141110.

(174) Tran, H.; Pham, T.; Margetis, J.; Zhou, Y.; Dou, W.; Grant, P. C.; Grant, J. M.; Al-Kabi, S.; Sun, G.; Soref, R. A.; Tolle, J.; Zhang, Y. H.; Du, W.; Li, B.; Mortazavi, M.; Yu, S. Q. Si-Based GeSn Photodetectors toward Mid-Infrared Imaging Applications.

ACS Photonics **2019**, *6*, 2807–2815.

(175) Mathews, J.; Roucka, R.; Xie, J.; Yu, S. Q.; Meńndez, J.; Kouvetakis, J. Extended Performance GeSn/Si(100) p-i-n Photodetectors for Full Spectral Range Telecommunication Applications. *Appl. Phys. Lett.* **2009**, *95*, 133506.

(176) Chang, G. E.; Basu, R.; Mukhopadhyay, B.; Basu, P. K. Design and Modeling of GeSn-Based Heterojunction Phototransistors for Communication Applications. *IEEE J. Sel. Top. Quantum Electron.* **2016**, *22* , 8200409.

(177) Tran, H.; Pham, T.; Du, W.; Zhang, Y.; Grant, P. C.; Grant, J. M.; Sun, G.; Soref, R. A.; Margetis, J.; Tolle, J.; Li, B.; Mortazavi, M.; Yu, S. Q. High Performance Ge0.89Sn0.11 Photodiodes for Low-Cost Shortwave Infrared Imaging. *J. Appl. Phys.* **2018**, *124*, 013101.

(178) Pham, T.; Du, W.; Tran, H.; Margetis, J.; Tolle, J.; Sun, G.; Soref, R. A.; Naseem, H. A.; Li, B.; Yu, S.-Q. Systematic Study of Si-Based GeSn Photodiodes with 26 Mm Detector Cutoff for Short-Wave Infrared Detection. *Opt. Express* **2016**, *24*, 4519.

(179) Conley, B. R.; Margetis, J.; Du, W.; Tran, H.; Mosleh, A.; Ghetmiri, S. A.; Tolle, J.; Sun, G.; Soref, R.; Li, B.; Naseem, H. A.; Yu, S. Q. Si Based GeSn Photoconductors with a 1.63 A/W Peak Responsivity and a 2.4 μ m Long-Wavelength Cutoff. *Appl. Phys. Lett.* **2014**, *105*, 221117.

(180) Pham, T. N.; Du, W.; Conley, B. R.; Margetis, J.; Sun, G.; Soref, R. A.; Tolle, J.; Li, B.; Yu, S. Q. Si-Based Ge0.9Sn0.1 Photodetector with Peak Responsivity of 2.85 A/W and Longwave Cutoff at 2.4 Mm. *Electron. Lett.* **2015**, *51*, 854–856.

(181) Zheng, J.; Liu, Z.; Xue, C.; Li, C.; Zuo, Y.; Cheng, B.; Wang, Q. Recent Progress in GeSn Growth and GeSn-Based Photonic Devices. *J. Semicond.* **2018**, *39*, 061006.

(182) Homewood, K. P.; Lourenço, M. A. Optoelectronics: The Rise of the GeSn Laser. *Nat. Photonics* **2015**, *9*, 78–79.

(183) Stange, D.; Wirths, S.; Geiger, R.; Schulte-Braucks, C.; Marzban, B.; Driesch, N. V. Den; Mussler, G.; Zabel, T.; Stoica, T.; Hartmann, J. M.; Mantl, S.; Ikonic, Z.; Grützmacher, D.; Sigg, H.; Witzens, J.; Buca, D. Optically Pumped GeSn Microdisk Lasers on Si. *ACS Photonics* **2016**, *3*, 1279–1285.

(184) von den Driesch, N.; Stange, D.; Rainko, D.; Povstugar, I.; Zaumseil, P.; Capellini, G.; Schröder, T.; Denneulin, T.; Ikonic, Z.; Hartmann, J. M.; Sigg, H.; Mantl, S.; Grützmacher, D.; Buca, D. Advanced GeSn/SiGeSn Group IV Heterostructure Lasers. *Adv. Sci.* **2018**, *5*, 1700955.

(185) Kim, M. G.; Cho, J. Nanocomposite of Amorphous Ge and Sn Nanoparticles as an Anode Material for Li Secondary Battery. *J. Electrochem. Soc.* **2009**, *156*, A277.

(186) Bodnarchuk, M. I.; Kravchyk, K. V.; Krumeich, F.; Wang, S.; Kovalenko, M. V. Colloidal Tin-Germanium Nanorods and Their Li-Ion Storage Properties. *ACS Nano* **2014**, *8*, 2360–2368.

(187) Doherty, J.; McNulty, D.; Biswas, S.; Moore, K.; Conroy, M.; Bangert, U.; O'Dwyer, C.; Holmes, J. D. Germanium Tin Alloy Nanowires as Anode Materials for High Performance Li-Ion Batteries. *Nanotechnology* **2020**, *31*, 165402.

(188) Du, W.; & Yu, S. Y. In *Mid-infrared Optoelectronics*, Tournié, E.; Laurent Cerutti,

L., Woodhead Publishing Elseier **2020**, Chapter 12 (Group IV photonics using (Si)GeSn technology toward mid-IR applications), pp493-538.

TOC graphic: